nature climate change

Article https://doi.org/10.1038/s41558-023-01736-y

Co-firing plants with retrofitted carbon capture and storage for power-sector emissions mitigation

In the format provided by the authors and unedited

Supplementary Information for "Co-firing plants with retrofitted carbon capture and storage for power sector mitigation"

Supplementary Figures:

Figure 1. Geographical regions in China (Data Credits: All the provincial administrative boundaries are from Ministry of Civil Affairs of the People's Republic of China (http://xzqh.mca.gov.cn/map, Map Content Approval Number: GS(2022)1873))

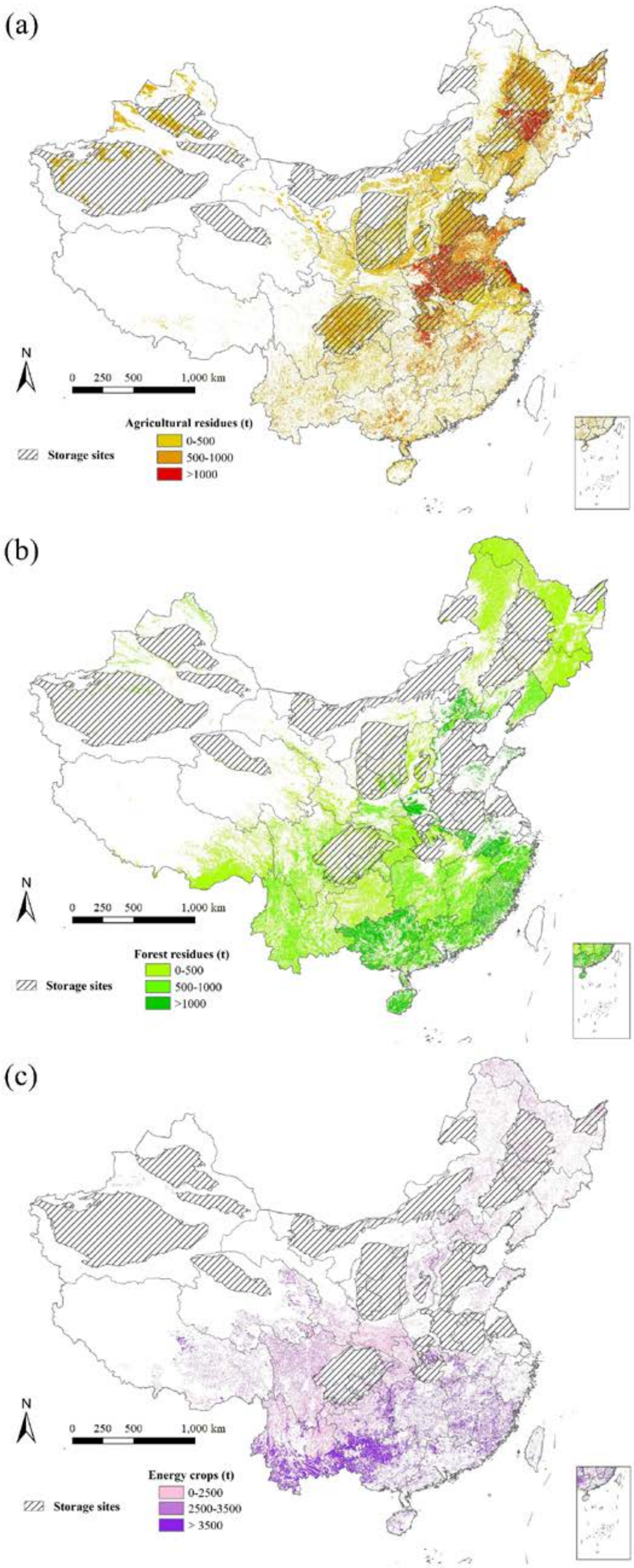

Figure 2. Spatial distribution of the yield of biomass resources in China in 2025 (**a,** agricultural residues; **b,** forest residues; **c,** energy crops. Data Credits: All the provincial administrative boundaries are from Ministry of Civil Affairs of the People's Republic of China (http://xzqh.mca.gov.cn/map, Map Content Approval Number: GS(2022)1873))

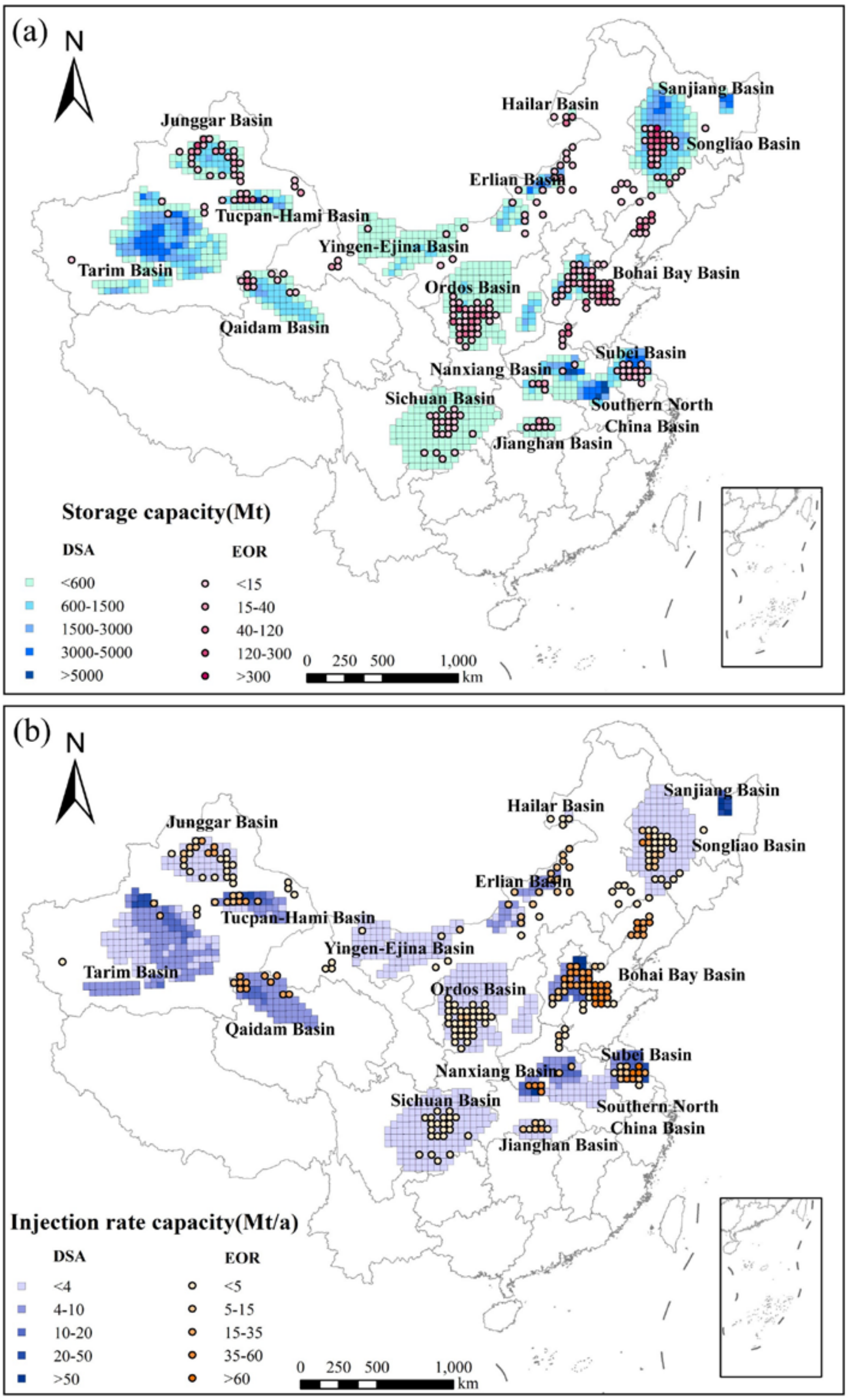

Figure 3. Spatial distribution of geological storage capacity and injection rate capacity in China (**a,** storage capacity; **b,** injection rate capacity. Data Credits: All the provincial administrative boundaries are from Ministry of Civil Affairs of the People's Republic of China (http://xzqh.mca.gov.cn/map, Map Content Approval Number: GS(2022)1873))

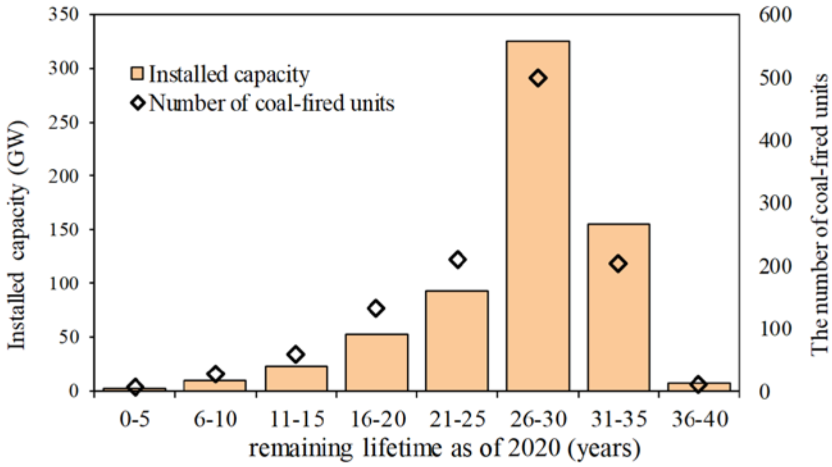

Figure 4. Remaining lifetime of the existing coal-fired units in China

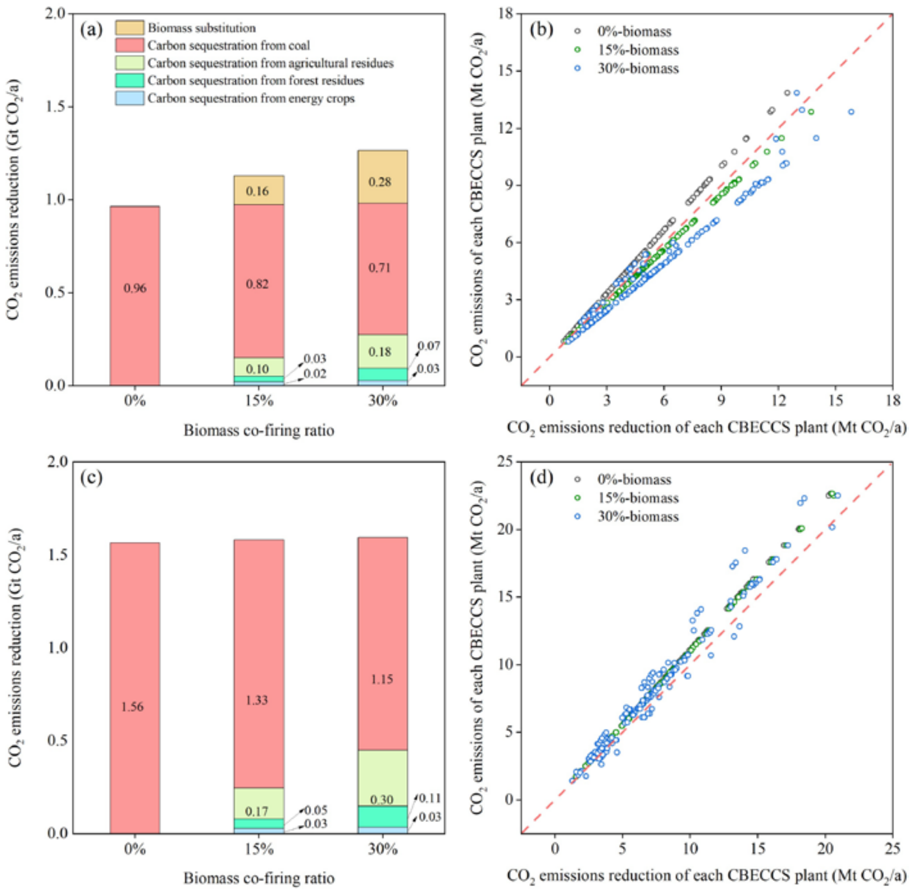

Figure 5. CO_2 emissions reduction of CBECCS plants under different co-firing ratios (**a.** supply potential in deployment year 2025; **b.** plant-level supply potential in deployment year 2025; **c.** mitigation contribution in planning year 2040; **d.** plant-level mitigation contribution in planning year 2040). Notes: 0%-biomass means that all CCS-qualified power plants can be retrofitted only with CCS technology; 15%-biomass shows the baseline scenario; and 30%-biomass shows a higher upper limit of the co-firing ratio of 30% with other assumptions unchanged. Additionally, note that the mitigation contribution is higher than the supply potential as the utilization hours of power generation are longer than the current status.

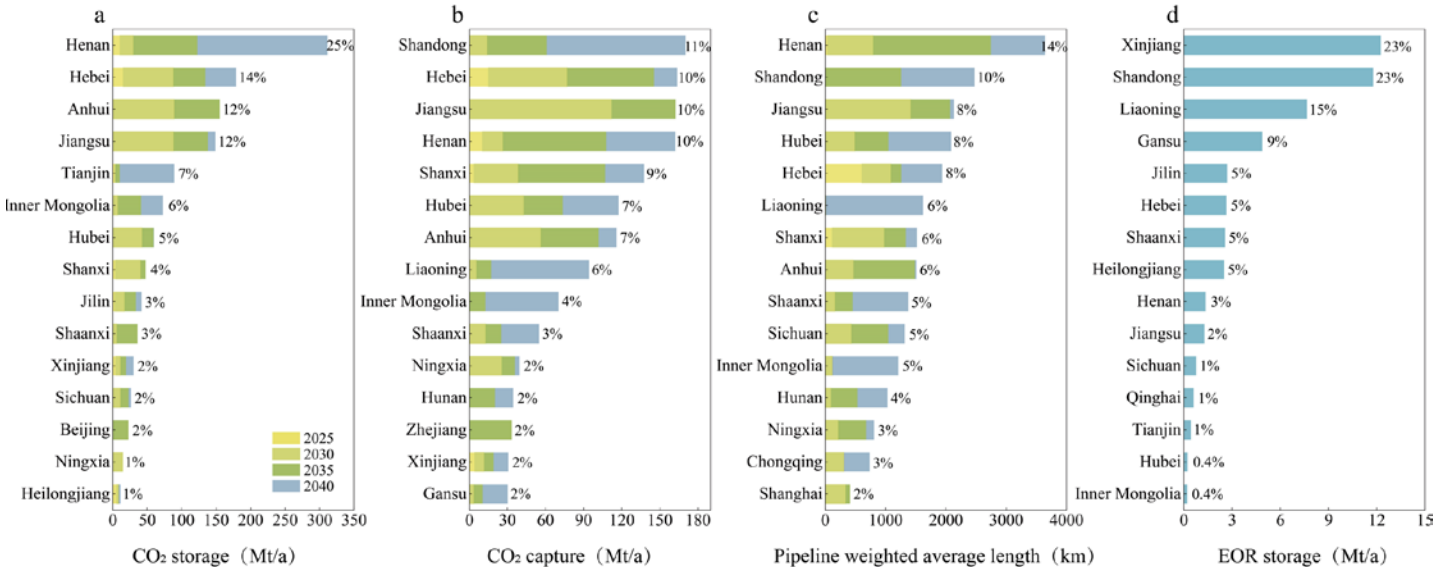

Figure 6. Optimal source-sink matching results of CBECCS by province. (**a, b** and **c** represent provincial CO_2 storage, CO_2 capture and CO_2 transport pipeline length in the carbon neutrality scenario, respectively; **d** represents provincial EOR storage in 2025 under the static scenario.)

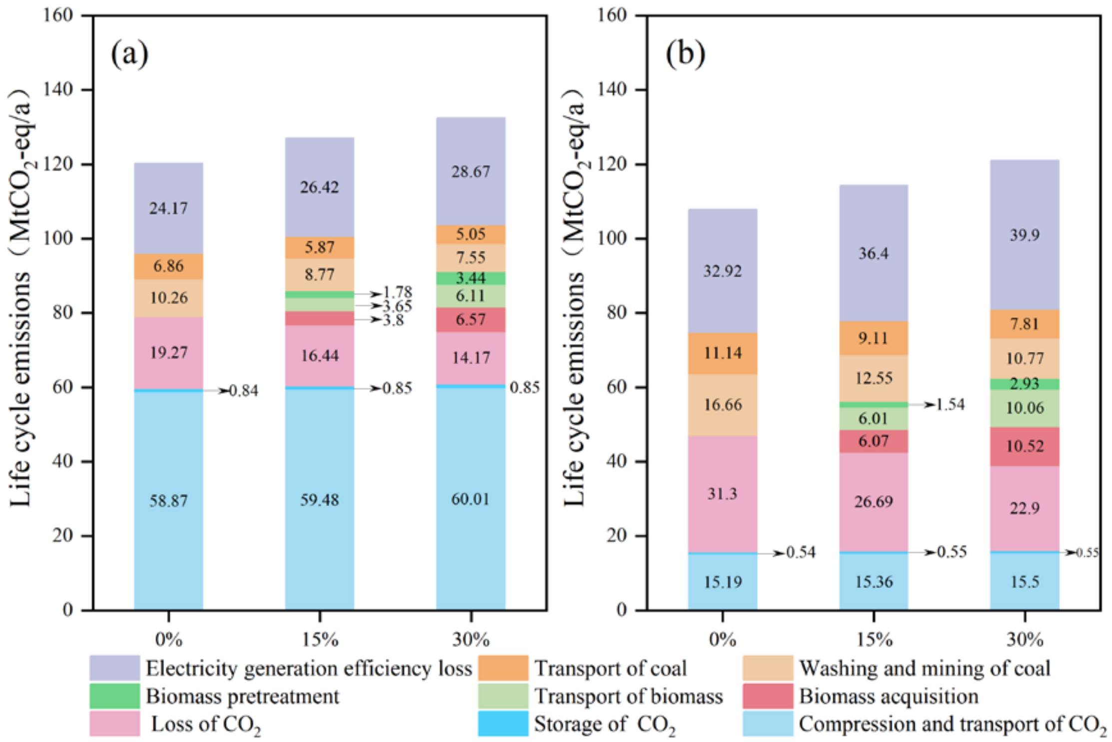

Figure 7. The life-cycle emission composition of CBECCS plants under different co-firing ratios. (**a.** total supply potential in deployment year 2025; **b.** total mitigation contribution in planning year 2040)

Supplementary Methods:

Soft linking mechanism of the CBECCS mitigation contribution assessment model

A combination model was developed for the assessment of the CBECCS technology mitigation contribution to carbon neutrality by 2060 in China, which softly links the dynamic recursive computable general equilibrium (CGE) model, the power system optimization model (PSOM) and the CBECCS source-sink matching model via various linking variables. The specific linking mechanism is that the CGE model is first softly linked to the PSOM model through the national dynamic electricity demand and CO_2 emissions trajectory of the power sector. Second, to make the simulation results of the PSOM model more reflective of reality and scientific validity, the maximum CBECCS retrofittable installed capacity in the PSOM model is feedback from the source-sink matching model. Finally, the PSOM model is softly linked to the CBECCS dynamic source-sink matching model through the retrofit installed capacity, electricity generation and mitigation contribution of CBECCS technology at each stage (every five years from 2020 to 2060). The technical parameters of CBECCS in the PSOM model and the source-sink matching model are set consistently and include the capital cost, the learning rate of the learning curve for dynamics capital cost and the CO_2 emission factor of the biomass resources. In addition, the three models are solved independently in GAMS by different solvers.

Calculation of biomass resource feedstocks

Agricultural residues. Agricultural residues are represented by the straw-based byproducts (e.g., stems, leaves, and branches) of harvested crops, including 16 types of crops, namely, rice, wheat, maize, other food crops, beans, tubers, cotton, peanuts, rapeseed, sesame, other oil crops, kenaf, flax, sugar cane, sugar beet and tobacco leaf. We estimated the biomass feedstock of agricultural residues by using the residue-to-product ratio (RPR, i.e., the conversion coefficient from crops to agricultural residues) and yields of the corresponding crops, as expressed in equation (S1).

$$M_p = \sum_b P_{b,p} \cdot \alpha_b \cdot \lambda_b \tag{S1}$$

where M_p is the biomass feedstock of the agricultural residues in province *p*; *b* denotes the 16 types of harvested crops; $P_{b,p}$ is the yield of crop *b* in province *p*; α_b is the RPR of crop *b* (Supplementary Table 4); and λ_b is the straw availability coefficient of crop *b*, which is set to 100% by assuming that agricultural residues can be fully collected for bioenergy utilization with technological progress and social awareness improvement [1]. The calculated agricultural residues in the various provinces were further spatialized into a 1×1 km^2 grid distribution across China based on high-resolution land-use information. Given the real cultivation environment, rice was assumed planted in paddy fields, while the other crops were planted in dry land.

Forest residues. In this study, we considered three types of forest residues sourced from forest harvesting and timber processing, tending and thinning, and wood recycling, whose current total quantity was derived from the actual national forest residue yield in China (924 million tons) [2], and future yields were estimated by using the predicted wood products in typical years (2025, 2030 and 2060) combined with their possible shares in forest residues [3, 4]. After combining the provincial proportion [2] and land-use change, 1×1 km^2 forest residues in 2025, 2030, and 2060 could be obtained, while grid-based values in the other years from 2025-2060 were estimated by using the linear interpolation method.

Energy crops. Miscanthus and switchgrass were chosen as representative energy crops due to their high productivity and notable growth adaptability [5]. Based on the land-use regulations in China [6], we first extracted marginal lands suitable for miscanthus and switchgrass planting and then calculated their corresponding yields per unit area to obtain their biomass feedstocks. Here, we introduced multifactor comprehensive evaluation indicators to screen suitable marginal lands based on literature investigations [7] and expert predictions. In the evaluation systems, a series of screening criteria were designated for miscanthus and switchgrass, including land use, terrain slope, meteorological characteristics (e.g., precipitation, temperature, and frost-free period), and soil content (Supplementary Tables 5-6). In regard to marginal lands suitable for the cultivation of both miscanthus and switchgrass, we adopted the principle of planting miscanthus as a priority due to its generally higher unit yield.

Calculation of the initial CO_2 emissions

Emissions originating from original coal-fired power plants. The initial CO_2 emissions of original coal-fired power plants at the unit level were calculated by using the Intergovernmental Panel on Climate Change (IPCC) accounting method [8], as expressed in equations (S2)-(S4):

$$CE_{i,u,t} = CO_{i,u,t} \cdot NCV^c \cdot C^c \cdot O^c \cdot (44/12) \tag{S2}$$

$$CO_{i,u,t} = U_u^{screen} IC_{i,u} \cdot RT_{i,t} \cdot PGCC_i / T^c \tag{S3}$$

$$TCE_{i,t} = \sum_u CE_{i,u,t} \tag{S4}$$

where $CE_{i,u,t}$ denotes the initial annual CO_2 emissions of unit *u* of power plant *i* in year *t*; $CO_{i,u,t}$ is the initial raw coal consumption of unit *u* of power plant *i* in year *t*; NCV^c is the lower heating value (LHV) of raw coal, at 20.91 MJ/kg; C^c is the carbon content in raw coal, at 26.59 kg/GJ; O^c is the oxidation rate of raw coal, at 0.92; 44/12 is the mass fraction ratio of CO_2 to carbon; U_u^{screen} is a binary variable that indicates whether unit *u* can meet the size requirements (>300 MW) and remaining life (>15 years) needed for CCS retrofitting (i.e., CCS-qualified coal-fired power unit) ($U_u^{screen} = 1$, if the size and lifetime requirements are met; otherwise, $U_u^{screen} = 0$); $IC_{i,u}$ is the installed capacity of unit *u* of power plant *i*; $RT_{i,t}$ denotes the annual operating hours of power plant i, which varies by province in supply potential assessment and are endogenously determined by the PSOM (within 6000 hours) in mitigation contribution assessment; $PGCC_i$ is the standard coal consumption per kWh of electricity generation in the various provinces; T^c is the conversion coefficient from raw coal to standard coal, at 0.714 tons of coal equivalent (tce)/t; and $TCE_{i,t}$ denotes the annual CO_2 emissions originating from CCS-qualified coal-fired power plant *i* in year *t*.

Matching model between biomass feedstocks and CCS-qualified coal-fired power plants

In the biomass and CCS-qualified coal-fired power plants matching model, the CCS-qualified coal-fired power units participating are identified by their size requirement (>300 MW) and remaining life (>15 years) based on the suitability standard for CCS retrofitting proposed by the IEA[9, 10]. Agbor, Zhang [11] noted that only a minimal modification is needed for coal-fired power plants when the co-firing ratio reaches 10-15% by heat. Therefore, we assume that the main equipment of the biomass and coal co-firing process, such as coal-fired boilers, would have little or no modifications and assume that the maximum co-firing ratio is 15% by heat, i.e., the biomass feedstock collected by a power plant cannot exceed this upper limit relating to the actual bio-fuel demand. We further set the biomass collection radius as 50 km, considering the economic feasibility of the biomass collection process. This model was solved in Python software with ArcGIS. The objective functions are expressed as equations (S5)-(S6), and the related constraints are defined in equations (S7)-(S8):

$$\min F_t^{trans} = \sum_i \sum_s \sum_k m_{i,s,t} \cdot BQ_{i,s,k,t} \cdot DB_{i,s} \tag{S5}$$

$$\max F_t^{bio} = \sum_i \sum_s \sum_k BQ_{i,s,k,t} \cdot T_k \tag{S6}$$

$$\sum_s \sum_k BQ_{i,s,k,t} \cdot T_k \leq \sum_u U_u^{screen} \cdot IC_{i,u} \cdot RT_{i,t} \cdot PGCC_i \cdot \theta \tag{S7}$$

$$DB_{i,s} \leq R_{\max} \tag{S8}$$

where F_t^{trans} is the total biomass transport equivalent, and F_t^{bio} denotes the total biomass feedstocks, both calculated from all potential biomass sourcing sites to the CCS-qualified coal-fired power plants in year *t*. Moreover, $m_{i,s,t}$ is a binary variable that indicates whether sourcing site *s* can be optimally linked to power plant *i*, with $m_{i,s,t} = 1$, if the aforementioned is satisfied. Otherwise, $m_{i,s,t} = 0$. $BQ_{i,s,k,t}$ is the feedstock of biomass *k* at sourcing site *s* linked to power plant *i* in year *t*; *k*=1, 2, and 3 denotes agricultural residues, forest residues, and energy crops (including miscanthus and switchgrass), respectively; $DB_{i,s}$ is the straight-line distance between sourcing site *s* and power plant *i*; T_k is a conversion coefficient from biomass *k* to standard coal, with values of 0.51, 0.57, 0.52 (miscanthus), and 0.66 (switchgrass) tce/t, respectively; θ is the maximum co-firing ratio by heat, at 15% or 30%; and $R_{\max}$ is the maximum biomass collection radius of 50 km.

Thus, the total biomass feedstock linked to a specific power plant can be calculated by summing those obtained from all possible biomass sourcing sites, as expressed in equation (S9):

$$BQ_{i,k,t}^s = \sum_s m_{i,s,t} \cdot BQ_{i,s,k,t} \tag{S9}$$

where $BQ_{i,k,t}^s$ is the total feedstock of biomass *k* linked to power plant *i* in year *t*.

Calculation of the CO_2 emissions before CCS deployment

Emission reduction resulting from biomass substitution for coal. Biomass feedstocks can provide additional emission reduction benefits by replacing coal, as expressed in equations (S10) -(S11):

$$SCE_{i,t}^r = SCO_{i,t}^r \cdot NCV^c \cdot C^c \cdot O^c \cdot (44/12) \tag{S10}$$

$$SCO_{i,t}^r = \sum_k BQ_{i,k,t}^s \cdot T_k / T^c \tag{S11}$$

where $SCE_{i,t}^r$ is the emission reduction resulting from biomass substitution for coal at CBECCS plant *i* in year *t*; $SCO_{i,t}^r$ is the raw coal consumption replaced by biomass feedstock at CBECCS plant *i* in year *t*; and $BQ_{i,k,t}^s$ can be calculated with equation (S9).

Emissions originating from CBECCS plants due to coal combustion. Coal combustion-related CO_2 emissions can be calculated based on the actual coal consumption of CBECCS plants, as expressed in equation (S12):

$$RCE_{i,t} = (\sum_{u} CO_{i,u,t} - SCO^{r}_{i,t}) \cdot NCV^{c} \cdot C^{c} \cdot O^{c} \cdot (44/12) \tag{S12}$$

where $RCE_{i,t}$ denotes the emissions resulting from the actual coal combustion after biomass substitution at CBECCS plant *i* in year *t*; $CO_{i,u,t}$ can be determined with equation (S3); and $SCO^{r}_{i,t}$ can be obtained with equation (S11).

Flue gas emissions originating from CBECCS plants before CO_2 capture. The direct CO_2 emissions in flue gas originating from CBECCS plants can be subsequently captured, including those due to the actual coal combustion and biomass combustion, as calculated with equations (S13) and (S14), respectively.

$$DCE_{i,t} = RCE_{i,t} + \sum_{k} CE^{b}_{i,k,t} \tag{S13}$$

$$CE^{b}_{i,k,t} = BQ^{s}_{i,k,t} \cdot NCV^{b}_{k} \cdot C^{b}_{k} \cdot O^{b} \cdot (44/12) \tag{S14}$$

where $DCE_{i,t}$ denotes the direct emissions in flue gas originating from CBECCS plant *i* in year *t*; $RCE_{i,t}$ can be obtained with equation (S12); $CE^{b}_{i,k,t}$ denotes the annual CO_2 emissions resulting from direct combustion of biomass *k* at CBECCS plant *i* in year *t*; $BQ^{s}_{i,k,t}$ can be calculated with equation (S9); NCV^{b}_{k} is the LHV of biomass *k*, with values of 14.89, 16.73, 15.24 (miscanthus), and 16.19 (switchgrass) MJ/kg; C^{b}_{k} is the carbon content in biomass *k*, with values of 27.3, 30.5, 30.8 (miscanthus), and 29.6 (switchgrass) kg/GJ; and O^{b} is the oxidation rate of biomass, at 0.9. The cumulative flue gas emissions of CBECCS plants from the various deployment years to 2060 can be calculated with equation (S15):

$$DCE^{Total}_{i} = \sum_{t=t_0}^{2060} DCE_{i,t} \tag{S15}$$

where DCE^{Total}_{i} denotes the cumulative flue gas emissions originating from CBECCS plant *i* over the t_0~2060 period, and t_0 denotes the various CBECCS deployment years for both the static and dynamic assessments.

Calculation of the CO_2 storage potential and injection rate capacity

We consider 17 saline aquifer basins (53 reservoirs) and existing oil fields in China as available CO_2 storage sites and calculate the CO_2 storage potential and injection capacity of all reservoirs under each basin with the US Department of Energy's storage potential calculation method and Darcy's law, respectively. To improve the accuracy of the results, these reservoirs are first divided into 5×5 km^2 high-resolution grids, and the storage potential and injection rate capacity of these grids are obtained by spatial superposition and weighted average for different reservoirs in the same basin at the same spatial location. Finally, they are aggregated into 40×40 km^2 grids for CO_2 storage in the source-sink matching model, where each grid is considered a storage site.

CO_2 storage potential calculation. Referring to previous studies [12-14], the CO_2 storage potential of a given saline aquifer reservoir is calculated by equation (S16).

$$SP_{BA,R} = A_{BA,R} \cdot h_{BA,R} \cdot \phi_{BA,R} \cdot E^{saline} \cdot \rho_{BA,R}^{CO_2} \quad \text{(S16)}$$

where $SP_{BA,R}$ is the CO_2 storage potential of reservoir R in basin BA (kg); $A_{BA,R}$ is the area of reservoir R in basin BA (m^2); $h_{BA,R}$ is the gross thickness of reservoir R in basin BA (m); $\phi_{BA,R}$ is the porosity of reservoir R in basin BA; E^{saline} is the CO_2 storage efficiency factor of saline aquifers, taken as 2.4% [15]; and $\rho_{BA,R}^{CO_2}$ is the CO_2 density determined by the pressure and temperature of reservoir R in basin BA (kg/m^3), as shown in equation (S17):

$$\rho_{BA,R}^{CO_2} = 0.4649 \cdot \ln(P_{BA,R}^{pre} / T_{BA,R}^{tem}) + 1.2417 \quad \text{(S17)}$$

where $P_{BA,R}^{pre}$ is the pressure of the given reservoir (Pa) and $T_{BA,R}^{tem}$ is the temperature of the given reservoir (°C).

The CO_2 storage potential of EOR at the oil field level is calculated by equation (S18) [13, 16]:

$$SP_j^{EOR} = \sum_{\zeta} OOIP_{\zeta} / \rho^{oil} \cdot V^{oil} \cdot E^{oil} \cdot ER \cdot (P_{\zeta}^{LCO_2} \cdot R^{LCO_2} + P_{\zeta}^{HCO_2} \cdot R^{HCO_2}) \quad \text{(S18)}$$

$$ER = \begin{cases} 5.3\% & (API \le 31) \\ (1.3 \cdot API - 35)\% & (31 < API < 41) \\ 18.3\% & (API \ge 41) \end{cases} \quad \text{(S19)}$$

$$API = (141.5 / \rho^{oil}) - 131.5 \quad \text{(S20)}$$

where SP_j^{EOR} is the total CO_2 storage potential via EOR (t); $OOIP_{\zeta}$ is the recoverable reserve in oil field ζ (m^3); ρ^{oil} is the density of crude oil, taken as 0.81 t/m^3; V^{oil} is the formation volume factor that brings the oil volume from standard conditions to in situ conditions, taken as 1.18 [17]; E^{oil} is the factor of storage efficiency, taken as 75% [18]; ER is the efficiency of EOR, calculated by equation (S19); P^{LCO_2} and P^{HCO_2} are the lowest and the highest probabilities of API [18] (Supplementary Table 1); R^{LCO_2} and R^{HCO_2} are the fixed values of 2.113 and 3.522 (t/m^3) [18]; and API is the American Petroleum Institute gravity.

Table 1 Four EOR cases with different depths and API gravity conditions [18]

Depth (m)	API	P^{LCO_2}	P^{HCO_2}
<2000	>35	100%	0%
	⩽35	66%	33%
>2000	>35	33%	66%
	≤35	0%	100%

CO_2 injection rate capacity calculation. The allowable injection capacity per well is calculated based on Darcy's law for single-phase flow, as shown in equation (S21) [12, 19]:

$$Q_{BA,R} = \frac{2\pi \cdot \gamma_{BA,R} \cdot h_{BA,R} \cdot \Delta P_{BA,R}}{\mu^{CO_2} \cdot \ln(r^e_{BA,R} / r^w)} \tag{S21}$$

where $Q_{BA,R}$ is the volumetric flow rate at the injection point of reservoir R in basin BA, m^3/s; $\gamma_{BA,R}$ is the reservoir permeability of reservoir R in basin BA, μm^2; $\Delta P_{BA,R}$ is the pressure differential at the injection well of reservoir R in basin BA, defined in equation (S22), Pa; μ^{CO_2} is the dynamic viscosity of CO_2, taken as 6.8×10^{-5} Pa·s; $r^e_{BA,R}$ is the radius of the pressure influence of reservoir R in basin BA, defined in equation (S23), m; and r^w is the radius of the wellbore, taken as 0.1 m.

The pressure differential in equation (S22) is determined using the hydrostatic pressure and a maximum allowable pressure difference of 50% for the hydrostatic pressure.

$$\Delta P_{BA,R} = \rho^{water} \cdot g \cdot d_{BA,R} \cdot 50\% \tag{S22}$$

where ρ^{water} is the density of water, taken as 1000 kg/m^3; g is the gravitational acceleration, taken as 9.81 m/s^2; and $d_{BA,R}$ is the depth from the surface to the center of reservoir R in basin BA, m.

$$r^e_{BA,R} = \left(\frac{2 \cdot \gamma_{BA,R} \cdot TS}{\phi_{BA,R} \cdot \mu \cdot c^r}\right)^{1/2} \tag{S23}$$

where TS is the total number of the injection timeframe, taken as 9.5×10^8 s (30 years) and c^r is the compressibility of the rocks, taken as 1×10^{-9} Pa^{-1} [19].

Then, we introduce the weighted-average injection rate capacity (an extension of ref. [19]) of different formations as a constraint on each CO_2 storage site in China. The injection capacity of the reservoir ($IJC^r_{BA,R}$) and each storage site in the basin (IJC^b_{BA}) is calculated by equations (S24) and (S25):

$$IJC^r_{BA,R} = Q_{BA,R} \cdot TS / 30 \cdot \rho^{CO_2} \tag{S24}$$

$$IJC^b_{BA} = \frac{\sum_{R\in BA} IJC^r_{BA,R} \cdot SP_{BA,R}}{\sum_{R\in BA} SP_{BA,R}} \tag{S25}$$

Based on the above calculation, the geological storage capacity of saline aquifers ranges from 0.2~10,726.7 Mt per site, while that of oil fields ranges from 0.01~706.7 Mt per site (Supplementary Fig. 3a). In addition, saline aquifers show injection rate capacities ranging from 0.003~122.8 Mt/a per site, and oil fields show a rate capacity ranging from 0.006~134.8 Mt/a per site (Supplementary Fig. 3b).

Calculation of the CO_2 transportation cost

The CO_2 transportation cost consists of the capital cost and O&M cost for the proposed pipelines. The capital (i.e., pipeline construction) cost per unit length of pipeline is calculated by equation (S26):

$$Peq_d = MC^{pip}_d + VSC^{pip}_d + ISC^{pip}_d + OCC^{pip}_d \tag{S26}$$

where Peq_d is the capital cost per unit length of pipeline with diameter *d*, as shown in equation (1) in Methods, including primary raw material cost MC_d^{pip}, valve station cost VSC_d^{pip}, installation cost ISC_d^{pip}, and other construction costs OCC_d^{pip}, respectively. Specifically, VSC_d^{pip} equals MC_d^{pip} multiplied by 30% [20]; ISC_d^{pip} equals MC_d^{pip} multiplied by 50% [20]; and OCC_d^{pip} equals the sum of MC_d^{pip}, VSC_d^{pip}, and ISC_d^{pip} multiplied by 10% [21].

Material cost. The cost of primary raw material includes steel and insulation. Due to relatively long transport distances, the insulation material is selected as cheaper mineral wool with a price of 43.5 USD/m^3 [22]. The material cost is calculated by equation (S27).

$$MC_d^{pip} = C^{steel}\rho^{steel}\pi((r_d^{pip1})^2 - d^2) + C^{insulation}((r_d^{pip2})^2 - (r_d^{pip1})^2) \tag{S27}$$

where, C^{steel} is the steel cost, taken as 745.5 USD/t by referring to the average price of steel in China in 2021 [23]; ρ^{steel} is the density of steel, taken as 7.85 t/m^3; r_d^{pip1} is the outer diameter of the pipe determined by referring to the related thickness from Lu, Ma [24,] Lu, Ma [25]; *d* is the inner diameter of the pipe, as shown in equation (1) in Methods; $C^{insulation}$ is the price of the pipe insulation layer; r_d^{pip2} is the outer diameter of the pipe insulation layer determined by referring to the related thickness from the Ministry of Petroleum Industry SYJ1021-82 and the national standard GB4272-84 [26].

Specifically, the pipe size determines its upper CO_2 flow limit, as shown in equation (S28) [20]:

$$d = 0.363\left(\frac{Prate_d}{\rho^{CO_2\text{-}super}}\right)^{0.45}(\rho^{CO_2\text{-}super})^{0.13}(\mu^{CO_2})^{0.025} \tag{S28}$$

where $Prate_d$ is the upper CO_2 flow rate of the pipe; $\rho^{CO_2\text{-}super}$ is the CO_2 density of 0.448 t/m^3 in the supercritical state; and μ^{CO_2} is the dynamic viscosity of CO_2, taken as 6.8×10^{-5} Pa·s, as shown in equation (S21) [19].

Equation (S28) can be deformed by equation (S29):

$$Prate_d = \sqrt[0.45]{\frac{d}{0.363(\rho^{CO_2\text{-}super})^{0.13}(\mu^{CO_2})^{0.025}}} \cdot \rho^{CO_2\text{-}super} \tag{S29}$$

The O&M cost per unit length of pipeline with diameter *d*, i.e., Pom_d, is calculated by equation (S26) multiplied by 4% [18].

Calculation of the EOR revenue

When the captured CO_2 is used for EOR, it will generate additional crude oil revenue that benefits CBECCS plants, as shown in equation (S30):

$$EOR_t^{annual} = p_t^{oil} \cdot R^{oil} \cdot (1/4) \tag{S30}$$

where EOR_t^{annual} is the annual EOR revenue per unit of CO_2 for oil fields in year *t*; p_t^{oil} is the predicted crude oil price in year *t*, ranging from 45 \$/bbl to 25 \$/bbl over the period 2025-2060 [21]; R^{oil} is the replacement ratio of barrels and tons, taken as 7.3 bbl/t; and the replacement ratio of CO_2 to oil is 4:1 [27].

Calculation of the CBECCS extra life-cycle greenhouse gas (GHG) emissions

GHG emissions components resulting from biomass acquisition. The GHG emissions resulting from biomass acquisition were obtained by summing those resulting from the acquisition of the three biomass types. In detail, we considered the direct and indirect CO_2-equivalent emissions originating from the product supply chain of the input for the cultivation of agricultural residues and energy crops, the CO_2-equivalent emissions of the diesel used during collection, the N_2O emissions resulting from the application of nitrogen fertilizer (converted into equivalent amounts of CO_2), and the CO_2-equivalent emissions due to land-use and land cover change (for the cultivation of energy crops in marginal lands). The input products of the agricultural residues include phosphorus, potash, and nitrogen fertilizers to compensate for the lost nutrients in soils when agricultural residues are removed from the land, while those of the energy crops include seeds, herbicides, and phosphorus, potash, and nitrogen fertilizers for the cultivation of energy crops in marginal lands. The GHG emissions in the biomass acquisition phase are calculated by equation (S31):

$$CE_{i,t}^{b\_acq} = CE_{i,t}^{acq\_a} + CE_{i,t}^{acq\_f} + CE_{i,t}^{acq\_e} \tag{S31}$$

where $CE_{i,t}^{b\_acq}$ is the GHG emissions in the biomass acquisition phase; $CE_{i,t}^{acq\_a}$ is the GHG emissions from agricultural residue acquisition; $CE_{i,t}^{acq\_f}$ is the GHG emissions from forestry residue acquisition; and $CE_{i,t}^{acq\_e}$ is GHG emissions from energy crop acquisition.

GHG emissions from agricultural residue acquisition. Agricultural residues are assumed to be the byproducts of agricultural products, and their life-cycle emissions start at their collection from the field and end at the CBECCS power plant boiler. The GHG emissions from agricultural residue acquisition are calculated by equation (S32):

$$\begin{aligned} CE_{i,t}^{acq\_a} = BQ_{i,t}^{a}(&CF^{P}\cdot R^{acq\_agrp} + CF^{K}\cdot R^{acq\_agrk} + CF^{N}\cdot R^{acq\_agrn} \\ &+\partial^{n}\cdot NF\cdot GWP_{n}\cdot R^{acq\_agrn} + EF^{diesel}\cdot R^{diesel\_acqa}) \end{aligned} \tag{S32}$$

where $BQ_{i,t}^{a}$ is the total amount of agricultural residues matched with CBECCS plant *i* in year *t*, from the case of k = 1 of $BQ_{i,k,t}^{s}$; CF^{P}, CF^{K} and CF^{N} are the carbon footprints of input products, i.e., direct and indirect the CO_2-equivalent emissions from the product supply chain of the phosphorus, potash, and nitrogen fertilizers, with the values of 1.1, 0.64, and 3.6 kgCO_2-eq/kg [28], respectively; R^{acq_agrp}, R^{acq_agrk} and R^{acq_agrn} are the consumption of phosphorus, potash, and nitrogen fertilizers needed to compensate for the lost nutrients in soils when agricultural residues are taken away from the land, with the values of 2.1, 18.1, and 1.8 kg/t biomass [29], respectively; ∂^{n} is the amount of N_2O emitted from N applications to soils, with a value of 0.01 kg N_2O/kg N [30]; NF is the nitrogen content of nitrogen fertilizer, with a value of 0.03 kg N /kg [30]; GWP_n is the global warming potential (100 year-basis) index of the N_2O compared CO_2, with a value of 264 [31]; EF^{diesel} is the emission factor of diesel, with a value of 3.4 kgCO_2-eq/L [28]; and R^{diesel_acqa} is the amount of diesel consumed in the agricultural residue collection phase, with a value of 1 L/t agricultural residues [28].

GHG emissions from forestry residue acquisition. The GHG emissions from forestry residue acquisition come from the diesel consumption required to collect forestry residues, which can be calculated by equation (S33):

$$CE_{i,t}^{acq-f} = BQ_{i,t}^{f} \cdot EF^{diesel} \cdot R^{diesel\_acqf} \quad \text{(S33)}$$

where $BQ_{i,t}^{f}$ is the total amount of forestry residues matched with CBECCS plant *i* in year *t*, from the case of *k* = 2 of $BQ_{i,k,t}^{s}$; EF^{diesel} is the emission factor of diesel; R^{diesel_acqf} is the amount of diesel consumed in the forestry residues acquisition collection phase, with the values of 5.2 L/t forestry residues [32].

GHG emissions from energy crop acquisition. The GHG emissions from energy crop acquisition are calculated by equation (S34):

$$\begin{aligned} CE_{i,t}^{acq-e} = BQ_{i,t}^{e}(&CF^{S} \cdot R^{acq-enrs} + CF^{H} \cdot R^{acq-enrh} + CF^{P} \cdot R^{acq-enrp} + CF^{K} \cdot R^{acq-enrk} + CF^{N} \cdot R^{acq-enrn} \\ &+ \partial^{n} \cdot NF \cdot GWP_{n} \cdot R^{acq-enrn} + EF^{diesel} \cdot R^{diesel\_acqe} + LUC^{acqe}) \end{aligned} \quad \text{(S34)}$$

where $BQ_{i,t}^{e}$ is the total amount of the energy crop matched with CBECCS plant *i* in year *t*, from the case of *k* = 3 of $BQ_{i,k,t}^{s}$; CF^{S} and CF^{H} are the carbon footprints of the seed and herbicides, with values of 0.06 and 20.3 $kgCO_2$-eq/kg[28], respectively; CF^{P}, CF^{K} and CF^{N} are the carbon footprints of the phosphorus, potash, and nitrogen fertilizers, respectively; and $R^{acq-enrs}$, $R^{acq-enrh}$, $R^{acq-enrp}$, $R^{acq-enrk}$ and $R^{acq-enrn}$ are the consumption of seed, herbicides, and phosphorus, potash, and nitrogen fertilizers for growing energy crops on marginal lands, with values of 0.06, 0.04, 10.2, 8.1, and 9.3 kg/t energy crop [28], respectively. The average values of the inputs required for miscanthus and switchgrass were taken as the amount of inputs required for energy crops; ∂^{n}, NF, and GWP_{n} are the amount of N_2O emitted from N applications to soils, the nitrogen content of nitrogen fertilizer and the global warming potential (100 year-basis) index of the N_2O compared CO_2, respectively; EF^{diesel} is the emission factor of diesel; R^{diesel_acqe} is the amount of diesel consumed in the energy crop acquisition phase, with a value of 4.6 L/t energy crop [32]; and LUC^{acqe} is the CO_2-equivalent emissions due to the land use and land cover change associated with growing one ton of an energy crop, with a value of 1.34 $kgCO_2$-eq/t energy crop [28].

GHG emissions resulting from biomass transportation. The GHG emissions resulting from biomass transportation are caused by biomass transportation from fields or forests to CBECCS plants using trucks fueled by diesel. The transportation distance for each CBECCS plant is the actual average distance derived from the biomass-plant matching model. The GHG emissions from biomass transportation are calculated by equation (S35):

$$CE_{i,t}^{b-tra} = \sum_{k} BQ_{i,k,t}^{s} \cdot DB_{i,k.t} \cdot EF^{diesel} \cdot R^{diesel\_b\_tra} \quad \text{(S35)}$$

where $CE_{i,t}^{b-tra}$ is the GHG emissions from biomass transportation, shown in equation (8) in the Methods section; $BQ_{i,k,t}^{s}$ is the total amount of biomass *k* matched with CBECCS plant *i* in year *t*, shown in equation (S9); $DB_{i,k.t}$ is the average distance for biomass *k* between various sourcing sites *s* and corresponding power plant *i* in year *t*, derived from the biomass and coal-fired power plant matching model; EF^{diesel} is the emission factor of diesel; and $R^{diesel\_b\_tra}$ is the amount of diesel required to transport one ton of biomass over one km by vehicles (using diesel), with a value of 0.0125 L/(t· km) [30].

GHG emissions resulting from biomass pretreatment. The GHG emissions resulting from biomass pretreatment are due to diesel and electricity consumption, and the annual electricity emission factors were calculated based on the future projected Chinese power generation mix. Referring to Fajardy and Mac Dowell [33], it was assumed that the moisture content in agricultural residues and energy crops available to the CBECCS plants could reach the fuel combustion requirements, while forest residues must be dried to 15%. In addition, we assumed a mass loss rate of 4% on average for biomass before consumption [34]. The GHG emissions from biomass pretreatment are caused by diesel and electricity consumption. The loss rate of biomass feedstock was set as 4% by referring to the situation in China described in Qin, Mohan [34] and Lu, Cao [30]. The calculation is presented in equation (S36):

$$CE_{i,t}^{b-pre} = 0.96 \cdot \sum_{k} BQ_{i,k,t}^{s} (EF^{diesel} \cdot R_{k}^{diesel\_bpre} + EF_{t}^{ele} \cdot R_{k}^{ele\_bpre}) \tag{S36}$$

where $CE_{i,t}^{b-pre}$ is the GHG emissions from pretreatment, shown in equation (8) in Methods; 0.96 is the proportion of biomass that is pretreated after deducting the loss during transportation and storage; $BQ_{i,k,t}^{s}$ is the total amount of biomass *k* matched with CBECCS plant *i* in year *t*, as shown in equation (S9); EF^{diesel} is the emission factor of diesel; $R_{k}^{diesel\_bpre}$ is the diesel consumption of the pretreatment process for biomass *k*, with values of 3.89 [32] and 3.36 [28] L/t biomass for chopping forestry residues and energy crops, respectively; EF_{t}^{ele} is the electricity emission factor in year *t* and is estimated through the carbon neutrality scenario of the power system optimization model; $R_{k}^{ele\_bpre}$ is the electricity consumption of the pretreatment process for biomass *k*, with values of 75 [35], 257.4 [28], and 34.4 [28] kWh/t biomass for finely grinding agricultural residues, grinding and drying forestry residues and grinding energy crop, respectively.

CO_2 emissions resulting from coal mining and washing. The CO_2 emissions resulting from coal mining and washing are mainly due to the corresponding fuel used, as expressed in equation (S37):

$$\begin{aligned} CE_{i,t}^{c-mw} = & (\sum_{u} CO_{i,u,t} - SCO_{i,t}^{r})(\sum_{g} EC_{g} \cdot NCV_{g}^{e} \cdot C_{g}^{e} \cdot O_{g}^{e} \cdot (44/12) + EF_{t}^{ele} \cdot R^{ele\_C_{mw}} \\ & + EE^{heat} \cdot R^{heat\_C_{mw}}) \end{aligned} \tag{S37}$$

where $CE_{i,t}^{c-mw}$ denotes the CO_2 emissions resulting from coal mining and washing for CBECCS plant *i* in year *t*; $CO_{i,u,t}$ is the initial raw coal consumption of unit *u* of power plant *i* in year *t*, as expressed in equation (S3); $SCO_{i,t}^{r}$ is the raw coal consumption substituted by biomass feedstocks at CBECCS plant *i* in year *t*, as expressed in equation (S11); EC_{g} is the amount of fuel *g* consumed during mining and washing per unit of raw coal; *g* =1, ..., 15 denotes raw coal, other washed coal, coke, coke oven gas, blast furnace gas, other gas, other coking products, crude oil, gasoline, kerosene, diesel, fuel oil, liquefied petroleum gas, other petroleum products, and natural gas; NCV_g^e is the LHV of fuel *g*, MJ/kg or MJ/m^3; C_g^e is the carbon content in fuel *g*, kg/GJ; O_g^e is the oxidation rate of fuel *g*; EF_t^{ele} is the electricity emission factor in year *t* and can be estimated with the PSOM through the carbon neutrality scenarios, with values ranging from 0.017-0.127 kg CO_2/kWh from 2025-2060; $R^{ele-C_{mw}}$ is the electricity consumed during mining and washing per unit of coal, with a value of 26.69 [36] kWh/t raw coal; EE^{heat} is the emission factor of heat, with a value of 0.125 t CO_2/GJ [37]; and $R^{heat-C_{mw}}$ is the heat consumed during mining and washing per unit of raw coal, with a value of 1.834 MJ/t raw coal [36].

GHG emissions resulting from coal transportation. The GHG emissions resulting from coal transportation depend on the means of transportation, including trains, ships, and trucks, and the amount of raw coal being transported, as expressed in equation (S38):

$$CE_{i,t}^{c-tra} = (\sum_u CO_{i,u,t} - SCO_{i,t}^r)(w^R \cdot TCF_t^R + w^H \cdot TCF_t^H + w^W \cdot TCF_t^W) \tag{S38}$$

where $CE_{i,t}^{c-tra}$ denotes the GHG emissions resulting from raw coal transportation at CBECCS plant *i* in year *t*; $CO_{i,u,t}$ is the initial raw coal consumption of unit *u* of power plant *i* in year *t*, as expressed in equation (S3); $SCO_{i,t}^r$ is the raw coal consumption substituted by biomass feedstocks at CBECCS plant *i* in year *t*, as expressed in equation (S11); w^R, w^H and w^W are the shares of trains, ships, and trucks in China's coal transportation mode, respectively, with values of 0.8, 0.13 and 0.07 [38], respectively; TCF_t^R, TCF_t^H and TCF_t^W are the GHG emissions of trains, ships, and trucks, respectively, during transportation, kg CO_2-eq/t raw coal. The GHG emissions of coal transportation by trains, ships, and trucks are estimated based on equations (S39)-(S41):

$$TCF_t^R = T^R(\alpha_t^{ele} \cdot EF_t^{ele} \cdot R^{ele\_train} + (1-\alpha_t^{ele}) \cdot EF^{diesel} \cdot R^{diesel\_train}) \tag{S39}$$

$$TCF_t^H = T^H(EF^{diesel} \cdot R^{diesel\_ship}) \tag{S40}$$

$$TCF_t^W = T^W(EF^{diesel} \cdot R^{diesel\_truck}) \tag{S41}$$

where TCF_t^R, TCF_t^H and TCF_t^W are GHGs emissions of coal transportation by trains, ships, and trucks, kgCO_2-eq /t raw coal, respectively, shown in equation (S38); T^R, T^H and T^W are the average transport distance of trains, ships, and trucks, respectively [38]; and α_t^{ele} is the share of electric locomotives in railway transportation in China, which is assumed to be 1 by the period of 2050 to 2060 [39]; the shares for other years were obtained using linear interpolation, with a value of 0.63 in 2020. EF_t^{ele} is the electricity emission factor in year *t*, shown in equation (S37); R^{ele_train} is the electricity consumption of electric locomotives, with a value of 0.015 kWh/(t· km) [40]; EF^{diesel} is the emission factor of diesel; R^{diesel_train} is the diesel consumption of internal combustion locomotives, with a value of 0.882× 10^{-3} kg/(t· km) [37]; R^{diesel_ship} is the diesel consumption of ships, with a value of 2.15×10^{-3} kg/t raw coal [41]; and R^{diesel_truck} is the diesel consumption of trucks, based on the assumption that all trucks use diesel, with a value of 0.1848 kg/(t· km) [37].

CO_2 leakage of coal combustion-induced emissions in the CO_2 transport process. The CBECCS plants were assumed to have 2% [42] of the CO_2 emissions related to coal combustion released into the atmosphere because of CO_2 transport process losses (including compression).

CO_2 emissions caused by power generation efficiency loss. The generation efficiency of power plants will decrease after CBECCS retrofitting, resulting in an increased electricity demand that compensates for the efficiency loss. The CO_2 emissions caused by the generation efficiency loss can be calculated with equation (S42):

$$CE_{i,t}^{\eta} = 0.1 \cdot TCE_{i,t} \cdot \left[(\eta_t^{coal} / f^{coal}) \cdot (f^{bio-coal} / \eta_t^{CBECCS}) - 1 \right] \tag{S42}$$

where $CE_{i,t}^{\eta}$ denotes the CO_2 emissions due to the generation efficiency loss; the CO_2 uncaptured rate is 0.1 [27]; $TCE_{i,t}$ denotes the annual initial CO_2 emissions of power plant i in year t, as expressed in equation (S4); η_t^{coal} is the generation efficiency of the coal-fired plant in year t, with smooth change values ranging from 0.4 in 2020 to 0.5 in 2060; f^{coal} is the emission factor of raw coal, with a value of 0.0895 t CO_2/MJ; $f^{bio-coal}$ is the emission factor for the combustion of coal and biomass mixtures determined by their actual fuel shares, with values of 0.0909 t CO_2/MJ under the scenario with a 15% co-firing ratio limit and 0.0923 t CO_2/MJ under the scenario with a 30% co-firing ratio limit; and η_t^{CBECCS} is the generation efficiency of the CBECCS plant in year t, with smooth change values ranging from 0.28 in 2020 to 0.43 in 2060.

CO_2 emissions resulting from CO_2 transportation and CO_2 storage. The energy penalty-related CO_2 emissions resulting from CO_2 transportation (including compression) and CO_2 storage can be attributed to the increased electricity consumption in this process, as expressed in equation (S43):

$$CE_{i,t}^{CO_2\_comtrastr} = 0.9 \cdot DCE_{i,t} \cdot EF_t^{ele} (R^{ele\_CO_2comtra} \cdot D_i + 0.98 \cdot R^{ele\_CO_2sto}) \tag{S43}$$

where $CE_{i,t}^{CO_2\_comtrastr}$ denotes the total CO_2 emissions resulting from CO_2 transportation (including compression) and CO_2 storage; the CO_2 capture rate is 0.9 [27]; $DCE_{i,t}$ denotes the direct emissions in flue gas originating from CBECCS plant i in year t, which is the sum of the CO_2 emissions related to coal and biomass feedstock combustion, as expressed in equation (S13); EF_t^{ele} is the electricity emission factor in year t, as expressed in equation (S37); $R^{ele\_CO_2comtra}$ is the electricity consumption for CO_2 transportation (including compression), at 1.3 kWh/(t km) [37, 43]; D_i is the distance from CBECCS plant i to the storage sites, which is a weighted average of the distance from plant i to each storage site; 0.98 is the proportion of CO_2 captured and stored after deducting leakage during transportation (including compression); and $R^{ele\_CO_2sto}$ is the electricity consumption for CO_2 storage, at 7 kWh/t CO_2 [42].

Calculation of the uncaptured CO_2 emissions

The CBECCS plant with CO_2 capture equipment exhibits uncaptured CO_2 emissions related to coal combustion due to the 90% capture rate, as expressed in equation (S44).

$$CE_{i,t}^{CO_2\_uncap} = 0.1 \cdot RCE_{i,t} \tag{S44}$$

where $CE_{i,t}^{CO_2\_uncap}$ denotes the total uncaptured CO_2 emissions related to coal combustion; the CO_2 uncaptured rate is 0.1 [27]; and $RCE_{i,t}$ denotes the CO_2 emissions due to the actual coal combustion after biomass substitution at CBECCS plant i in year t, as expressed in equation (S12).

Calculation of the CBECCS levelized cost

Levelized CO_2 sequestration cost. The levelized CO_2 sequestration cost for a given CBECCS plant can be calculated with equation (S45) [30, 34, 44]. It should be noted that in the CBECCS source-sink matching optimization model, the CO_2 transportation cost and CO_2 storage cost (EOR revenue) are determined by each constructed pipeline and activated storage site, respectively, not corresponding to a specific CBECCS plant directly. Thus, we propose a specific cost allocation mechanism to move those costs or revenues from storage sites and pipelines to the respective linked CBECCS plants, as expressed in equations (S47)-(S48) for CO_2 storage and EOR revenue, and equations (S49)-(S50) for CO_2 transportation.

$$LCO_i^{seq} = \frac{\sum_{t=1}^{Period}(CCS_{i,t}^{C} + CCS_{i,t}^{S} - EOR_{i,t} + CCS_{i,t}^{T\text{-}OM})\cdot(1+r)^{-t} + CCS_i^{T\text{-}initial}}{\sum_{t=1}^{Period} Scap_{i,t}^{annual}\cdot(1+r)^{-t}}, \ \forall i \in I \quad \text{(S45)}$$

where LCO_i^{seq} is the levelized CO_2 sequestration cost of CBECCS plant *i*; *Period* denotes the entire period from the various CBECCS deployment years to 2060; $CCS_{i,t}^{C}$ and $CCS_{i,t}^{S}$ are the annual CO_2 capture and storage costs, respectively, of CBECCS plant *i* in year *t*, as expressed in equations (S46) and (S47), respectively; $EOR_{i,t}$ is the annual EOR revenue achieved by CBECCS plant *i* in year *t*, which can be calculated by using a time-phased allocation coefficient of the EOR revenue, as expressed in equation (S48); $CCS_{i,t}^{T\text{-}OM}$ is the annual O&M cost for the proposed pipelines used by CBECCS plant *i* in year *t*, which can be calculated by using a time-phased allocation coefficient of the O&M cost for CO_2 transportation, as expressed in equation (S49); r is the discount rate; $CCS_i^{T\text{-}initial}$ is the capital cost for the construction of the proposed pipelines used by CBECCS plant *i*, discounted to 2025, which can be calculated by using an allocation coefficient of the capital cost for CO_2 transportation, as expressed in equation (S50); and $Scap_{i,t}^{annual}$ is the annual CO_2 capture amount of CBECCS plant *i* in year *t* both for the static and dynamic assessments.

$$CCS_{i,t}^{C} = Scap_{i,t}^{annual}\cdot Ccost_t^{annual}, \ \forall i \in I \quad \text{(S46)}$$

$$CCS_{i,t}^{S} = \sum_j Q_{i,j}^{storage}\cdot Rsto_{j,t}^{annual}\cdot Scost_t^{annual}\cdot R_j\cdot w_{i,t,j}^{storage}, \ \forall i \in I \quad \text{(S47)}$$

$$EOR_{i,t} = \sum_j Q_{i,j}^{storage}\cdot Rsto_{j,t}^{annual}\cdot EOR_t^{annual}\cdot E_j\cdot w_{i,t,j}^{EOR}, \ \forall i \in I;\ j \in J \quad \text{(S48)}$$

$$CCS_{i,t}^{T\text{-}OM} = \sum_{(n,m)}\sum_d Q_{i,(n,m)}^{arc}\cdot Pom_d^{annual}\cdot Dist_{(n,m)}\cdot P_{(n,m),d}\cdot w_{i,t,(n,m)}^{T\text{-}OM}, \ \forall i \in I;\ (n,m)\in Arc(n,m);\ d \in DM \quad \text{(S49)}$$

$$CCS_i^{T\text{-}initial} = \sum_{(n,m)}\sum_d Q_{i,(n,m)}^{arc}\cdot Peq_d\cdot Dist_{(n,m)}\cdot P_{(n,m),d}\cdot w_{i,(n,m)}^{T\text{-}ini}, \ \forall i \in I;\ (n,m)\in Arc(n,m);\ d \in DM \quad \text{(S50)}$$

where $Ccost_t^{annual}$ is the annual capture costs per unit of CO_2 considering the technological learning rate; $Q_{i,j}^{storage}$ is a binary variable that indicates whether CBECCS plant *i* can be linked to storage site *j*; $Rsto_{j,t}^{annual}$ is the annual CO_2 storage at storage site *j* in year *t* both for the static and dynamic assessments; $Scost_t^{annual}$ is the annual storage costs per unit of CO_2 considering the technological learning rate; EOR_t^{annual} is the annual EOR revenue per unit of CO_2 in year *t* considering the predicted crude oil prices by 2060 and the replacement ratio of oil to CO_2; R_j is a binary variable that indicates whether storage site *j* can be activated for CO_2 injection; E_j is a binary variable that indicates whether storage site *j* can be identified as an oil field site with EOR revenue, as expressed in equation (1) in Methods; $w_{i,t,j}^{storage}$ and $w_{i,t,j}^{EOR}$ are allocation coefficients of the storage cost and EOR revenue in year *t*, respectively, due to the newly added CO_2 flow from later retrofitted CBECCS plants that can be injected at the previously used storage sites for dynamic assessment, which can be calculated as the cumulative CO_2 capture amount of CBECCS plant *i* divided by the sum of the cumulative amounts of CO_2 captured from relevant CBECCS plants linked to storage site *j*; $Q_{i,(n,m)}^{arc}$ is a binary variable that indicates whether CO_2 captured from CBECCS plant *i* can flow into arc (n,m); Pom_d^{annual} is the annual O&M cost per unit of the length for pipelines with diameter *d* (i.e., 4% of Peq_d in the initial deployment year; more calculation details are provided in the Supplementary Methods); $Dist_{(n,m)}$ is the pipeline length following the actual geographic path with arc (n,m); $P_{(n,m),d}$ is a binary variable that indicates whether arc (n,m) with diameter *d* can be used for CO_2 flow transportation; Peq_d is the initial capital cost per unit of the length for pipelines with diameter *d*, as expressed in equation (1) in Methods; $w_{i,t,(n,m)}^{T\text{-}OM}$ is an allocation coefficient of the O&M cost for CO_2 transportation in year *t* due to the newly added CO_2 flow from later retrofitted CBECCS plants flowing through the previously built pipelines for dynamic assessment; and $w_{i,(n,m)}^{T\text{-}ini}$ is an allocation coefficient of the capital cost for CO_2 transportation. Both $w_{i,t,(n,m)}^{T\text{-}OM}$ and $w_{i,(n,m)}^{T\text{-}ini}$ can be calculated as the cumulative amount of CO_2 captured from CBECCS plant *i* divided by the sum of the cumulative amounts of CO_2 captured from relevant CBECCS plants linked to arc (n,m).

Levelized CO_2 sequestration cost related to saline aquifers and oil fields. In order to clearly demonstrate the cost difference between CBECCS plants linked by oil field sites and saline aquifer sites, the levelized CO_2 sequestration cost for a given CBECCS plant could be split into two separate costs. Specifically, we introduce a weight coefficient calculated by summing those cumulative CO_2 storage in saline aquifer sites (or oil field sites) attributed to a specific CBECCS plant divided by its cumulative CO_2 storage in all activated storage sites, as shown in equations (S51)-(S52):

$$LCO_i^{seq-DSA} = \frac{(\sum_{t=1}^{Period}(CCS_{i,t}^{C} + CCS_{i,t}^{S} + CCS_{i,t}^{T\text{-}OM})\cdot(1+r)^{-t} + CCS_i^{T\text{-}initial})\cdot w_i^{R\text{-}DSA}}{\sum_{t=1}^{Period}(Rsto_{i,t}^{annual\text{-}DSA})\cdot(1+r)^{-t}},\ \forall i\in I;\ j\in J \quad (S51)$$

$$LCO_i^{seq\text{-}EOR} = \frac{(\sum_{t=1}^{Period}(CCS_{i,t}^{C} + CCS_{i,t}^{S} + CCS_{i,t}^{T\text{-}OM})\cdot(1+r)^{-t} + CCS_i^{T\text{-}initial})\cdot w_i^{R\text{-}EOR} - \sum_{t=1}^{Period} EOR_{i,t}\cdot(1+r)^{-t}}{\sum_{t=1}^{Period}(Rsto_{i,t}^{annual\text{-}EOR})\cdot(1+r)^{-t}},\ \forall i\in I;\ j\in J \quad (S52)$$

where $LCO_i^{seq-DSA}$ is the sequestration cost related to saline aquifers storage; $LCO_i^{seq-EOR}$ is the sequestration cost related to oil fields storage; $CCS_{i,t}^{C}$ and $CCS_{i,t}^{S}$ are the annual CO_2 capture and storage cost, respectively, of CBECCS plant *i* in year *t*; $CCS_{i,t}^{T\text{-}OM}$ is the annual O&M cost for proposed pipelines used by CBECCS plant *i* in year *t*; $CCS_i^{T\text{-}initial}$ is the capital cost for proposed pipelines construction used by CBECCS plant *i*; $EOR_{i,t}$ is the annual EOR revenue achieved by CBECCS plant *i* in year *t*; $w_i^{R\text{-}DSA}$ is a weight coefficient calculated by the cumulative CO_2 storage in saline aquifer sites attributed to CBECCS plant *i* divided by its cumulative CO_2 storage in all activated storage sites; $w_i^{R\text{-}EOR}$ is a weight coefficient calculated by the cumulative CO_2 storage in oil field sites attributed to CBECCS plant *i* divided by its cumulative CO_2 storage in all activated storage sites; $Rsto_{i,t}^{annual\text{-}DSA}$ is the annual CO_2 storage in saline aquifers, which is calculated by summing total CO_2 injected into those saline aquifer sites linked by CBECCS plant *i* in year *t*; $Rsto_{i,t}^{annual\text{-}EOR}$ is the annual CO_2 storage in oil fields, which is calculated by summing total CO_2 injected into those oil field sites linked by CBECCS plant *i* in year *t*; and both $Rsto_{i,t}^{annual\text{-}DSA}$ and $Rsto_{i,t}^{annual\text{-}EOR}$ are accumulated from various CBECCS deployment years to 2060 for static and dynamic assessments.

Life-cycle levelized CO_2 abatement cost. The life-cycle levelized CO_2 abatement cost for a given CBECCS plant mainly includes the capital and O&M costs of retrofitting co-firing boilers, the acquisition and transportation cost due to the actual coal consumption, and the additional costs due to biomass combustion and CCS-related processes, as expressed in equation (S53) [30, 44, 45].

$$LCO_i^{abatement} = \frac{LACOE_i}{EF_i^{CFPP} - EF_i^{CBECCS}}, \forall i \in I \tag{S53}$$

where $LACOE_i$ is the life-cycle levelized additional cost of electricity, as expressed in equation (S54), and EF_i^{CFPP} and EF_i^{CBECCS} are the life-cycle CO_2 emission factors per kWh of coal-fired power plant *i* without CBECCS retrofitting and CBECCS plant *i*, respectively.

$$LACOE_i = \frac{\sum_{t=1}^{Period}(Bio_{i,t}^{annual} + CCS_{i,t}^{annual} + P_{i,t}^{A\text{-}coal} + P_{i,t}^{T\text{-}coal} + Bio_i^{OM} - EOR_{i,t})\cdot(1+\mathrm{r})^{-t} + B_i^{Initial} + CCS_i^{T\text{-}initial}}{\sum_{t=1}^{Period}\sum_{u} IC_{i,u}\cdot RT_{i,t}\cdot(1+\mathrm{r})^{-t}}, \forall i \in I \tag{S54}$$

where for CBECCS plant *i*, $Bio_{i,t}^{annual}$ denotes the additional annual costs due to biomass combustion considering the annual actual co-firing ratio and variable cost per unit; $CCS_{i,t}^{annual}$ denotes the additional annual costs resulting from the CCS-related process; $P_{i,t}^{A\text{-}coal}$ and $P_{i,t}^{T\text{-}coal}$ are the annual acquisition and transportation costs, respectively, of coal (excluding coal substituted by biomass) considering the annual actual co-firing ratio and variable cost per unit; Bio_i^{OM} is the annual O&M cost of retrofitting co-firing boilers (excluding fuel); $EOR_{i,t}$ is the annual EOR revenue achieved in year *t*; $B_i^{Initial}$ is the capital cost of retrofitting co-firing boilers, discounted to 2025; $CCS_i^{T\text{-}initial}$ is the capital cost for proposed pipeline construction; $IC_{i,u}$ is the installed capacity of unit *u*; and $RT_{i,t}$ denotes the annual operating hours in year *t*, as expressed in equation (S3).

Cost of retrofitting co-firing boilers. The cost of retrofitting co-firing boilers includes the capital cost and related O&M cost. The capital cost is calculated based on equations (S55)-(S56):

$$B_i^{Initial} = \sum_u IC_{i,u}\cdot UC_i^{bio} \tag{S55}$$

$$UC_i^{bio} = UC^{r\text{-}bio}\cdot(\sum_u IC_{i,u}/IC^r)^{scale\ factor} \tag{S56}$$

where $B_i^{Initial}$ is the capital cost of retrofitting co-firing boilers of CBECCS plant *i*, mainly caused by the ash removal system; $IC_{i,u}$ is the installed capacity of unit *u* of CBECCS plant *i*, as shown in equation (S3); UC_i^{bio} is the unit capital cost of retrofitting co-firing boilers of CBECCS plant *i* at a 15% co-firing ratio; $UC^{r\text{-}bio}$ is the unit capital cost of 50 USD/kW for the 500 MW boiler at a 15% co-firing ratio [46]; IC^r is the reference installed capacity of 500 MW; and the scale factor is 0.79 [47].

The O&M cost is calculated based on equation (S57):

$$Bio_i^{OM} = B_i^{Initial}\cdot 3\% \tag{S57}$$

where Bio_i^{OM} is the annual O&M cost, which is 3% of the capital cost of retrofitting co-firing boilers.

Cost of coal acquisition. The cost of coal acquisition includes coal mining and washing processes, which is calculated based on equation (S58):

$$P_{i,t}^{A\text{-}coal} = (\sum_u CO_{i,u,t} - SCO_{i,t}^r) \cdot p_t^{coal} \tag{S58}$$

where $P_{i,t}^{A\text{-}coal}$ is the annual cost of coal acquisition for CBECCS plant *i* in year *t*; $CO_{i,u,t}$ is the initial raw coal consumption for unit *u* of CBECCS plant *i* in year *t*, as shown in equation (S3); $SCO_{i,t}^r$ is the raw coal consumption replaced by biomass feedstock for CBECCS plant *i* in year *t*, as shown in equation (S11); and p_t^{coal} is the predicted coal mine mouth price of 80~50 USD/t over the period 2020-2050 [21].

Cost of coal transportation. The cost of coal transportation depends on the means of transportation, including trains, ships, and trucks, as shown in equations (S59)-(S60):

$$P_{i,t}^{T\text{-}coal} = (\sum_u CO_{i,u,t} - SCO_{i,t}^r) \cdot UP^{T\text{-}coal} \tag{S59}$$

$$UP^{T\text{-}coal} = CP^{t1} \cdot T^R \cdot w^R + CP^{t2} \cdot T^H \cdot w^H + CP^{t3} \cdot T^W \cdot w^W \tag{S60}$$

where $P_{i,t}^{T\text{-}coal}$ is the annual cost of coal transportation for CBECCS plant *i* in year *t*; $UP^{T\text{-}coal}$ is the unit cost of coal transportation via trains, ships, and trucks; CP^{t1}, CP^{t2}, and CP^{t3} are the unit transportation costs for trains, ships, and trucks, respectively [48]; T^R, T^H, and T^W are the average transport distances for trains, ships, and trucks, respectively [49], as shown in equations (S39) -(S41); and w^R, w^H and w^W are the shares of trains, ships, and trucks designated for China's coal transportation, respectively [38], as shown in equation (S38).

Additional costs of biomass combustion. The additional costs caused by biomass combustion are associated with the energy penalty, biomass acquisition, biomass transportation, and biomass pretreatment, respectively, as shown in equation (S61):

$$Bio_{i,t}^{annual} = BC_{i,t}^{energy} + BC_{i,t}^{acq} + BC_{i,t}^{trans} + BC_{i,t}^{pre}, \forall i \in I \tag{S61}$$

where $Bio_{i,t}^{annual}$ is the additional annual cost caused by the biomass combustion of CBECCS plant *i* considering the annual actual co-firing ratio and variable cost per unit.

$$BC_{i,t}^{energy} = \sum_u IC_{i,u} \cdot RT_{i,t} \cdot \eta^{bio} \cdot p^{c\text{-}power} \tag{S62}$$

where $BC_{i,t}^{energy}$ is the additional annual cost of energy penalty caused by the biomass combustion of CBECCS plant *i* in year *t*, respectively; $IC_{i,u}$ is the installed capacity of unit *u* of CBECCS plant *i*, and $RT_{i,t}$ is the annual operating hours of CBECCS plant i in year *t*, as shown in equation (S3); η^{bio} is the power generation efficiency reduction caused by biomass combustion, which is defined as 0.56% according to China's engineering experience of co-firing boilers at a 15% co-firing ratio; $p^{c\text{-}power}$ is the feed-in tariff for coal-fired power plants in China, which has stabilized at 50.0 USD/MWh in recent years [50].

$$BC_{i,t}^{acq} = \sum_k BQ_{i,k,t}^s \cdot p_k^{b\text{-}acq} \tag{S63}$$

where $BC_{i,t}^{acq}$ is the additional annual cost of biomass acquisition (i.e., biomass purchase and collection) caused by the biomass combustion of CBECCS plant *i* in year *t*, respectively; $BQ_{i,k,t}^{s}$ is the total biomass feedstock of biomass *k* linked by power plant *i* in year *t*, as shown in equation (S9); $p_k^{b\text{-}acq}$ is the unit acquisition cost of agricultural residues, forest residues, and energy crops in China, which has stabilized at 35 USD/t, 35 USD/t, and 120 USD/t, respectively [45, 47, 51-54].

$$BC_{i,t}^{trans} = \sum_k BQ_{i,k,t}^{s} \cdot (2.9 + 0.03 \cdot DB_{i,k,t}) \tag{S64}$$

where $BC_{i,t}^{trans}$ is the additional annual cost of biomass transportation caused by the biomass combustion of CBECCS plant *i* in year *t*, respectively [45, 47, 51, 54]; $DB_{i,k.t}$ is the average distance for biomass k between various sourcing sites *s* and corresponding power plant *i* in year *t*, derived from the biomass and coal-fired power plant matching model, as shown in (S65).

$$BC_{i,t}^{pre} = \sum_k BQ_{i,k,t}^{s} \cdot p_k^{b\text{-}pre} \tag{S65}$$

where $BC_{i,t}^{pre}$ is the additional annual cost of biomass pretreatment (including compression, crushing, storing, and drying for forest residues) caused by biomass combustion of CBECCS plant *i* in year *t*, respectively; $p_k^{b\text{-}pre}$ is the unit pretreatment cost of agricultural residues, forest residues, and energy crops in China, which has stabilized at 10 USD/t, 36 USD/t, and 10 USD/t, respectively [45, 51, 55].

Additional costs of the CCS-related process. The additional costs caused by the CCS-related process are associated with CO_2 capture, energy penalty, O&M for proposed pipelines, and CO_2 storage, as shown in equation (S66):

$$CCS_{i,t}^{annual} = CCS_{i,t}^{C} + CCS_{i,t}^{energy} + CCS_{i,t}^{T\text{-}OM} + CCS_{i,t}^{S} \tag{S66}$$

where $CCS_{i,t}^{annual}$ is the additional annual costs caused by the CCS-related process of CBECCS plant *i* in year *t*; $CCS_{i,t}^{C}$ and $CCS_{i,t}^{S}$ are the annual CO_2 capture and storage costs of CBECCS plant *i* in year *t*, as shown in equations (S46) and (S47); $CCS_{i,t}^{energy}$ is the annual energy penalty caused by CO_2 capture after considering the power generation efficiency increase and CCS-related efficiency loss decrease in the future; and $CCS_{i,t}^{T\text{-}OM}$ is the annual O&M cost for the proposed pipelines used by CBECCS plant *i* in year *t*, as shown in equation (S49).

$$CCS_{i,t}^{energy} = \sum_u IC_{i,u} \cdot RT_{i,t} \cdot \varepsilon_t / \eta_t^{coal} \cdot p^{c\text{-}power} \tag{S67}$$

where $IC_{i,u}$ is the installed capacity of unit *u* of CBECCS plant *i* and $RT_{i,t}$ is the annual operating hours of CBECCS plant i in year *t*, as shown in equation (S3); ε_t is the CCS-related coal-fired power generation efficiency loss in year *t*, which is projected to decrease from 10% to 5% over 2020-2060 [56]; η_t^{coal} is the original coal-fired power generation efficiency in year *t*, which is projected to increase from 40% to 50% over 2020-2060, as shown in equation (S42); $p^{c\text{-}power}$ is the feed-in tariff for coal-fired power plants in China, which has stabilized at 50.0 USD/MWh in recent years [50].

Recursive dynamic computable general equilibrium model

Production functions. The production activities of the production module are mainly described by a nested constant elasticity of substitution (CES) production function. Depending on the differences in the production structure of different sectors, the production activities can be divided into three categories: 1) general sectors (Supplementary Fig. 8); 2) sectors with natural resources or land inputs (Supplementary Fig. 9); and 3) sectors with energy as a raw material input (taking the refined oil sector as an example, as shown in Supplementary Fig. 10). In each production function, fossil energy inputs require carbon emission permits when they are used, and carbon emission permits enter the production chain as a scarce input factor so that the economic system is linked to the energy system.

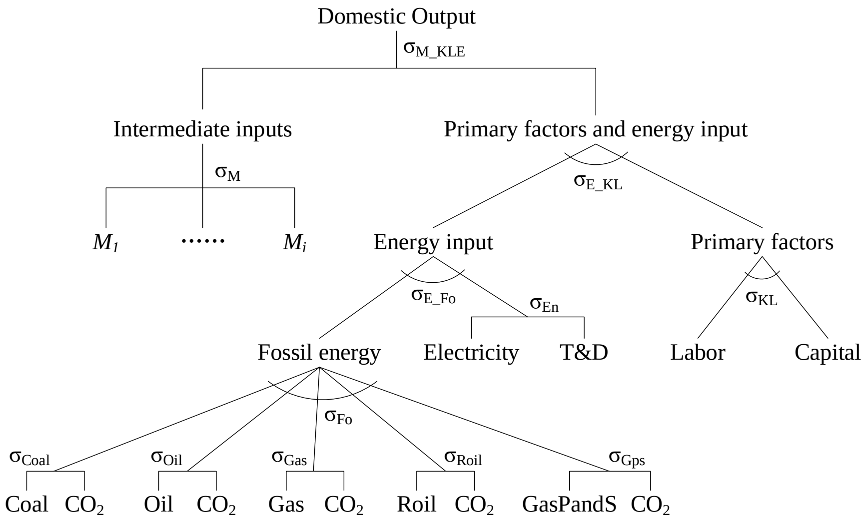

Figure 8. Nested CES production structure of general sectors. Notes: σ denotes the elasticity of substitution; the right-angle connections represent the fixed proportion input-output relationships, which follow the Leontief function, a special case of the CES function (σ = 0); T&D denotes the transmission and distribution of electricity; Roil denotes refined oil; and GasPandS denotes the production and supply of refined gas.

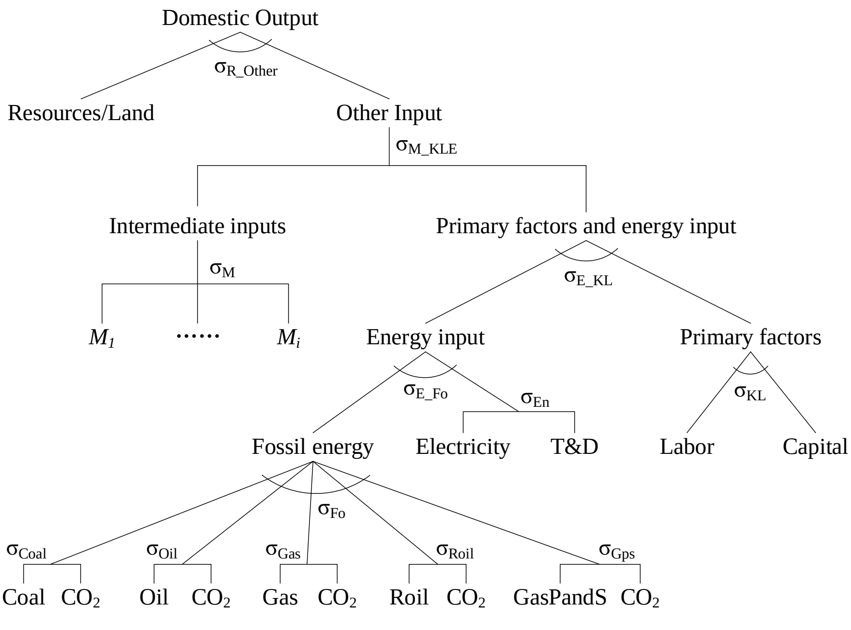

Figure 9. Nested CES production structure of sectors with natural resources or land inputs. Notes: σ denotes the elasticity of substitution; the right-angle connections represent the fixed proportion

input-output relationships, which follow the Leontief function, a special case of the CES function ($\sigma = 0$); T&D denotes the transmission and distribution of electricity; Roil denotes refined oil; and GasPandS denotes the production and supply of refined gas.

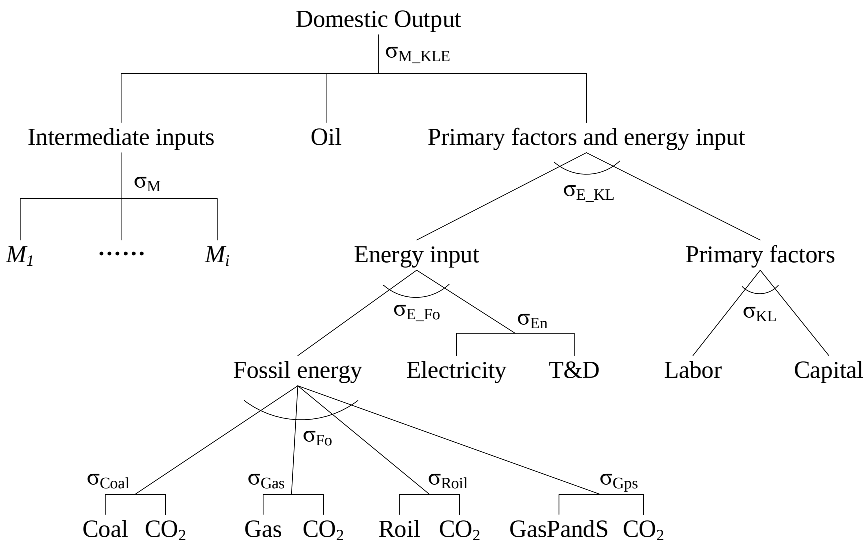

Figure 10. Nested CES production structure of the refined oil sector with oil as a raw material input. Notes: σ denotes the elasticity of substitution; the right-angle connections represent the fixed proportion input-output relationships, which follow the Leontief function, a special case of the CES function ($\sigma = 0$); T&D denotes the transmission and distribution of electricity; Roil denotes refined oil; and GasPandS denotes the production and supply of refined gas.

Consumption functions. For rural and urban households, the total income comes mainly from labor income, returns on capital (including the income from natural resources and land), profit distribution from enterprises and transfer payments from government and abroad. The total income of households, after deducting all taxes paid to the government, gives the disposable income. The disposable income of households is partly used for household savings and partly used for the consumption of various commodities. Similar to the production function, the consumption function is described by a nested CES function (Supplementary Fig. 11). Enterprises earn their income mainly from the return on capital (including the income from natural resources and land). The total income of enterprises, after deducting income taxes paid to the government and adding transfer payments from the government, gives the net profit of the enterprise. Part of the net profit of the enterprise is used as enterprise savings for reproduction expansion, and part is distributed to households as profit. Government revenues, which consist of various taxes and foreign transfer payments, are mainly used for government consumption, government transfer payments to enterprises and households, and export tax rebates. The government's consumption function is also represented by the CES function.

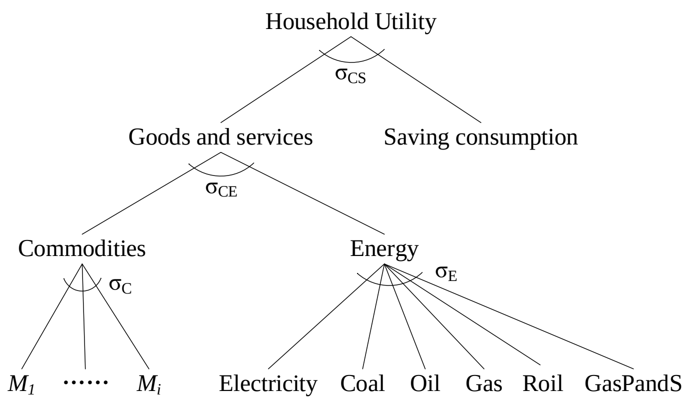

Figure 11. Nested CES structure of consumption. Notes: σ denotes the elasticity of substitution; Roil denotes refined oil; and GasPandS denotes the production and supply of refined gas.

Dynamic mechanism. The dynamic mechanism of the CGE model is mainly driven by the time-series changes in production factors, including changes in the labor force and the accumulation of capital. The change in the labor force depends on the changes in population and employment rates in each year, as shown in equation (S68)-(S69).

$$L_t = L_{t-1} \cdot g_t \tag{S68}$$

$$g_t = \frac{POP_t \cdot ER_t}{POP_{t-1} \cdot ER_{t-1}} \tag{S69}$$

where L_t denotes the labor force supply in year *t*. g_t denotes the labor force growth rate in year *t*. POP_t denotes the national population in year *t*. ER_t denotes the national employment rate in year *t*.

The supply of capital depends on the capital stock, depreciation rates and new capital added in each year. The CGE model divides capital into rigid capital and malleable capital. The capital already in use by each sector is rigid capital, and the new capital invested every year is malleable capital. Rigid capital cannot flow between sectors, while malleable capital is allocated between sectors according to the relative return on capital. The accumulation of capital is shown in equations (S70)-(S71).

$$K^r_{v,t} = K^r_{v,t-1} \cdot (1-\delta_v) + K^m_{v,t} \tag{S70}$$

$$\sum_v K^m_{v,t} = I_t \tag{S71}$$

where $K^r_{v,t}$ denotes the supply of rigid capital to sector *v* in year *t*; $K^m_{v,t}$ denotes the allocation of malleable capital to sector *v* in year *t*. δ_v is the depreciation rate of sector *v*. I_t denotes the total new investments added in year *t*.

Detailed representation of power generation technologies in the CGE model. With the accelerated electrification and development of renewable energy generation technologies, electricity will play an increasingly critical role in China's future energy consumption. According to energy sources, the model categorizes power generation technologies into seven conventional power generation technologies in the power sector: coal-fired power, natural gas-fired power, hydropower, nuclear, wind, solar, and biomass, and three advanced power generation technologies, which include coal-fired with CCS, natural gas-fired with CCS, and BECCS. Due to concern regarding the availability of wind, solar and biomass resources, the model treats these three types of power generation technologies as imperfect substitutes for other power generation technologies, as shown in Supplementary Fig. 12. Furthermore, the production function of CCS technologies varies depending on whether negative emissions are generated, as shown in Supplementary Figs. 13-14. A fixed factor input at the top of the production function is set for CCS technologies to control their penetration rate to avoid overturning growth [57].

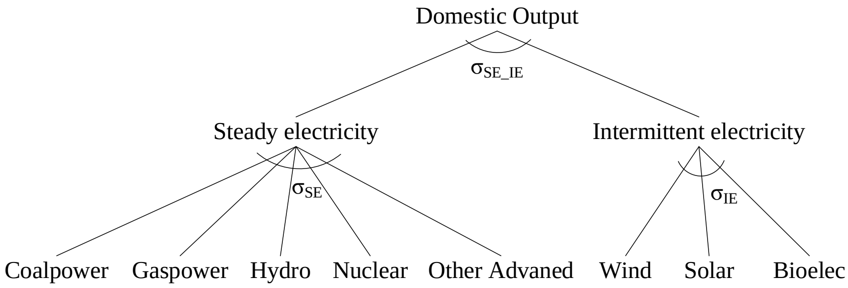

Figure 12. Nested CES production structure of the power sector. Note: σ denotes the elasticity of substitution.

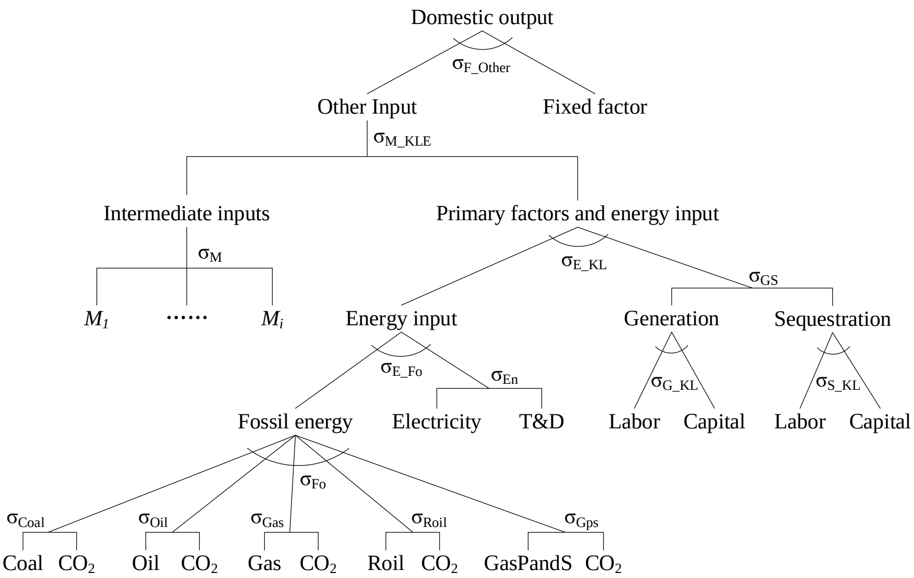

Figure 13. Nested CES production structure of CCS technology without negative emissions. Notes: σ denotes the elasticity of substitution; the right-angle connections represent the fixed proportion input-output relationships, which follow the Leontief function, a special case of the CES function (σ = 0); T&D denotes the transmission and distribution of electricity; Roil denotes refined oil; and GasPandS denotes the production and supply of refined gas.

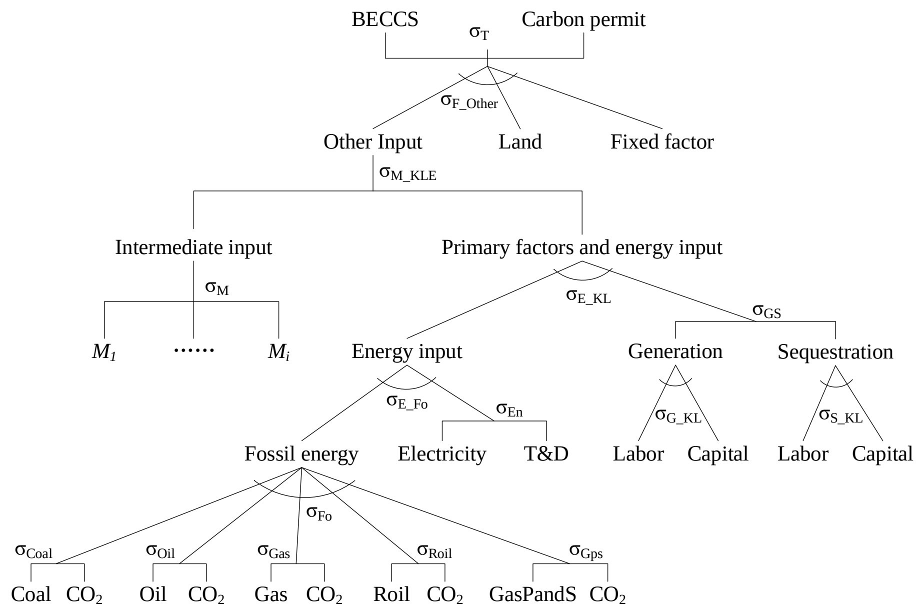

Figure 14. Nested CES production structure of CCS technologies with negative emissions. Notes: σ denotes the elasticity of substitution; the right-angle connections represent the fixed proportion input-output relationships, which follow the Leontief function, a special case of the CES function (σ = 0); T&D denotes the transmission and distribution of electricity; Roil denotes refined oil; and GasPandS denotes the production and supply of refined gas.

Solving Method and Code Implementation. The CGE model is written in the General Algebraic Modeling System (GAMS) software using the Mathematical Programming System for General Equilibrium (MPSGE) modeling language and is solved by the PATH solver.

Power system optimization model

Assumptions. To simplify the model and make the optimization problem tractable, the installed capacity of generation units and energy storage units are simplified. Generation units and energy storage units of the same type across the country are aggregated as one unit, and the installed capacities are modelled as continuous variables. The model adopts the K-means algorithm to create 25 categories in which to cluster representative days based on the hourly real-time data of onshore wind, offshore wind, solar and electricity demand for 365 days a year across the country. On the basis of the typical workday and holiday load curves of each province provided by the National Development and Reform Commission[58], the monthly electricity consumption of each province in 2019 and the actual hourly electricity consumption in reference to a typical province (Anhui), the hourly electricity demand of each province in 2019 is calculated, and the data are calibrated to 2020. The national hourly electricity demand is the sum of the hourly electricity demand of each province. Load shedding is the demand side response in the model. The cost of load shedding in this paper is set to 6899.6 CNY/MWh [59]. The model considers only CO_2 emissions caused by electricity generation. Carbon emissions during the manufacturing process of the units are not considered. We take the price of CNY in 2020 as the power market price benchmark. The exchange rate of CNY to USD is set at the average exchange rate in 2020, that is, 1 CNY= 0.144982 USD.

Technology classification. The PSOM model considers 15 technologies (denoted by *ig*), including 13 types of power generation technologies (denoted by *igp*) and two kinds of power storage technologies (denoted by *is*). Specifically, *igp* includes the power generation technologies of coal-fired power, natural gas-fired power, hydropower, nuclear power, biomass power, onshore wind power, offshore wind power, solar PV, newly built coal-fired power coupled with CCS technology, newly built natural gas-fired power coupled with CCS technology, newly built BECCS, coal-biomass co-firing coupled with CCS technology and dedicated coal-fired power coupled with CCS technology. Coal-biomass co-firing coupled with CCS technology and dedicated coal-firing coupled with CCS technology are two retrofitting technologies for coal-fired units (denoted by *ir*), which are innovatively considered in the model. The *is* includes pumped-hydro storage technology and battery storage technology. According to the type of energy source, *igp* is divided into thermal and nuclear power (denoted by *itn*), hydropower (denoted by *ihy*) and variable renewable power (denoted by *ivre*). The *itn* includes the power generation technologies of coal-fired power, natural gas-fired power, biomass power, newly built coal-fired power coupled with CCS technology, newly built natural gas-fired power coupled with CCS technology, newly built BECCS, coal-biomass co-firing coupled with CCS technology, dedicated coal-fired coupled with CCS technology and nuclear power. The *ivre* includes the power generation technologies of onshore wind power, offshore wind power and solar PV. According to the stability of the power supply, technologies such as coal-fired power, natural gas-fired power, hydropower, nuclear power, biomass power, newly built coal-fired power coupled with CCS technology, newly built natural gas-fired power coupled with CCS technology, newly built BECCS, coal-biomass co-firing coupled with CCS technology, dedicated coal-fired coupled with CCS technology, pumped-hydro storage technology and battery storage technology are regarded as steady power technologies (denoted by *ic*). In addition, except for coal-fired power generation technology, all other technologies consider endogenous technology cost learning (denoted by *il*).

Objective function. The total system cost includes the investment cost, maintenance cost, operating cost, start-up cost and penalty cost of load shedding during the planning periods, as expressed in equation (S72):

$$\min TSC = \sum_{a} (1+r)^{-5(a-1)} \cdot (COST_a^{INV} + COST_a^{MAT} + COST_a^{OP} + COST_a^{StartUp} + COST_a^{Plshed}) \quad \text{(S72)}$$

where *TSC* denotes the total system cost, and *a* (*a*=1, 2 …, 9) denotes the planning year, i.e., 2020 is represented by *a*=1, and 2060 is represented by *a*=9. The total system cost in each planning year was converted into the present value at the end of 2020 by the $(1+r)^{-5(a-1)}$ term, where *r* is the discount rate; $COST_a^{INV}$, $COST_a^{MAT}$, $COST_a^{OP}$, $COST_a^{StartUp}$, and $COST_a^{Plshed}$ denote the investment cost, maintenance cost, operating cost, start-up cost, and penalty cost of load shedding, respectively, for all technologies in planning year *a*.

Specifically, first, the investment cost in each planning year can be calculated by the endogenous cumulative investment cost in the current year minus the endogenous cumulative investment cost in the previous year, as expressed in equation (S73):

$$COST_a^{INV} = \sum_{ig}\left(\sum_{x=1}^{45-5a}(1+r)^{-x}\right)\cdot\frac{r}{1-(1+r)^{-LT_{ig}}}\cdot(y_{ig,a}-y_{ig,a-1})\ ,\ a>1 \quad \text{(S73)}$$

where *ig* denotes all technologies, including power generation technologies and energy storage technologies; LT_{ig} is the designed lifetime of technology *ig*; $y_{ig,a}$ denotes the cumulative investment cost for technology *ig* in planning year *a* and can be endogenously obtained from the model; and the investment costs in planning year *a* are converted into capital costs during the lifetime via multiplication ($\left(\sum_{x=1}^{45-5a}(1+r)^{-x}\right)\cdot\frac{r}{1-(1+r)^{-LT_{ig}}}$).

Second, the maintenance cost in each planning year can be calculated as the unit maintenance cost multiplied by the installed capacity, as expressed in equation (S74). In terms of coal-fired units, the installed capacity should exclude the installed capacity retrofitted in each planning year *a*, as expressed in equation (S75):

$$COST_a^{MAT} = \sum_{il}\left(\sum_{x=1}^{5}(1+r)^{-x}\right)\cdot MATEX_{il,a}\cdot C_{il,a} + COST_a^{MAT-coal} \quad \text{(S74)}$$

$$COST_a^{MAT-coal} = \left(\sum_{x=1}^{5}(1+r)^{-x}\right)\cdot MATEX_{coal,a}\cdot(C_{coal,a}-\sum_{ir}C_{ir,a}) \quad \text{(S75)}$$

where *il* denotes the technology type considering endogenous cost learning; *ir* denotes the CCS retrofitting technology for the coal-fired power plants; $MATEX_{il,a}$ denotes the maintenance cost per MW for technology *il* in planning year *a*; $C_{il,a}$ denotes the installed capacity for technology *il* in planning year *a*; $COST_a^{MAT-coal}$ denotes the maintenance cost for coal-fired power technology in planning year *a*; $MATEX_{coal,a}$ denotes the maintenance cost per MW for coal-fired power technology in planning year *a*; $C_{coal,a}$ is the installed capacity for coal-fired power technology in planning year *a*; and $C_{ir,a}$ denotes the installed capacity for retrofitted technology *ir* in planning year *a*.

Third, the operating cost in each planning year can be calculated as the unit operating cost multiplied by the power generation, as expressed in equation (S76):

$$COST_a^{OP} = \sum_{ig}\sum_{c}(phiD_c\cdot\sum_{h}OPEX_{ig,a}\cdot P_{ig,a,c,h}) \quad \text{(S76)}$$

where *c* (*c*=1, …, 25) denotes the number of clusters, in which we clustered the 365 days of a given year into 25 categories (refer to the description of K-means clustering below for more information); *h* (*h*=1, …, 24) denotes the hours in a day; $phiD_c$ denotes the days of cluster *c*; $OPEX_{ig,a}$ denotes the operating cost per MWh for technology *ig* in planning year *a*; and $P_{ig,a,c,h}$ is the power output of technology *ig* per hour of cluster *c* in planning year *a*.

Fourth, the start-up cost of thermal and nuclear power generation technologies can be calculated as the unit start-up cost multiplied by the installed capacity, as expressed in equation (S77):

$$COST_a^{StartUp} = \sum_{itn}\sum_{c}(phiD_c\cdot(\sum_{h}StartUp_{itn}\cdot Coni_{itn,a,c,h})) \quad \text{(S77)}$$

where *itn* denotes the thermal and nuclear power generation technologies; $StartUp_{itn}$ denotes the start-up cost per MW for thermal and nuclear power generation technology *itn*; and $Coni_{itn,a,c,h}$ is the operation capacity increment for thermal and nuclear power generation technology *itn* per hour of cluster *c* in planning year *a*.

Finally, the penalty cost of load shedding in each planning year can be calculated as the unit penalty cost multiplied by the load shedding amount, as expressed in equation (S78):

$$COST_a^{Plshed} = \sum_c (phiD_c \cdot \sum_h Plshed_{a,c,h}) \cdot CLS \tag{S78}$$

where $Plshed_{a,c,h}$ denotes the load shedding amount per hour of cluster *c* in planning year *a* and *CLS* is the penalty cost per MWh of load shedding.

Installed capacity constraints. For *a*=1, the initial installed capacity of each technology should be consistent with the actual installed capacity, as expressed in equation (S79). For *a*>1, the installed capacity of each technology in each planning year should equal the installed capacity in the previous planning year minus the retired installed capacity plus the incremental capacity in the current planning year. The model considered the lifetime of the unit for the different technologies. Hence, the installed capacity can be calculated differently depending on the unit lifetime, as expressed in equations (S80)-(S82). Equation (S80) applies to the period until the end of the initial installed lifetime for the various technologies. Equation (S81) applies to the period from the end of the initial installed lifetime to the end of the lifetime of the first newly built unit, and Equation (S82) applies to the period after the end of the lifetime of the first newly built unit. In addition to the initial year, the capacity increment is constrained by the upper limit of the capacity increment multiplied by the planning time step width and maturity of technology, as shown in equation (S83). The total installed capacity of each technology in each year should not exceed the upper installed capacity limit of each technology in consideration of the limitations of construction capability and the environment, as shown in equation (S84).

$$C_{ig,a} = CIni_{ig} \;,\; \forall ig \text{ and } a = 1 \tag{S79}$$

$$C_{ig,a} = C_{ig,a-1} - C_{ig,a-\frac{LTIni_{ig}}{\Delta a}} + Ci_{ig,a} \;,\; \forall ig \text{ and } 1 < a \le \frac{LTIni_{ig}}{\Delta a} + 1 \tag{S80}$$

$$C_{ig,a} = C_{ig,a-1} + Ci_{ig,a} \;,\; \forall ig \text{ and } \frac{LTIni_{ig}}{\Delta a} + 1 < a \le \frac{LT_{ig}}{\Delta a} + 1 \tag{S81}$$

$$C_{ig,a} = C_{ig,a-1} - Ci_{ig,a-\frac{LT_{ig}}{\Delta a}} + Ci_{ig,a} \;,\; \forall ig \text{ and } a > \frac{LT_{ig}}{\Delta a} + 1 \tag{S82}$$

$$0 \le Ci_{ig,a} \le Cir_{ig} \cdot \Delta a \cdot MA_{ig,a} \;,\; \forall ig \setminus ir \text{ and } a > 1 \tag{S83}$$

$$0 \le C_{ig,a} \le CMax_{ig} \;,\; \forall ig, a \tag{S84}$$

where *ig* denotes all technologies, including power generation technologies and energy storage technologies; $C_{ig,a}$ is the installed capacity for technology *ig* in planning year *a*; $CIni_{ig}$ denotes the initial installed capacity for technology *ig* in 2020; $LTIni_{ig}$ denotes the remaining lifetime of the initial capacity of technology *ig*; LT_{ig} is the designed lifetime of technology *ig*, as expressed in equation (S73); Δa denotes the planning time step, which is set to 5 years; $Ci_{ig,a}$ denotes the capacity increment for technology *ig* (including the retrofitted installed capacity for retrofitting technology *ir*) in planning year *a*; Cir_{ig} denotes the upper limit of the capacity increment for technology *ig* in every year; $MA_{ig,a}$ denotes the maturity of technology *ig* in planning year *a*, if technology *ig* is mature, $MA_{ig,a}$ =1, otherwise $MA_{ig,a}$ =0; and $CMax_{ig}$ is the upper limit of the installed capacity for technology *ig* for all planning years.

Retrofittable capacity constraints on the retrofitting technologies. The retrofitting technologies include coal-biomass co-firing power generation coupled with CCS technology (i.e., CBECCS) and dedicated coal-fired power generation coupled with CCS retrofitting technology. Based on information on China's existing coal-fired power generation units in 2020 and the evaluation results of their corresponding retrofittable potential retrieved from the static source–sink matching model, the model selects the initial installed capacity of the coal-fired power generation units that can be retrofitted, as expressed in equation (S85). When the remaining lifetime of the coal-fired power generation unit is greater than or equal to 10 years, the remaining retrofittable installed capacity of the coal-fired power generation units satisfying the retrofitted conditions in each planning year equals that in the last planning year minus the installed capacity retrofitted in this planning year, as expressed in equation (S86). When the remaining lifetime of the coal-fired power generation unit is less than 10 years, the retrofitted conditions are not satisfied, as expressed in equation (S87). In addition, the retrofitted installed capacity of the coal-fired power generation units in each planning year should not exceed the remaining retrofittable installed capacity in the previous year, as expressed in equation (S88):

$$RC_a = RCIni \ , \ a = 1 \tag{S85}$$

$$RC_a = RC_{a-1} - \sum_{ir} Ci_{ir,a} \ , \ 1 < a < \frac{LTIni_{coal} - 10}{\Delta a} + 1 \tag{S86}$$

$$RC_a = 0 \ , \ a \geq \frac{LTIni_{coal} - 10}{\Delta a} + 1 \tag{S87}$$

$$\sum_{ir} Ci_{ir,a} \leq RC_{a-1} \ , \ a > 1 \tag{S88}$$

where *ir* denotes the CCS retrofitting technology for coal-fired power plants, including CBECCS and dedicated CCS retrofitting technology; RC_a denotes the remaining retrofittable installed capacity of coal-fired power generation units in planning year *a*; *RCIni* denotes the initial retrofittable installed capacity of coal-fired power generation units, which are screened by the source–sink matching model according to the installed capacity and remaining lifetime of the existing coal-fired power units, biomass availability, storage site accessibility, and pipeline network accessibility; and $Ci_{ir,a}$ is the installed capacity retrofitted for retrofitting technology *ir* in planning year *a*.

Operation capacity constraints. The hourly operation capacity of the thermal and nuclear units of cluster *c* cannot exceed the total installed capacity in planning year *a*, as shown in equation (S89). In terms of coal units, the sum of the retrofitted and un-retrofitted hourly operation capacities of cluster *c* should not exceed the total installed capacity of coal units in planning year *a*, as shown in equation (S90). The hourly operation capacity of thermal and nuclear power is supposed to satisfy the balance of start-up capacity and shut-down capacity in each hour, as shown in equation (S91).

$$0 \le Con_{itn,a,c,h} \le C_{itn,a} \ , \ \forall itn,a,c,h \tag{S89}$$

$$\sum_{ir} Con_{ir,a,c,h} + Con_{Coal,a,c,h} \le C_{coal,a} \ , \ \forall c,h \text{ and } a < \frac{LTIni_{coal}}{\Delta a} + 1 \tag{S90}$$

$$Con_{itn,a,c,h} - Con_{itn,a,c,h-1} = Coni_{itn,a,c,h} - Cond_{itn,a,c,h} \ , \ \forall itn,a,c \text{ and } h > 1 \tag{S91}$$

where *itn* denotes the thermal power generation technologies and nuclear power generation technologies; $Con_{itn,a,c,h}$ denotes the operation capacity per hour of cluster *c* for thermal and nuclear power generation technology *itn* in planning year *a*; $C_{itn,a}$ is the installed capacity for thermal and nuclear power generation technology *itn* in planning year *a*; $Con_{ir,a,c,h}$ denotes the operation capacity per hour of cluster *c* for retrofitting technologies *ir* in planning year *a*; $Con_{coal,a,c,h}$ denotes the operation capacity per hour of cluster *c* of coal-fired power generation unit in planning year *a*; $LTIni_{coal}$ denotes the lifetime of initial capacity of coal-fired power generation unit; and $Coni_{itn,a,c,h}$ and $Cond_{itn,a,c,h}$ represent the start-up capacity and shut-down capacity per hour of cluster *c* for thermal and nuclear power generation technology *itn*, respectively, in planning year *a*.

Electricity balance constraints. The hourly electricity supplied to the demand side by the generation and storage technologies should satisfy the hourly electricity demand of each cluster, as expressed in equation (S92). The hourly capacity of load shedding cannot exceed the load demand, and the total amount of loading shedding cannot exceed 5% of the total load demand, as shown in equations (S93)-(S94). The initial generation of each technology should be consistent with the actual generation in 2020, as shown in equation (S95).

$$[\sum_{igp} P_{igp,a,c,h} + \sum_{is} (Pdis_{is,a,c,h} - Pch_{is,a,c,h})] \cdot (1 - lr) = PD_{a,c,h} - Plshed_{a,c,h} \ , \ \forall a,c,h \tag{S92}$$

$$0 \le Plshed_{a,c,h} \le PD_{a,c,h} \ , \ \forall a,c,h \tag{S93}$$

$$\sum_{c} (phiD_c \cdot \sum_{h} Plshed_{a,c,h}) \le 0.05 \sum_{c} (phiD_c \cdot \sum_{h} PD_{a,c,h}) \ , \ \forall a \tag{S94}$$

$$\sum_{c} (phiD_c \cdot \sum_{h} P_{ig,a,c,h}) = PIni_{ig} \ , \ \forall ig \text{ and } a = 1 \tag{S95}$$

where *igp* denotes all the power generation technologies; *is* denotes all the energy storage technologies; $P_{igp,a,c,h}$ denotes the power output of power generation technology *igp* per hour of cluster *c* in planning year *a*; $Pdis_{is,a,c,h}$ and $Pch_{is,a,c,h}$ denote the electricity discharging and charging amounts, respectively, of the energy storage technology per hour of cluster *c* in planning year *a*; *lr* denotes the line losses of the power grid in the transmission process, at 0.056 [60]; $PD_{a,c,h}$ denotes the load demand per hour of cluster *c* in planning year *a*; and $Plshed_{a,c,h}$ denotes the load shedding amount per hour of cluster *c* in planning year *a* (refer to equation (S78)); $PD_{a,c,h}$ denotes the load demand per hour of cluster *c* in planning year *a*; $phiD_c$ denotes the days of cluster *c*;

$P_{ig,a,c,h}$ denotes the power output of technology *ig* per hour of cluster *c* in planning year *a*; and $PIni_{ig}$ denotes the initial generation of technology *ig* in 2020.

Electricity generation constraints. The output of thermal and nuclear units is restrained by the unit minimum and maximum output rate, as shown in equation (S96). The output of the nuclear power plant is not allowed to change within a day, as shown in equation (S97).

$$Con_{itn,a,c,h} \cdot PMin_{itn} \le P_{itn,a,c,h} \le Con_{itn,a,c,h} \cdot PMax_{itn} \ , \ \forall itn,a,c,h \tag{S96}$$

$$P_{inu,a,c,h} = P_{inu,a,c,h-1} \ , \ \forall a,c \text{ and } h > 1 \tag{S97}$$

where $PMin_{itn}$ and $PMax_{itn}$ are the minimum and maximum output rates of thermal and nuclear power generation technology *itn*, respectively; $P_{itn,a,c,h}$ denotes the power output of thermal and nuclear power generation technology *itn* per hour of cluster *c* in planning year *a*; *inu* denotes the nuclear power generation technologies; and $P_{inu,a,c,h}$ denotes power the output of nuclear technology *inu* per hour of cluster *c* in planning year *a*.

In terms of renewable power, the hourly power output of hydropower cannot exceed the installed capacity in planning year *a*, as shown in equation (S98). The actual hourly power output of wind power and solar PV is limited by the installed capacity and availability factor, as shown in equation (S99).

$$0 \le P_{ihy,a,c,h} \le C_{ihy,a} \ , \ \forall a,c,h \tag{S98}$$

$$0 \le P_{ivre,a,c,h} \le C_{ivre,a} \cdot \mathrm{AF}_{ivre,c,h} \ , \ \forall ivre,a,c,h \tag{S99}$$

where *ihy* denotes the hydropower generation technologies; $P_{ihy,a,c,h}$ denotes the power output of hydropower technology *ihy* per hour of cluster *c* in planning year *a*; $C_{ihy,a}$ is the installed capacity for hydropower technology *ig* in planning year *a*; *ivre* denotes the variable renewable energy power generation technologies, including onshore wind power, offshore wind power and solar PV; $P_{ivre,a,c,h}$ denotes the power output of variable renewable energy technology *ivre* per hour of cluster *c* in planning year *a*; $C_{ivre,a}$ is the installed capacity for variable renewable energy technology *ig* in planning year *a*; and $\mathrm{AF}_{ivre,c,h}$ denotes the availability factor for variable renewable energy technology *ivre* per hour of cluster *c*, with a value of 0~1.

In terms of energy storage technologies, the discharging and charging power cannot exceed the installed capacity of the energy storage unit, as shown in equation (S100). The stored energy should satisfy the charging-discharging balance, and cannot exceed the upper limit of energy storage technologies, as shown in equations (S101)-(S102) The energy in the storage unit should be unchanged after the intraday dispatch, as shown in equation (S103).

$$0 \le Pch_{is,a,c,h}, Pdis_{is,a,c,h} \le C_{is,a} \ , \ \forall is,a,c,h \tag{S100}$$

$$SP_{is,a,c,h} = SP_{is,a,c,h-1} + Pch_{is,a,c,h} \cdot etaS_{is} - Pdis_{is,a,c,h} / etaS_{is} \ , \ \forall is,a,c \text{ and } h>1 \tag{S101}$$

$$0 \le SP_{is,a,c,h} \le TMax_{is} \cdot C_{is,a} \ , \ \forall is,a,c,h \tag{S102}$$

$$SP_{is,a,c,h=1} = SP_{is,a,c,h=24} \ , \ \forall is,a,c \tag{S103}$$

where *is* denotes all the energy storage technologies; $Pch_{is,a,c,h}$ and $Pdis_{is,a,c,h}$ denote charging electricity and discharging electricity for energy storage technology *is* per hour of cluster *c* in planning year *a*, respectively; $C_{is,a}$ is the installed capacity for energy storage technology *is* in planning year *a*; $SP_{is,a,c,h}$ denotes the stored energy for energy storage technology *is* per hour of cluster *c* in planning year *a*; $etaS_{is}$ denotes the efficiency of storage charging and discharging for energy storage technology *is*; and $TMax_{is}$ denotes the maximum storage duration for energy storage technology *is*.

Average capacity factor constraints. During unit operation, it is not possible to guarantee that the unit will always operate at the maximum power output throughout the year due to downtime caused by maintenance or limited power generation resources. Furthermore, owing to policy requirements or necessary unit operation conditions, the power output of power generation technology should be sufficient. Consequently, the generation capacity factor of power generation technology should be clipped by the minimum and maximum capacity factors in each year, as expressed in equation (S104):

$$CFMin_{igp} \cdot C_{igp,a} \le \sum_{c} (phiD_c \cdot \sum_{h} p_{igp,a,c,h}) / 8760 \le CFMax_{igp} \cdot C_{igp,a} \ , \ \forall igp,a \tag{S104}$$

where $C_{igp,a}$ is the installed capacity for power generation technology *igp* in planning year *a*, and $CFMin_{igp}$ and $CFMax_{igp}$ denote the lower and upper limits, respectively, of the capacity factor for power generation technology *igp*. For specific $CFMin_{igp}$ and $CFMax_{igp}$ values for the various power generation technologies, please refer to Supplementary Table 11.

Carbon emission constraints. The total CO_2 emitted by the generation unit should not exceed the given carbon emission reduction goals, as shown in equation (S105).

$$\sum_{c} (phiD_c \cdot \sum_{igp,h} P_{igp,a,c,h} \cdot EF_{igp,a}) \le ET_a \ , \ \forall a \tag{S105}$$

where *igp* denotes all the power generation technologies; $P_{igp,a,c,h}$ denotes the power output of power generation technology *igp* per hour of cluster *c* in planning year *a*; $EF_{igp,a}$ denotes the emission factor for power generation technology *igp* in planning year *a*; and ET_a is the upper CO_2 emission limit of the power system in planning year *a*.

Power reserve requirements. To guarantee security during unexpected accidents, the power reserve capacity provided by technology should be larger than the peak load in each year and meet a certain proportion of reserve requirements, as shown in equation (S106).

$$\sum_{ig} C_{ig,a} \cdot CCr_{ig} \ge PL_a \cdot (1 + RSr) \ , \ \forall a \tag{S106}$$

where CCr_{ig} is the credit capacity rate of technology *ig*; PL_a denotes the peak load in planning year *a*; and *RSr* is the required reserve rate of the power system.

Spinning reserve capacity constraints represent the flexibility requirements during power system operation. Due to the uncertainties in the load and variable renewable energy output, the actual value may fluctuate greatly in a short time. Hence, the system must have sufficient spinning reserve capacity to supplement potential power shortages; we define the spinning reserve capacity as the output increments provided by steady power generation technology within 10 minutes [61]. The constraints of the spinning reserve capacity are as shown in equations (S107)-(S110).

$$\sum_{ic} Chot_{ic,a,c,h} \geq hr_{load} \cdot PD_{a,c,h} + hr_{ivre} \cdot \sum_{ivre} P_{ivre,a,c,h} \ , \ \forall a,c,h \tag{S107}$$

$$0 \leq Chot_{itn,a,c,h} \leq \min\{Con_{itn,a,c,h} - P_{itn,a,c,h}, Con_{itn,a,c,h} \cdot RP_{itn}\} \ , \ \forall itn,a,c,h \tag{S108}$$

$$0 \leq Chot_{ihy,a,c,h} \leq C_{ihy,a} - P_{ihy,a,c,h} \ , \ \forall a,c,h \tag{S109}$$

$$0 \leq Chot_{is,a,c,h} \leq \min\{C_{is,a,c,h} - Pdis_{is,a,c,h} + Pch_{is,a,c,h}, 6 \cdot SP_{is,a,c,h} \cdot etaS_{is}\} \ , \ \forall is,a,c,h \tag{S110}$$

where *ic* denotes the steady power generation technologies; $Chot_{ic,a,c,h}$, $Chot_{itn,a,c,h}$, $Chot_{ihy,a,c,h}$ and $Chot_{is,a,c,h}$ denote the spinning reserve capacity for steady power generation technology *ic*, thermal and nuclear power generation technology *itn*, hydropower technology *ihy* and energy storage technology *is* per hour of cluster c in planning year *a*, respectively; hr denotes the spinning factor; RP_{itn} denotes the maximum ramp rate within 10 minutes provided by thermal and nuclear power generation technology *itn*; and $6 \cdot SP_{is,a,c,h} \cdot etaS_{is}$ denotes the maximum power that energy storage technology can provide when discharging the whole energy storage within 10 minutes [61].

System inertia constraints. The total inertia provided by steady technology should not be less than the power system inertia requirements, as shown in equations (S111)-(S114).

$$\sum_{ic} H_{ic,a,c,h} \geq \alpha \cdot SI \cdot PD_{a,c,h} \ , \ \forall a,c,h \tag{S111}$$

$$H_{itn,a,c,h} = IP_{itn} \cdot Con_{itn,a,c,h} \ , \ \forall itn,a,c,h \tag{S112}$$

$$H_{ihy,a,c,h} = IP_{ihy} \cdot C_{ihy,a} \ , \ \forall a,c,h \tag{S113}$$

$$H_{is,a,c,h} = IP_{is} \cdot C_{is,a} \ , \ \forall is,a,c,h \tag{S114}$$

where $H_{ic,a,c,h}$, $H_{itn,a,c,h}$, $H_{ihy,a,c,h}$ and $H_{is,a,c,h}$ denote the inertia requirements offered by steady power generation technology *ic*, thermal and nuclear power generation technology *itn*, hydropower technology *ihy* and energy storage technology *is* per hour of cluster *c* in planning year *a*; α denotes a constant reflecting the tolerance of the system inertia drop relative to the current system inertia level, taken as 0.7 [61]; *SI* denotes the inertia level for China's current power system; IP_{itn}, IP_{ihy} and IP_{is} denote the inertia constant of thermal and nuclear power generation technology *itn*, hydropower technology *ihy* and energy storage technology *is*, respectively.

Calculation of the endogenous technology cost. The PSOM model considers the endogenous technology cost learning by the "learning-by-doing" learning curve. According to Wright's law [62], the "learning-by-doing" learning curve theory can be described by an exponential correlation between the unit cost and the cumulative installed capacity (equation (S115)); that is, the unit cost of technology will decrease with increasing cumulative installed capacity. The learning rate (*LR*) of the learning curve is defined as a function of the cost reduction rate Z, as shown in equation (S116). The learning curve of CBECCS technology is shown in Supplementary Fig. 15a.

$$TUC_t = TUC_1 \cdot (\frac{CIC_t}{CIC_1})^{-Z} \tag{S115}$$

$$LR = 1 - 2^{-Z} \tag{S116}$$

where TUC_t denotes the technology unit cost in year t; TUC_1 denotes the initial technology unit cost; CIC_t is the cumulative installed capacity of the technology in year t; CIC_1 is the initial cumulative installed capacity of the technology; and Z denotes the cost reduction rate, which is a positive learning parameter.

The cost learning curve couples the unit cost with the cumulative installed capacity, both of which are endogenous variables. However, the direct multiplication of two endogenous variables will lead to nonlinear problems in the objective function, which is not applicable for linear programming. To avoid this problem, we referred to Heuberger, Rubin [63], adopting the piecewise linear learning curve method to convert the unit cost curve into cumulative cost curve. The piecewise linear learning curve and cumulative investment cost of CBECCS technology are shown in Supplementary Fig. 15b. Equation (S117) was used to ensure that only one segment of the piecewise linear learning curve can be selected. The endogenous cumulative installed capacity can be obtained with equations (S118) and (S119), and the corresponding cumulative investment cost can be calculated via linear interpolation, as expressed in equation (S120):

$$\sum_l \rho_{il,a,l} = 1 \ , \ \forall il, a \tag{S117}$$

$$Xlo_{il,l} \cdot \rho_{il,a,l} \le xs_{il,a,l} \le Xup_{il,l} \cdot \rho_{il,a,l} \ , \ \forall il, a, l \tag{S118}$$

$$\sum_{a'=1}^{a} Ci_{il,a'} = \sum_l xs_{il,a,l} \ , \ \forall il, a \tag{S119}$$

$$y_{il,a} = \sum_l [Ylo_{il,l} \cdot \rho_{il,a,l} + \frac{Yup_{il,l} - Ylo_{il,l}}{Xup_{il,l} - Xlo_{il,l}} \cdot (xs_{il,a,l} - Xlo_{il,l}) \cdot \rho_{il,a,l}] \ , \ \forall il, a \tag{S120}$$

where l denotes the line segments of the piecewise linear learning curve; $\rho_{il,a,l}$ is a binary variable indicating whether the cumulative capacity increment occurs in segment l of technology il in planning year a (if this is the case, $\rho_{il,a,l}$ =1; otherwise, $\rho_{il,a,l}$ =0); $xs_{il,a,l}$ denotes the cumulative capacity increment of line segment l of technology il in planning year a; $Xlo_{il,l}, Xup_{il,l}, Ylo_{il,l}, Yup_{il,l}$ denote the lower and upper values of the x-axis and y-axis of line segment l, respectively; $Ci_{il,a}$ denotes the installed capacity increment for technology il in planning year a; and $y_{il,a}$ denotes the cumulative investment cost of technology il in planning year a, as expressed in equation (S73).

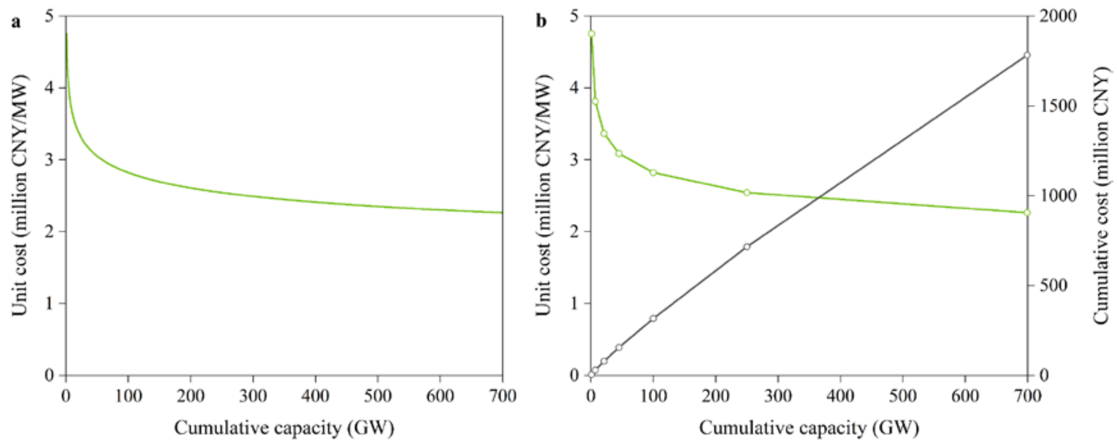

Figure 15. Piecewise linear learning curve of CBECCS. a Technology cost learning curve as a continuous. **b** Technology cost learning curve as a piecewise linear function of cumulative installed capacity.

Solving Method and Code Implementation. The power system optimization model is written in GAMS software using the mixed-integer linear programming (MIP) modeling language and is solved by the CPLEX solver.

Clustering of the hourly availability factor and electricity demand

Hourly wind power and solar PV availability factor. The hourly availability factor (AF) denotes the ratio of the real-time hourly wind power or solar PV output in one year to the yearly maximum output (ranging from 0 to 1). To calculate the AF value of wind power and solar PV in this study, we selected the capital cities of the provinces in China as representative points and obtained the hourly wind speed at 10 m from the Modern-Era Retrospective analysis for Research and Application version-2 (MERRA-2) database in 2019 [64, 65]. The hourly radiation intensity and ground surface temperature were obtained from Meteonorm software throughout 2019 [66]. Then, the real-time hourly power potential of onshore wind, offshore wind and solar PV are predicted separately by equations (S121)-(S123).

For wind power, onshore and offshore wind turbines are assumed to have the same specifications. The hourly wind speed at 10 m above ground at representative points in each province of China was selected from the NASA MERRA-2 database [64, 65]. The hourly power output per wind turbine in each province is calculated by equations (S121)-(S122).

$$Pw_{p,h}=\begin{cases}0, & V_{p,h}^{80}\le V^{ci}\ or\ V_{p,h}^{80}\ge V^{co}\\ \frac{1}{2}C^{P}\cdot\pi\cdot Ra^{2}\cdot\rho\cdot(V_{p,h}^{80})^{3}, & V^{ci}<V_{p,h}^{80}<V^{r}\\ P^{WR}, & V^{r}\le V_{p,h}^{80}<V^{co}\end{cases} \tag{S121}$$

$$V_{p,h}^{80}=V_{p,h}^{10}\cdot(\frac{80}{10})^{\beta} \tag{S122}$$

where $Pw_{p,h}$ denotes the hourly power output per wind turbine in province *p*; $V_{p,h}^{80}$ denotes the hourly wind speed at 80 m in province *p*; V^{ci} denotes the cut-in wind speed, taken as 3 m/s; V^{co} denotes the cut-out wind speed, taken as 25 m/s; C^{P} denotes the power coefficient of the wind turbine, taken as 0.5; *Ra* denotes the impeller radius of the wind turbine, taken as 49.5 m [67]; ρ denotes the air density, taken as 1.29 kg/m^3; P^{WR} denotes the rated wind turbine power, taken as

2 MW [67]; V^r denotes the rated wind speed, taken as 12 m/s; $V_{p,h}^{10}$ denotes the real-time wind speed at 10 m in province *p*; and β denotes the wind shear index, taken as 0.143 [68].

For solar PV, the power output of solar PV panels is referenced to the PVWatts model developed by the National Renewable Energy Laboratory [69], combined with real-time radiation intensity and surface temperature from meteorological stations in each province of China obtained from Meteonorm software[66], as shown in equation (S123).

$$Ps_{p,h} = Y^v \cdot \frac{R_{p,h}}{R^{STC}} \cdot [1 + \phi \cdot (T_{p,h} - T^{STC})] \cdot (1-\gamma) \tag{S123}$$

where $Ps_{p,h}$ denotes the hourly power output per solar PV panel in province *p* (W); Y^v is the rated power of the solar PV panel, taken as 300 W; $R_{p,h}$ denotes the actual solar radiation intensity per hour in province *p* (W/m^2); R^{STC} denotes the light intensity under standard test conditions, taken as 1000 W/m^2 [69]; and ϕ denotes the temperature coefficient of the solar PV module, taken as -0. 35%/°C; $T_{p,h}$ denotes the actual surface temperature per hour in province *p* (°C); T^{STC} denotes the temperature at standard test conditions, taken as 25 °C [69]; and γ denotes the shading factor of the solar PV array, taken as 10%.

The hourly AF value of wind power and solar PV in each province can be calculated with equation (S124). Then, the national AF value of wind power and solar PV can be calculated as a weighted average of the provincial AF values, weighted by the provincial electricity demand, as expressed in equation (S125).

$$RAF_{ivre,p,h} = \frac{P_{ivre,p,h}}{PMax_{ivre,p}} \tag{S124}$$

where *ivre* denotes the different variable renewable energy power generation technologies, $RAF_{ivre,p,h}$ denotes the AF value of variable renewable energy technology *ivre* per hour in province *p*, $P_{ivre,p,h}$ denotes the real-time hourly power output of variable renewable energy technology *ivre* in province *p*, and $PMax_{ivre,p}$ denotes the maximal power output of variable renewable energy technology *ivre* in province *p*.

$$NAF_{ivre,h} = \sum_p \frac{RAF_{ivre,p,h} \cdot EDe_p}{\sum_p EDe_p} \tag{S125}$$

where $NAF_{ivre,h}$ denotes the national AF value of variable renewable energy technology *ivre* per hour, and EDe_p denotes the electricity demand in province *p* in 2019.

Hourly real-time hourly electricity demand. The hourly electricity demand in each province was calculated based on the typical workday and holiday load curves of each province released by the National Development and Reform Commission of China, the monthly variation in the electricity demand in each province [70], and the actual hourly electricity consumption in reference to Anhui Province. Limited by the data availability, we only had access to the data for 2019. Thus, we first calculated the real-time hourly electricity demand in each province in 2019. Then, the hourly electricity demand data were calibrated to 2020 according to the ratio of the sum of the provincial electricity consumption in 2020 to the sum of the provincial electricity consumption in 2019. The national hourly electricity demand was determined as the sum of the hourly electricity demand in each province. Finally, the future hourly electricity demand was proportionally calculated based on the CGE model forecast results. The specific calculation process for the real-time hourly electricity demand of each province is as follows:

First, according to the monthly electricity demand of each province and referring to the typical hourly electricity load on workday and holiday in each province in 2019 [70], the corresponding hourly electricity load on workday and holiday for each month is calculated.

Second, using the number of workday and holiday in each month, the average hourly baseline electricity load at the same hour for each month is obtained, as shown in equation (S126):

$$AEL_{h,mo,p} = \frac{EL^{wd}_{h,mo,p} \cdot num^{wd}_{mo} + EL^{ho}_{h,mo,p} \cdot num^{ho}_{mo}}{num^{day}_{mo}}, \ \forall h, \forall mo, \forall p \tag{S126}$$

where $AEL_{h,mo,p}$ represents the average electricity load at hour *h* in month *mo* of province *p*; $EL^{wd}_{h,mo,p}$ represents the electricity load at hour *h* of workdays for month *mo* of province *p*; num^{wd}_{mo} represents the number of workdays in month *mo*; $EL^{ho}_{h,mo,p}$ represents the electricity load at hour *h* of holiday for month *mo* of province *p*; num^{ho}_{mo} represents the number of holiday in month *mo*; and num^{day}_{mo} represents the total number of days in month *mo*.

Third, according to the actual hourly electricity consumption in 2019 in Anhui Province, the variation proportion of electricity demand in each hour is calculated, as shown in equation (S127).

$$PP^{Anhui}_{h,da,mo} = EL^{Anhui}_{h,da,mo} / \left(\frac{\sum_{da} EL^{Anhui}_{h,da,mo}}{num^{day}_{mo}}\right) \tag{S127}$$

where $PP^{Anhui}_{h,da,mo}$ represents the Anhui province's variation proportion of actual electricity demand to the average electricity demand at hour *t* on day *da* in month *mo*; $EL^{Anhui}_{h,da,mo}$ represents the actual electricity demand of the Anhui province at hour *t* on day *da* in month *mo*.

Finally, the hourly electricity demand for each province of the whole year is calculated referring to the hourly electricity demand variation proportion of Anhui Province, as shown in Equation (S128):

$$EL_{h,da,mo,pr} = AEL_{h,mo,pr} \cdot PP^{Anhui}_{h,da,mo} \tag{S128}$$

where $EL_{h,da,mo,pr}$ represents the electricity demand of province *pr* at hour *t* on day *da* in month *mo*, which is eventually used to calculate the national electricity demand.

K-means clustering. In this study, we applied the K-means data clustering method to reduce the hourly granular data of wind power, solar PV AF, and electricity demand to obtain a manageable size. The K-means data clustering method assigns the original data into *c* clusters and minimizes the Euclidean distance between the data points in the clusters and the cluster mean or centroid [71]. According to the hourly AF values of wind power (including onshore and offshore wind power) and solar PV and the national hourly electricity demand, we first normalized the 4-dimensional data space to achieve equal weights for all input vectors (the electricity demand and the AF values of onshore wind, offshore wind and solar PV). Then, these data were clustered into 25 categories. In this way, the days of cluster *c* ($phiD_c$), the AF value per hour of cluster *c* of variable renewable energy technology *ivre* ($AF_{ivre,c,h}$), and the electricity demand per hour of cluster *c* in planning year *a* ($PD_{a,c,h}$) could be obtained. The specific clustering results are shown in Supplementary Table 2 and Supplementary Fig. 16.

Table 2. The duration days of a representative day in each cluster

Cluster	Duration days	Cluster	Duration days
1	15	14	30
2	10	15	23
3	26	16	12
4	3	17	25
5	14	18	9
6	3	19	20
7	21	20	9
8	24	21	25
9	3	22	8
10	8	23	9
11	20	24	12
12	12	25	17
13	7		

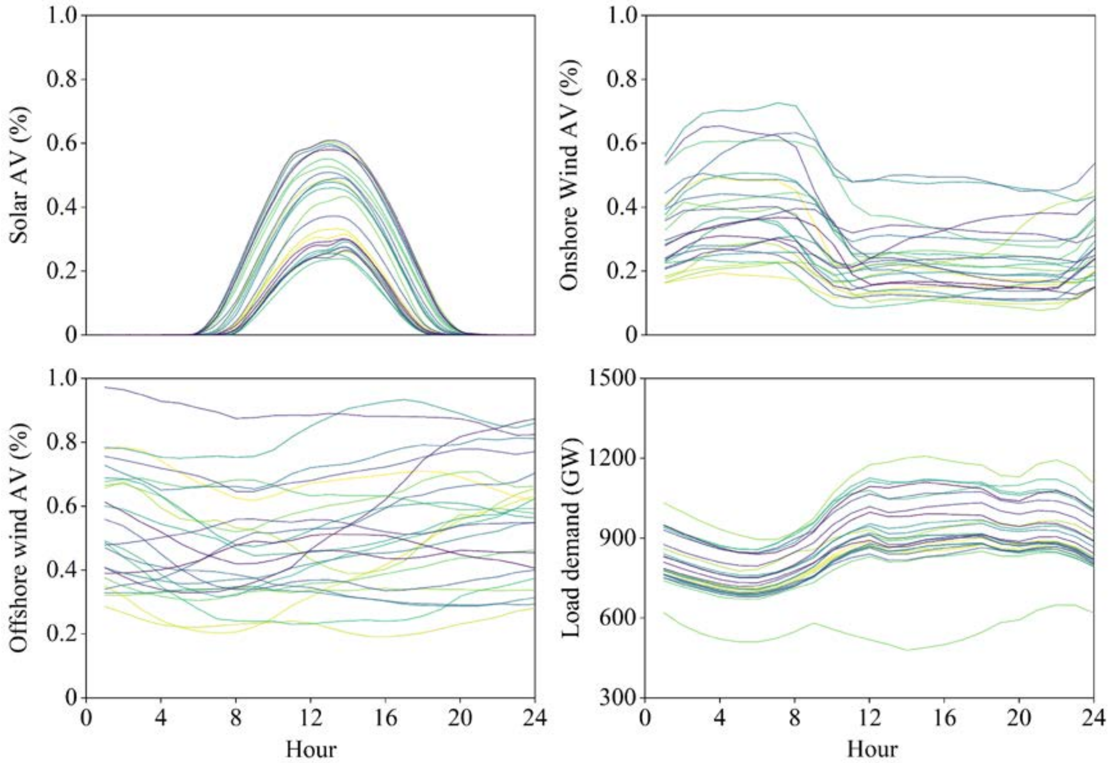

Figure 16. The 25-class clustering results for the load demand and the availability factor of solar, onshore wind and offshore wind (each line represents a different cluster).

CBECCS dynamic source–sink matching optimization model

Referring to the static model, all screened CBECCS-ready plants, storage sites, and disaggregated pipelines were compiled into nodes and arcs as model inputs, with the same dataset definitions of N, n, I, J, and $Arc(n,m)$.

Objective function. The model objective was to minimize the total cost of full-chain CCS technical links attributed to the retrofitted CBECCS plants across all phases, as expressed in equation (S129):

$$\begin{aligned} min\ COST^{dyn} &= \sum_i \sum_a Scap_{i,a}^{dyn\text{-}cum} \cdot Ccost_a^{aver} \cdot S_{i,a} + \sum_j \sum_a Rsto_{j,a}^{dyn\text{-}cum} \cdot Scost_a^{aver} \cdot R_{j,a} \\ &+ \sum_{(n,m)} \sum_d \sum_a (Peq_{d,a} + Pom_{d,a}) \cdot Dist_{(n,m)} \cdot P_{(n,m),d,a} \end{aligned} \tag{S129}$$

where a (a=1, 2 …, 9) denotes the planning year derived from the PSOM, i.e., 2020 is represented by a=1, and 2060 is represented by a=9; $COST^{dyn}$ is the total cost of CBECCS deployment across all phases; $S_{i,a}$ is a binary variable that indicates whether CBECCS-ready plant i can be matched with storage sites via pipelines (i.e., the plant can be retrofitted as a CBECCS plant) in planning year a (if this is the case, $S_{i,a} = 1$; otherwise, $S_{i,a} = 0$); $Scap_{i,a}^{dyn\text{-}cum}$ is the cumulative amount of CO_2 captured from CBECCS plant i from planning year a to 2060, which equals DCE_i^{Total} (by summing $DCE_{i,t}$ from planning year a to 2060) multiplied by a 90% capture rate, as expressed in equation (S15); $Ccost_a^{aver}$ is the average capture cost per unit of CO_2 from planning year a to 2060 after considering the time-phased technological learning rate and discount rate; $R_{j,a}$ is a binary variable that indicates whether storage site j can be linked to CBECCS plants via pipelines in planning year a (i.e., the site can be activated for CO_2 injection), with $R_{j,a} = 1$ if this is the case and $R_{j,a} = 0$ otherwise; $Rsto_{j,a}^{dyn\text{-}cum}$ is the newly added cumulative CO_2 storage at storage site j from planning year a to 2060; $Scost_a^{aver}$ is the average storage cost per unit of CO_2 from planning year a to 2060 after considering the time-phased technological learning rate and discount rate; $P_{(n,m),d,a}$ is a binary variable that indicates whether arc (n,m) with diameter d can be used for CO_2 flow transportation in planning year a, with $P_{(n,m),d,a} = 1$ if this is the case and $P_{(n,m),d,a} = 0$ otherwise; $Dist_{(n,m)}$ is the pipeline length following the actual geographic path of arc (n,m); $Peq_{d,a}$ is the initial capital cost per unit of the length for pipelines with diameter d in planning year a, discounted to 2025, including the primary raw material cost, valve station cost, and installation cost; $Pom_{d,a}$ is the cumulative O&M cost per unit of the length for pipelines with diameter d from planning year a to 2060 considering the discount rate.

Constraints. First, some CBECCS-ready plants can be retrofitted to satisfy their dynamic CBECCS mitigation demands under carbon neutrality, as expressed in equation (S130):

$$\sum_i Scap_{i,a}^{dyn\text{-}cum} \cdot S_{i,a} \geq T_a^{dyn\text{-}cum},\ \forall a \tag{S130}$$

where $T_a^{dyn\text{-}cum}$ is the newly added cumulative CO_2 sequestration that must be achieved from planning year a to 2060 derived from the PSOM.

Second, a specific CBECCS plant can only be retrofitted once at most across all phases and can continue to be operated until 2060, as expressed in equation (S131):

$$\sum_a S_{i,a} \leq 1,\ \forall i \in I \tag{S131}$$

Third, CO_2 flow conservation within the CO_2 pipeline network across all phases can be obtained with equation (S132):

$$\begin{gathered} Rsto_{n,a}^{dyn\text{-}cum} \cdot R_{n,a}^N = Scap_{n,a}^{dyn\text{-}cum} \cdot S_{n,a}^N + \sum_{(m,n)} amount_{(m,n),a}^{annual} \cdot Period_a - \sum_{(n,m)} amount_{(n,m),a}^{annual} \cdot Period_a \\ \forall a;\ n \in N \end{gathered} \tag{S132}$$

where n is any possible node (e.g., CO_2 sources, CO_2 sinks, and other intersections) that belongs to the overall node dataset N (if node n is identified as a storage site in planning year a, then $R_{n,a}^N = 1$, and otherwise, $R_{n,a}^N = 0$; if node n is identified as a CBECCS plant in planning year a, then $S_{n,a}^{N}=1$, and otherwise, $S_{n,a}^{N}=0$); $amount_{(n,m),a}^{annual}$ is the newly added CO_2 flow within arc (n,m) from nodes *n* to *m* in planning year *a*, while $amount_{(m,n),a}^{annual}$ denotes the opposite flow; and $Period_a$ is the entire period from the various deployment planning years to 2060.

Fourth, one proposed pipeline can only be built once by following the same arc in the various deployment planning years, as expressed in equation (S133):

$$\sum_d \sum_a P_{(n,m),d,a} \le 1,\ \forall (n,m) \in Arc(n,m) \tag{S133}$$

Fifth, the actual CO_2 flow in arc (n,m) cannot exceed the upper flow limit based on the selected diameter *d*, and the newly added CO_2 flows from later retrofitted CBECCS plants can be transported via previously built pipelines, as expressed in equation (S134):

$$\sum_a amount_{(n,m),a}^{annual} \le \sum_d \sum_a P_{(n,m),d,a} \cdot Prate_d,\ \forall (n,m) \in Arc(n,m) \tag{S134}$$

where $Prate_d$ is the upper flow limit for pipelines with diameter *d*.

Sixth, the cumulative CO_2 storage at storage site *j* cannot exceed the storage potential across all phases, as expressed in equation (S135):

$$\sum_a Rsto_{j,a}^{dyn\text{-}cum} \le Csto_j,\ \forall j \in J \tag{S135}$$

where $Csto_j$ is the storage potential of storage site *j*.

Finally, the annual CO_2 storage at storage site *j* cannot exceed the injection rate capacity across all phases, as expressed in equation (S136):

$$\sum_a \frac{Rsto_{j,a}^{dyn\text{-}cum}}{Period_a} \le Vin_j \cdot 50,\ \forall j \in J \tag{S136}$$

where Vin_j is the single-well injection rate capacity at storage site *j*, and 50 injection wells were assumed for each site based on engineering experience.

Calculation of the CO_2 emission reduction through CBECCS deployment

The total CO_2 captured through CBECCS can be calculated by equation (S137):

$$Scap_{i,t}^{annual} = 0.9 \cdot DCE_{i,t} \tag{S137}$$

where $Scap_{i,t}^{annual}$ is the total CO_2 captured from power plant *i* in year *t*, including the emissions resulting from both coal and biomass combustion, with a CO_2 capture rate of 0.9 [27]; and $DCE_{i,t}$ denotes the direct CO_2 emissions in flue gas from CBECCS plant *i* in year *t*, as expressed in equation (S13).

Thus, the total CO_2 emission reduction, the net negative emissions through CBECCS deployment, and the net emissions associated with extra life-cycle emissions can be calculated with equations (S138)-(S140):

$$TRE_{i,t} = Scap_{i,t}^{annual} + SCE_{i,t}^{r} \tag{S138}$$

$$\Delta TRE_{i,t} = TRE_{i,t} - TCE_{i,t} \tag{S139}$$

$$NCE_{i,t} = \Delta TRE_{i,t} + CE_{i,t}^{lc} \tag{S140}$$

where $TRE_{i,t}$ is the total CO_2 emission reduction at CBECCS plant *i* in year *t* due to the sequestration of CO_2 emissions resulting from both coal and biomass combustion, as well as biomass substitution; $SCE_{i,t}^{r}$ is the emission reduction caused by biomass substitution at CBECCS plant *i* in year *t*, as expressed in equation (S10); $\Delta TRE_{i,t}$ denotes the net negative emissions of CBECCS plant i in year t, i.e., the difference between the total CO_2 emission reduction and the initial CO_2 emissions before CBECCS retrofitting; $TCE_{i,t}$ denotes the annual initial CO_2 emissions of power plant i in year t, as expressed in equation (S4); $NCE_{i,t}$ denotes the net emissions associated with the extra life-cycle emissions of CBECCS plant i in year t; and $CE_{i,t}^{lc}$ denotes the extra life-cycle emissions of CBECCS plant i in year t, as expressed in equation (8) in Methods. Additionally, the cumulative CO_2 emission reduction, cumulative net negative emissions attributed to CBECCS deployment, and cumulative net emissions associated with the extra life-cycle emissions of CBECCS plant i can be obtained by summing the cumulative annual CO_2 capture amounts from the various CBECCS deployment years to 2060 for both the static and dynamic assessments. Note that the biomass substitution effect was only evaluated in the supply potential assessment instead of the mitigation contribution assessment.

APSIM model for energy crop estimation

In addition to the GIS-based land use model associated with suitable marginal land selection criteria, the production potential of switchgrass and miscanthus in China was also simulated by using the plant growth model, the Agricultural Production System Simulator (APSIM) model [72]. In this study, the APSIM model was applied to a spatial scale simulation. We first extract marginal lands suitable for planting switchgrass and miscanthus in China using ArcGIS and then calibrate the key parameters of the APSIM model related to meteorological, soil, and crop growth from the literature (see Supplementary Table 16 for details) and field observations [73-75]. With the marginal lands and key parameters, the future production of switchgrass and miscanthus could be finally simulated gird by grid via the APSIM model.

The future climate data used in the APSIM model has been widely used for climate impact assessments within the framework of the Inter-Sectoral Impact Model Intercomparison Project (ISIMIP) [76, 77], which were spatially downscaled and bias-corrected from the observation data [78]. The soil parameters were sourced partly from soil profile measurements collected before planting at the test site, and partly from the literature. Soil hydraulic parameters during the surface scale simulation were obtained from the database established by Dai, Shangguan [79]. Land use prediction data were mainly sourced from the database established by Liao, Liu [80] (https://geosimulation.cn/China_PFT_SSP-RCP.html).

Data sources and processing

Capture rate of CBECCS plants. In this study, we select a 90% capture rate to ensure economic benefit by using amine-based post-combustion capture for the coal-fired power sector, referring to previous literatures [81-83] and engineering practice of CCUS demonstration projects, e.g., the National Energy Group Jinjie Power Plant, China’s largest operational CCUS project for thermal power. The 90% capture rate is assumed to be unchanged over the study period considering its slow progress in previous decades [84]. To achieve net-zero emissions, we tend to address residual emissions due to incomplete capture via co-fire biomass with coal combustion combined with CCUS (i.e., CBECCS in this study), which is also viewed as a more economic approach than enhancing the CO_2 capture rate to near 100% [82, 85].

Biomass resources data. The data of various crop yields in the base year (2015) were collected from the Statistical Yearbook of China 2016, which included a total of 10 crops, i.e., rice, corn, wheat, cotton, oilseeds, beans, tubers, hemp, sugarcane, and beet, from 31 provinces across China (Supplementary Table 3). The residue to product ratio (RPR) values of the main crops that reflect straw productivity under current farming systems and cultivation technologies were obtained from a previous study [86] (Supplementary Table 4). The statistical data of the yield of forest residues in each province were collected from the "China Forestry Statistical Yearbook 2013", the "China Forest Resources Report (2009-2013)", the "China Forest Resources Statistics-The Seventh National Forest Resources Census", and the "China Forest Resources Statistics-The Eighth National Forest Resources Census".

Table 3. Selected crop yields in 2015 from 31 provinces across China (10,000 tons)

Province	rice	corn	wheat	cotton	oil	bean	potato	hemp	sugarcane	beet
Beijing	0.1	49.5	11.1	0.0	0.6	0.7	0.8	0.0	0.0	0.0
Tianjin	11.4	107.3	59.8	2.6	0.4	1.3	0.7	0.0	0.0	0.0
Hebei	54.5	1670.4	0.2	37.3	151.5	29.5	103.9	0.1	0.0	89.2
Shanxi	0.5	862.7	271.4	1.4	15.3	30.6	36.7	0.0	0.0	5.5
Inner Mongolia	53.2	2250.8	158.3	0.0	193.6	103.0	147.0	0.0	0.0	230.1
Liaoning	467.7	1403.5	2.7	0.0	46.1	27.2	48.0	0.0	0.0	5.2
Jilin	630.1	2805.7	0.1	0.0	76.4	48.6	59.5	0.0	0.0	1.3
Heilongjiang	2199.7	3544.1	21.8	0.0	18.3	437.3	100.3	2.0	0.0	7.3
Shanghai	84.0	2.1	19.9	0.0	1.2	0.8	0.6	0.0	0.6	0.0
Jiangsu	1952.5	252.2	1174.0	11.7	143.1	73.5	32.9	0.1	9.5	0.1
Zhejiang	578.1	31.1	35.1	2.0	31.4	35.8	60.8	0.0	62.2	0.0
Anhui	1459.3	496.3	1411.0	23.4	227.9	134.0	32.7	2.6	20.3	0.0
Fujian	485.0	21.5	0.6	0.0	30.7	23.3	128.4	0.0	43.6	0.0
Jiangxi	2027.2	12.8	2.6	11.5	124.0	33.1	71.4	0.7	65.8	0.0
Shandong	95.1	2050.9	2346.6	53.7	324.1	38.8	173.9	0.0	0.0	0.0
Henan	531.5	1853.7	3501.0	12.6	599.7	53.8	110.8	2.9	24.3	0.0
Hubei	1810.7	332.9	420.9	29.8	339.6	28.7	99.4	2.2	32.0	0.0
Hunan	2644.8	188.8	9.4	14.5	242.9	34.3	118.8	1.6	66.0	0.0
Guangdong	1088.4	77.9	0.3	0.0	110.3	21.6	167.7	0.0	1452.9	0.0
Guangxi	1137.8	280.7	0.9	0.3	64.7	23.9	78.4	1.1	7504.9	0.0
Hainan	153.3	0.0	0.0	0.0	11.3	2.1	28.6	0.1	264.8	0.0
Chongqing	506.4	259.7	22.9	0.0	59.9	47.9	306.8	0.9	9.8	0.0
Sichuan	1552.6	765.7	426.3	1.0	307.6	99.9	516.3	5.3	54.0	0.1
Guizhou	417.5	324.1	61.7	0.1	101.3	34.4	303.8	0.1	156.1	0.0
Yunnan	659.7	747.3	90.6	0.0	65.9	136.4	194.2	0.1	1930.1	0.0
Tibet	0.5	0.8	23.4	0.0	6.4	2.0	0.7	0.0	0.0	0.0
Shaanxi	91.9	543.1	458.1	3.9	62.7	21.2	85.7	0.1	0.1	0.0

Gansu	3.1	577.2	281.0	4.3	71.6	36.2	225.3	0.3	0.0	16.1
Qinghai	0.0	18.6	34.1	0.0	30.5	5.6	34.8	0.0	0.0	0.0
Ningxia	60.8	226.9	39.6	0.0	15.3	3.4	37.2	0.0	0.0	0.0
Xinjiang	65.1	705.1	698.3	350.3	62.9	20.8	20.0	0.0	0.0	448.3

Table 4. Residue-to-product-ratios of different crops

crop types		RPR	crop types	RPR
grain	rice	1.0	beans	1.7
	wheat	1.1	potato	1.0
	corn	2.0	hemp	1.7
cotton		3.0	sugarcane	0.1
oil		2.0	beet	0.1

The land use data required for the calculation of agricultural and forestry residues were collected from the "National Land Use/Cover Database of China 2015" (1 km×1 km resolution), provided by the Institute of Geographic Sciences and Natural Resources Research, CAS, where the pixel value represents both percentages of each current and future land use. The future farmland and forest land for selected years (2025, 2030, and 2060) were calculated using the CA-Markov model with the scenario-analysis method with the support of IDRISI (an integrated GIS and Image Processing software solution), taking 2015 as the starting point.

A multifactor comprehensive evaluation method was used to extract the marginal lands suitable for miscanthus and switchgrass cultivation nationwide. The evaluation index system of marginal land of miscanthus and switchgrass is based on previous studies, expert consultations, and relevant policies [87-91], as shown in Supplementary Tables 5-6. The minimum and maximum yield per unit area for miscanthus and switchgrass, which are used to calculate the total yield of these two energy crops on average, were estimated based on the literature [87, 91-96], as shown in Supplementary Table 7. We combined marginal lands of miscanthus and switchgrass according to the strategy of prioritizing the development of miscanthus, as shown in Supplementary Fig. 2c.

Table 5. The evaluation index system of marginal land of miscanthus

Categories	Parameters	Detailed descriptions
land use	land-use type	shrubbery, open woodland, grassland, mudflat, saline, and bare land
	nature reserve	exclusive of nature reserves
	grassland	exclusive of high and moderate coverage grasslands that belong to the provinces where the five major pastures are located (Qinghai, Xinjiang, Inner Mongolia, Tibet, Ningxia)
terrain data	slope/°	<25
soil	pH(H_2O)	4.2-8.0

	soil organic matter/%	>1.5
	annual mean temperature/°C	15-28
meteorological data	active accumulated temperature/°C	⩾400
	annual precipitation/mm	⩾600
	frost-free period/d	⩾110

Table 6. The evaluation index system of marginal land of switchgrass

Categories	Parameters	Detailed descriptions
land use	land-use type	shrubbery, open woodland, grassland, mudflat, saline, and bare land
	nature reserve	exclusive of nature reserves
	grassland	exclusive of high and moderate coverage grasslands that belong to the provinces where the five major pastures are located (Qinghai, Xinjiang, Inner Mongolia, Tibet, Ningxia)
terrain data	slope/°	<25
soil	pH (H_2O)	4.2-8.0
	soil organic matter/%	>1.5
meteorological data	annual precipitation/mm	＞350

Table 7. Yield per unit area of miscanthus and switchgrass

Energy crops	dry matter yield (t/ha)	
	min	max
miscanthus	15	60
switchgrass	8	35

The spatial data required for assessing energy crops were collected from various data sources shown in Supplementary Table 8, including databases related to land use, geographic information, natural environment, and ecological protection. For details, the Digital Elevation Model (DEM) database was used to show the geographic information derived from the Shuttle Radar Topography Mission V4 (SRTM V4). Based on this database, the corresponding slopes were calculated by the spatial analysis of ArcGIS. The 1:100,000 soil database of China was collected from the Resource and Environment Science Data Center (RESDC) and the Cold and Arid Regions Science Data Center (CARSDC) from the Chinese Academy of Sciences (CAS). It contains spatial information such as soil thickness, soil organic matter content, soil texture, and soil pH value. The meteorological database was derived from the China Meteorological Administration (CMA) and RESDC. The database of temporal and spatial variation in the frost-free period was obtained from the Global Change Data Publishing & Repository (GCdataPR).

Table 8. Databases required for data extraction of marginal land of energy crops

Categories		Formats	Detailed descriptions	Resolutions	Sources
land use	-	Grid	shrubbery, open woodland, grassland, mudflat, saline, and bare land	1 km	RESDC
geography	DEM	Grid	elevation and slope	1 km	SRTM V4
natural environment	soil	Grid/ Shapefile	soil texture, sand content, soil thickness, soil organic matter, and pH	1 km	RESDC
	temperature	Grid	monthly mean temperature, extreme temperature, and ≥10° accumulated temperature	1 km	CMA RESDC
	moisture	Grid	annual mean temperature	1 km	RESDC
	heat	Grid	frost-free period	1 km	GCdataPR
ecological protection	nature reserve	Shapefile	exclusive of nature reserves	1:10,000	RESDC

Note: Resource and Environment Science Data Center (RESDC); Shuttle Radar Topography Mission V4 (SRTM V4); China Meteorological Administration (CMA); Global Change Data Publishing & Repository (GCdataPR).

The three major types of biomass feedstock resources in China were finally obtained, i.e., agricultural residues (0.48 billion tons of coal equivalent, tce for abbreviation, in 2015), forest residues (0.68 billion tce in 2015), and potential energy crops (projected as 1.33 billion tce by 2025).

Biomass emissions calculation. The mean lower heating value (LHV)and conversion coefficient of raw coal, agricultural residues, and forestry residues were obtained from the "China Energy Statistics Yearbook" [97]. The carbon contents of agricultural residues and forest residues were obtained from the "2006 IPCC Guidelines for National Greenhouse Gas Inventory" [8]. The carbon contents and conversion coefficients of switchgrass and miscanthus were derived from the GREEN model, corresponding to the carbon emission factors in the model [98].

Geological storage potential and injection capacity data. The data on recoverable reserves, API, depth, locations, and porosities of oil fields were collected from the "Petroleum Basin Atlas of China" [99] and IHS Markit [100]. The depth and thickness of saline aquifers were derived from "Geological Surveys in China" [101]. The areas were calculated by ArcGIS, and the shapefiles of basins and reservoirs were obtained by vectorization of the original information.

Carbon emission caps in the CGE model. The CGE model considers only energy-related CO_2 emissions. We calculated the energy-related CO_2 emissions for the baseline year (2018) using the IPCC CO_2 emission accounting methodology based on the energy consumption by species from the China Energy Statistics Yearbook [102]. The time-series change in China's energy-related CO_2

emissions from 2018 to 2060 under the carbon neutrality target is referenced to the carbon emission distribution interval given in Zhang, Huang [103], as shown in Supplementary Fig. 17.

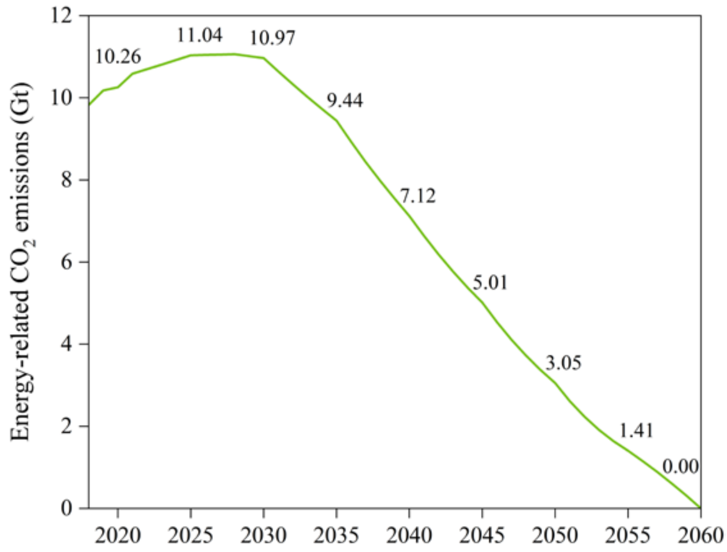

Figure 17. China's energy-related CO_2 emissions from 2018 to 2060.

Installed capacity and power generation data. The installed capacity and power generation data for various technologies are shown in Supplementary Table 9. Specifically, the data of initial installed capacity and power generation for various technologies in 2020 were collected from the "China Electric Power Yearbook 2021" [104], "Global Power Plant Database" [105], "Construction of biomass power generation in various provinces in 2020" [106], "Installed capacity of offshore wind for province at the end of 13th Five-year Plan" [107] and "White Papers of Research on Chinese Energy Storage Industry" [108]. The initial installed capacity and power generation of CCS technologies are set to zero because they are currently in the demonstration stage. The annual build rate limitation was calculated by the "China Energy & Electricity Outlook" [109]. We assume that no new coal-fired power plants without CCS will be built in China due to their high emissions and the current strict emission reduction targets. The annual build rate limitation of retrofitting technologies depends on the capacity of the coal-fired power generation units that can be retrofitted at each stage. Except for the retrofitting technologies, the maximum capacity deployment limitations for other technologies were calculated based on their construction capability and environment. The maximum capacity deployment limitation of retrofitting technologies was filtered from the data of existing coal-fired power generation units in China.

Table 9. Installed capacity and power generation data for various technologies

Technologies	Initial installed capacity (MW)	Initial power generation (TWh)	Annual build rate limitation (MW/year)	Maximum capacity deployment limitation (MW)
Coal	1079400	4629.6	0	1079400

RCoal CCS	0	0	-	350000
CBECCS	0	0	-	350000
Coal CCS	0	0	14640	150600
Gas	99900	252.5	7650	153450
Gas CCS	0	0	7740	76950
Hydro	338830	1321.8	11160	533386
Nuclear	49914	366.2	9770	233640
Biomass	29880	135.5	2502	120000
BECCS	0	0	2500	80000
Onshore Wind	271000	428.6	44800	2050000
Offshore Wind	9390	37.9	12000	450000
Solar	253560	261.1	121250	3800000
PHSto	31500	33.5	11995	450072
GenSto	3270	3.5	14000	300000

Designed lifetime and initial remaining lifetime data. The designed lifetime and initial remaining lifetime data for various technologies are shown in Supplementary Table 10. The designed lifetimes were derived from Liang, Yu [110], Heuberger, Rubin [63] and "Cost Projections for Utility-Scale Battery Storage" [111]. The remaining lifetime was calculated by the designed lifetime minus the average service life. The average service life of various technologies can be obtained from "Research on Flexible Operation and Life Extension Operation of Coal-fired Unit" [112] and "National Nuclear Power Operation" [113, 114]. The value was adjusted to a multiple of 5 according to the requirements of the model.

Table 10. Designed lifetime and remaining lifetime data for various technologies

Technologies	Designed lifetime (Year)	Remaining lifetime in 2020 (Year)
Coal	40	30
RCoal CCS	40	40
CBECCS	40	40
Coal CCS	40	40
Gas	30	25
Gas CCS	30	30
Hydro	80	75
Nuclear	60	55
Biomass	20	15
BECCS	20	20
Onshore Wind	25	20
Offshore Wind	30	30
Solar	25	20
PHSto	60	55
GenSto	15	15

Technical parameters data of the power system optimization model. The parameters of generation technologies and energy storage technologies, including minimum and maximum output, credit capacity rate, inertia constant reserve potential, minimum and maximum capacity factor, round-trip efficiency and maximum discharge time, were collected from Zhuo, Du [61] and Heuberger, Rubin [63], as shown in Supplementary Table 11.

Table 11. The parameters of generation technologies and energy storage technologies

Technology	Minimum output (%)	Maximum output (%)	Credit capacity rate (%)	Inertia Constant (s)	Reserve potential (%)	Minimum capacity factor (%)	Maximum capacity factor (%)	Round-trip Efficiency (%)	Maximum discharge time (h)
Coal	0.4	1	1	5.89	1	0	0.6	-	-
RCoal CCS	0.4	1	1	5.89	1	0.5	0.69	-	-
CBECCS	0.4	1	1	5.89	1	0.5	0.69	-	-
Coal CCS	0.4	1	1	5.89	1	0.5	0.69	-	-
Gas	0.3	1	1	4.97	1	0	0.45	-	-
Gas CCS	0.3	1	1	4.97	1	0.5	0.45	-	-
Hydro	0	1	1	2.83	1	0.4	0.54	-	-
Nuclear	0.5	1	1	4.07	1	0.7	0.91	-	-
Biomass	0.35	1	1	2.94	1	0	0.61	-	-
BECCS	0.35	1	1	5.89	1	0.5	1	-	-
Onshore Wind	0	1	0.38	0	0	0	1	-	-
Offshore Wind	0	1	0.42	0	0	0	1	-	-
Solar	0	1	0.17	0	0	0	1	-	-
PHSto	0	1	1	2.83	1	0	1	0.7	10
GenSto	0	1	1	5.89	1	0	1	0.85	4.5

Other parameter data of the power system. The other parameter data of the power system include the required reserve rate, line loss rate, spinning factor and system inertia, as shown in Supplementary Table 12. The required reserve rate is set to approximately 13%-15% based on the "reserve rate of power system" [115]. The line loss rate was obtained from the "China Electric Power Yearbook 2021" [104]. The remaining data were set according to the actual values for China's power system.

Table 12. Other parameters of the power system

Required reserve rate (%)	Line loss rate (%)	Spinning factor (%)	System inertia (%)
0.15	0.056	0.05	4

Power system carbon emission caps. The power system emission caps at each stage originated from the CGE model, as shown in Supplementary Table 13. The emission factors for various technologies at each stage were calculated according to the IPCC carbon emission accounting methodology, as shown in Supplementary Table 14.

Table 13. Power system emission caps at each stage ($GtCO_2$)

2020	2025	2030	2035	2040	2045	2050	2055	2060
3.78	3.89	3.34	2.44	1.58	0.94	0.39	-0.11	-0.40

Table 14. Emission factors for various technologies at each stage (tCO_2/MWh)

	2020	2025	2030	2035	2040	2045	2050	2055	2060
Coal	0.79	0.78	0.76	0.73	0.70	0.67	0.64	0.64	0.64
RCoal CCS	0.11	0.10	0.09	0.09	0.08	0.08	0.07	0.07	0.07
CBECCS	-0.07	-0.06	-0.06	-0.05	-0.05	-0.05	-0.04	-0.04	-0.04
Coal CCS	0.11	0.10	0.09	0.09	0.08	0.08	0.07	0.07	0.07
Gas	0.38	0.37	0.37	0.36	0.35	0.34	0.33	0.33	0.33
Gas CCS	0.05	0.05	0.04	0.04	0.04	0.04	0.04	0.04	0.04
Hydro	0.00	0.00	0.00	0.00	0.00	0.00	0.00	0.00	0.00
Nuclear	0.00	0.00	0.00	0.00	0.00	0.00	0.00	0.00	0.00
Biomass	0.00	0.00	0.00	0.00	0.00	0.00	0.00	0.00	0.00
BECCS	-2.38	-2.03	-1.77	-1.56	-1.40	-1.30	-1.21	-1.16	-1.10
Onshore Wind	0.00	0.00	0.00	0.00	0.00	0.00	0.00	0.00	0.00
Offshore Wind	0.00	0.00	0.00	0.00	0.00	0.00	0.00	0.00	0.00
Solar	0.00	0.00	0.00	0.00	0.00	0.00	0.00	0.00	0.00
PHSto	0.00	0.00	0.00	0.00	0.00	0.00	0.00	0.00	0.00
GenSto	0.00	0.00	0.00	0.00	0.00	0.00	0.00	0.00	0.00

Initial investment cost and learning rate of various technologies. The data on the initial investment cost for various technologies were collected from Zhuo, Du [61] and the “Report On China's Electric Power Development 2020”[116]. The learning rate for various technologies used in this study referred to NREL’s annual technology baseline (ATB) model results published in 2021 [117].

Table 15. Initial investment cost and learning rate of various technologies

	Initial investment cost (CNY/MW)	Learning rate (%)
Coal	3636000	-
Rcoal-PostCCS	4373000	0.0725
Bio-PostCCS	4751845	0.0755
Coal-PostCCS	8009000	0.0630
Gas	2104000	0.0291
Gas-PostCCS	6020000	0.0754
Hy	14561000	-0.0105
Nuclear	16000000	0.0380
Biomass	10528000	0.0440

BECCS	14901000	0.0590
Onshore Wind	6250000	0.0683
Offshore Wind	16000000	0.0878
Solar	3400000	0.0755
PHSto	5969000	0.0140
GenSto	3200000	0.1084

Parameters of the APSIM model. The data for planting switchgrass and miscanthus in different regions of China are shown in Supplementary Table 16.

Table 16. Experimental results of planting switchgrass and miscanthus in different regions of China based on the existing literature

Category	Dry matter yield (t/hm^2)	Sources
switchgrass	7.5-9 (Inner Mongolia, China)	118
	10-25 (The European Union/The US）	119
	8-35	95
	18 (Dingxi, China)	120
	3.47-44.22 (Yangling Area, China)	121
	23 (Beijing, China)	122
	20.03±1.02	123
	14-20	124
	6.77-28.33	125
	12.3-39.5 (The U.S.)	126
	6.91-18.45	127
miscanthus	30-60	128
	15-30	129
	15-22 (Loess Plateau of China)	130
	50-70	131
	29.96±0.99	123
	10.5-33	132
	29.6-43.8	133
	10-40	95
	29.7 (Beijing, China)	125
	12-16	134
	2.1–33 t/ha	135

Sensitivity analysis for some key assumptions

Biomass supply potential assessment model. In the biomass supply potential assessment, we applied a GIS-based land-use model with a high resolution of 1×1 km^2 grid instead of a plant growth model with a relatively low resolution, e.g., 10×10 km^2 [136], thus providing more accurate boundary identification to ensure fine spatial matching of power plants and the surrounding available biomass amounts. Nevertheless, we reconstructed a plant growth model (APSIM) and found that the predictions showed a slight decrease of 20%-26% in the total biomass feedstock with a similar spatial distribution over the 2025-2060 period (Supplementary Fig. 18).

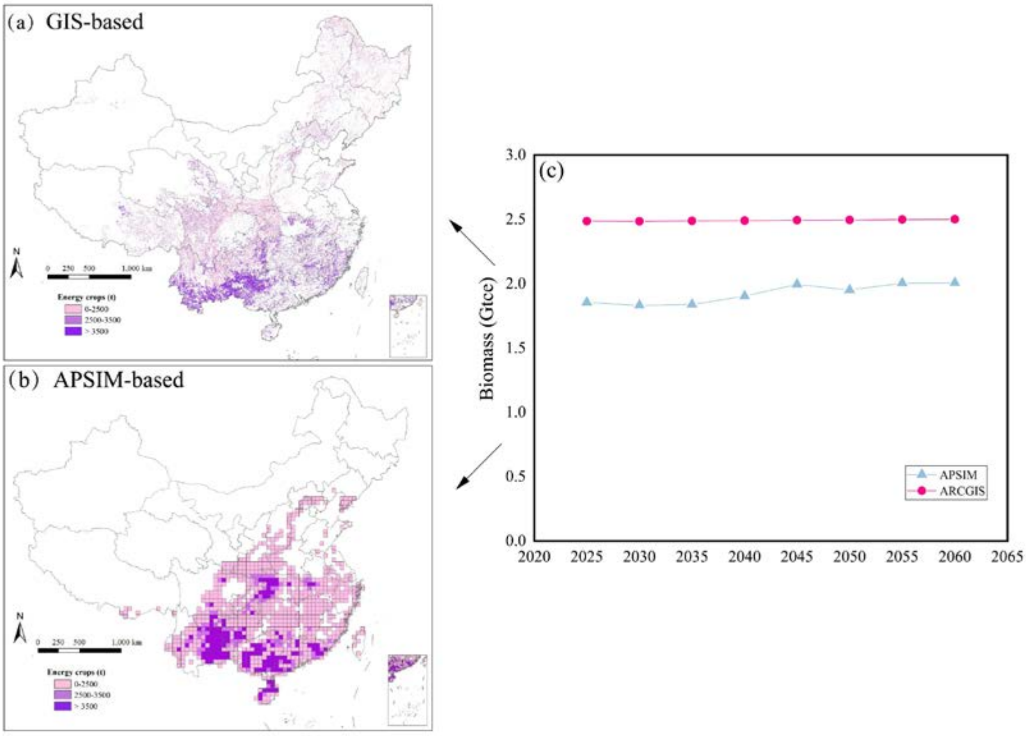

Figure 18. Total biomass feedstock and spatial distribution simulated by the GIS-based approach and APSIM. (**a**, the spatial distribution of energy crops by the GIS-based approach; **b**, the spatial distribution of energy crops by the APSIM; and **c**, the temporal variation in total biomass feedstock by the GIS-based approach and APSIM over the period 2025-2060. Note, the GIS-based approach is used in the major analysis of this study, while the APSIM-based approach is used for sensitivity analysis. Data Credits: All the provincial administrative boundaries are from Ministry of Civil Affairs of the People's Republic of China (http://xzqh.mca.gov.cn/map, Map Content Approval Number: GS(2022)1873))

CO_2 injection constraints and matching patterns in the CBECCS source-sink matching model. Whether or not injection rate capacity constraints are considered can have a significant impact on the optimal source-sink links between CBECCS plants and CO_2 storage sites. In the 2025 scenario, for instance, when there is no limit on the maximum CO_2 injection per year, more storage sites closer to CBECCS plants could be easily matched if their total storage potential is sufficient, resulting in the length of trunk pipeline construction being reduced by approximately 40%. Additionally, the CO_2 injection consideration will lead to a large variation in the number of matched storage sites. For example, in the Sichuan Basin where the injection rate capacity is relatively limited, 65 storage sites are matched with the CO_2 injection constraint, while only 28 are matched without the CO_2 injection constraint, indicating that there is no need to activate more remote CO_2 storage because more CO_2 injections are concentrated in large-capacity sites. In addition to a more realistic pipeline network-based matching approach, we provide a point-to-point matching pattern for comparison (Supplementary Fig. 19). With the same CBECCS plants involved in the 2025 scenario, the cost-optimized point-to-point matching network would require a total length of pipelines of over 84,000 km, or 1.7 times that of the proposed pipeline network.

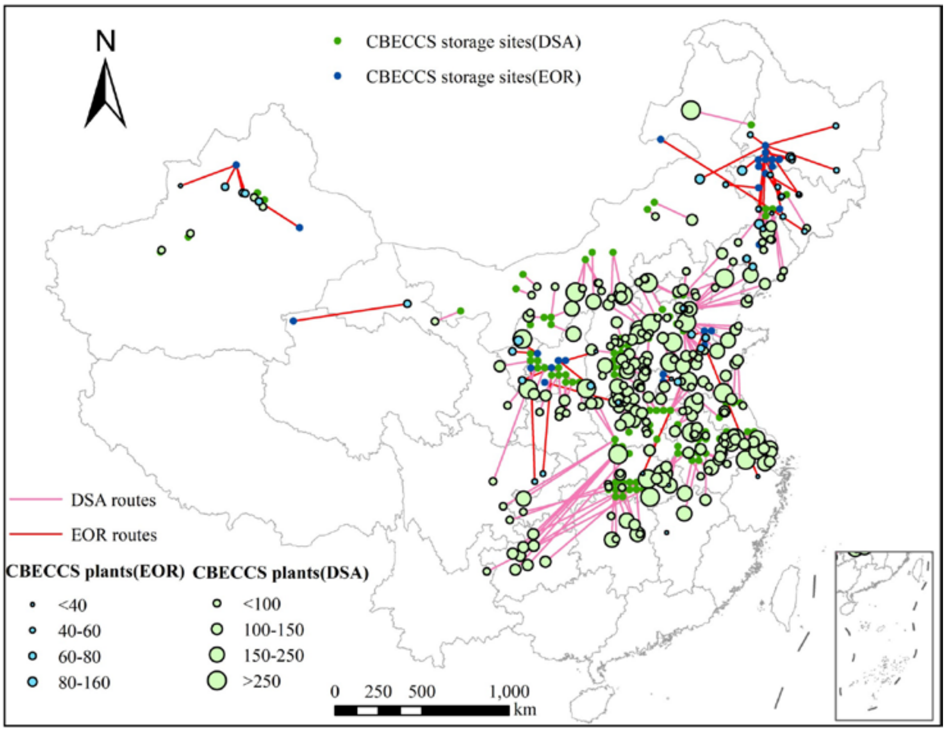

Figure 19. The cost-optimized point-to-point matching network with the same CO_2 sources and sinks in the 2025 scenario (Data Credits: All the provincial administrative boundaries are from Ministry of Civil Affairs of the People's Republic of China (http://xzqh.mca.gov.cn/map, Map Content Approval Number: GS(2022)1873))

Geological storage constraint in the power system optimization model. The geological storage constraint determines the maximum CBECCS retrofittable installed capacity in the power system optimization model and is also an important factor affecting the mitigation contribution of CBECCS technology. With other assumptions held constant, the mitigation contribution of the CBECCS technology in the scenario without consideration of the geological storage constraint is additionally simulated for comparison with the results of the scenario with consideration of the geological storage constraint. The results indicate that ignoring the geological storage constraint would overestimate the CBECCS mitigation contribution by 91.6% (from 1.4 to 2.7 Gt in 2060) (Supplementary Fig. 20). Therefore, considering the geological storage constraint can make the simulation results of the power system model more reflective of reality.

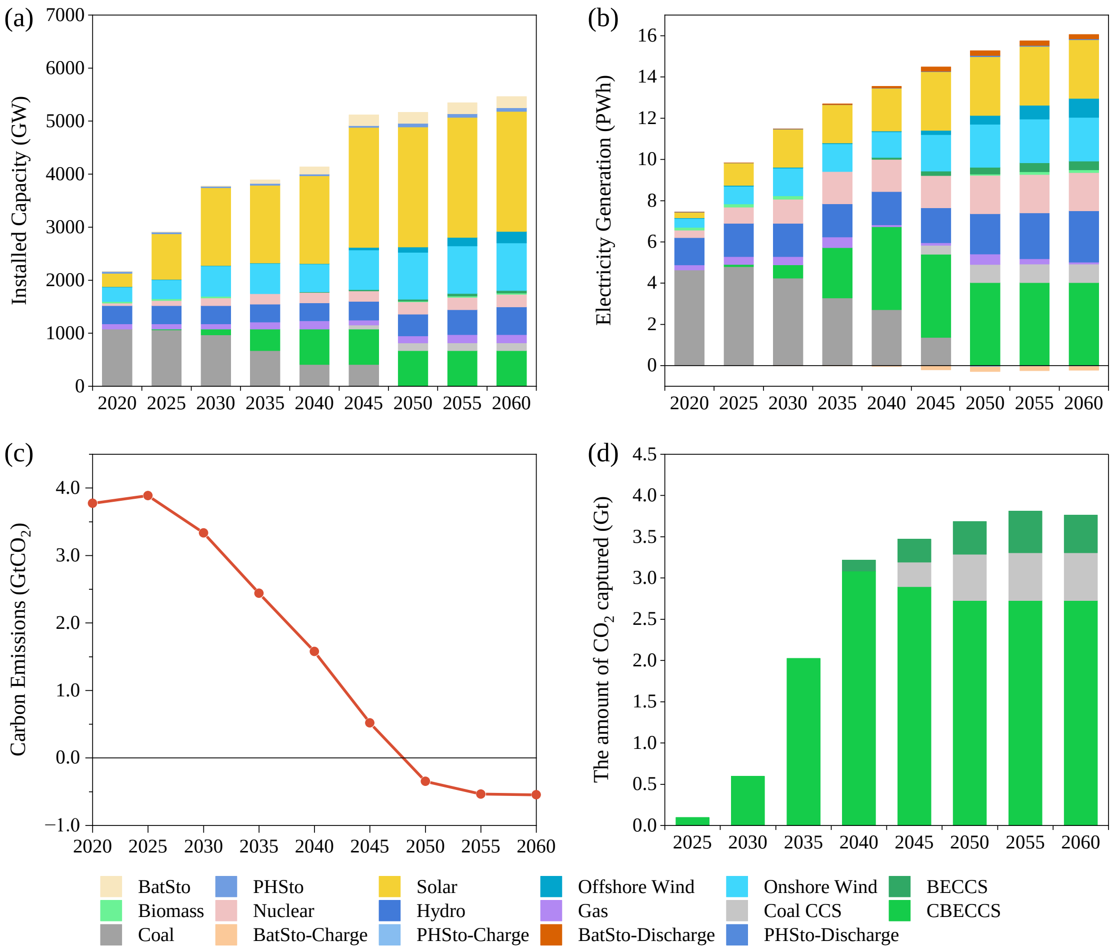

Figure 20. Power system model simulation results over the period 2020-2060 for the scenario including CBECCS technology without geographical sequestration constraints. (**a.** Installed capacity mix of China's power system (BatSto: battery storage; PHSto: pumped-hydro storage). **b.** The electricity generation mix of China's power system, where the negative values indicate the power charging of energy storage. **c.** The annual carbon emissions of China's power system. **d.** The amount of CO_2 captured by CCS-related technologies.)

CBECCS retrofit technology in the power system optimization model. The consideration of CBECCS technology in the power system optimization model can have a significant impact on the installed capacity mix, power generation mix and power supply costs of the power system. We additionally simulate the capacity expansion planning path of power system carbon neutrality under the scenario without considering CBECCS retrofit technology. The results indicate that if CBECCS retrofit technology is not considered, the total installed capacity share and power generation share of CCS-related technologies will decrease by 65% and 56% in 2060, respectively (Supplementary Fig. 21). Furthermore, we also note that ignoring CBECCS retrofit technology in China's power system modelling, as in the case in most existing integrated assessment models [137], would cause much higher system costs, e.g., by 10%-120% over the period 2045-2060 (Supplementary Fig. 22). The reason for this difference is that CBECCS retrofit technology is preferred by the power system optimization model due to the cost savings associated with the newly built plant infrastructure and the achievement of negative emissions.

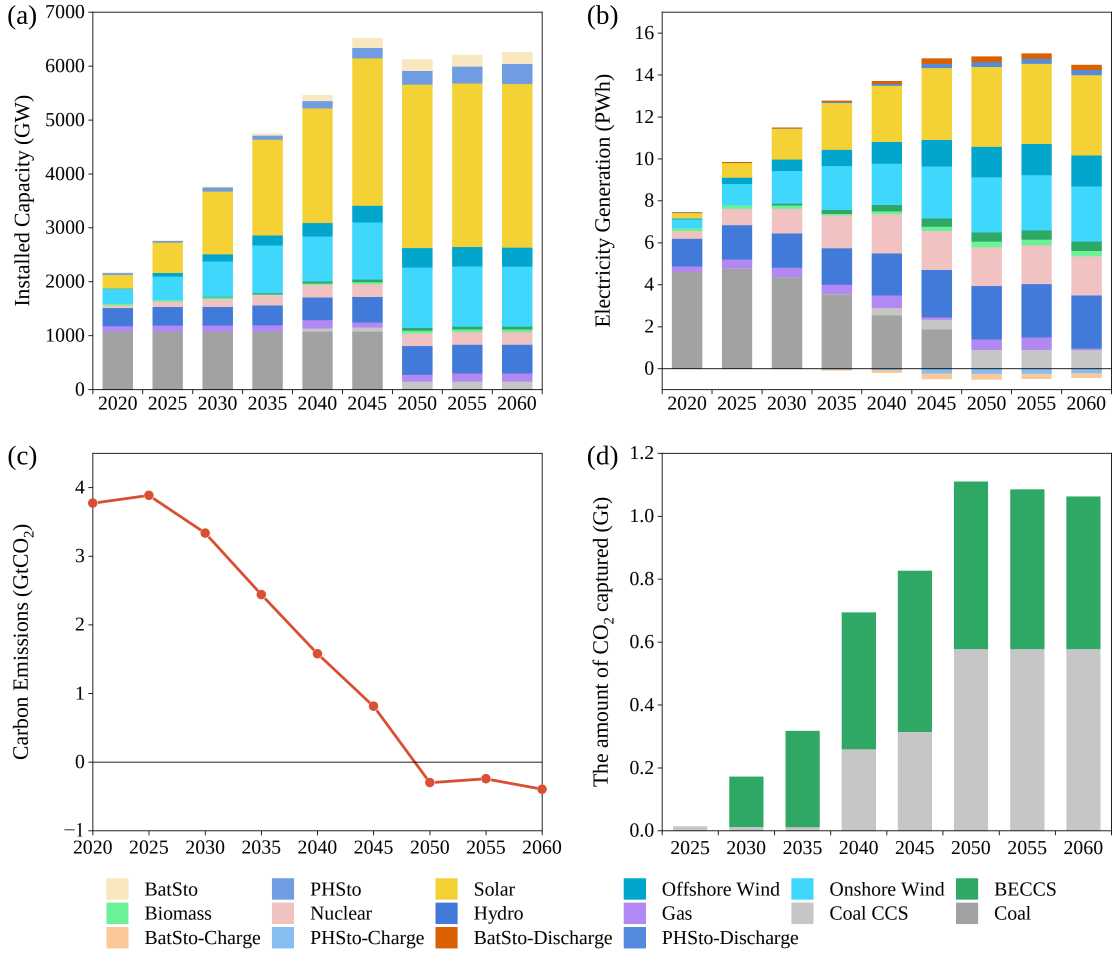

Figure 21. Power system model simulation results over the period 2020-2060 for the scenario without CCS retrofit technologies. (**a.** Installed capacity mix of China's power system (BatSto: battery storage; PHSto: pumped-hydro storage). **b.** The electricity generation mix of China's power system, where the negative values indicate the power charging of energy storage. **c.** The annual carbon emissions of China's power system. **d.** The amount of CO_2 captured by CCS-related technologies.)

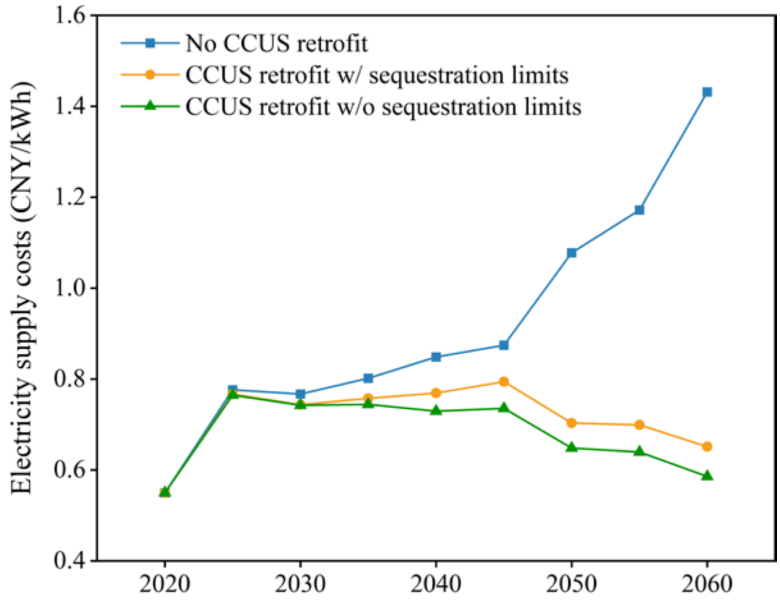

Figure 22. The annual electricity supply costs with and without CBECCS retrofit technology

The upper limit of the co-firing ratio. To investigate the technology supply potential and mitigation contribution caused by various co-firing ratios of the CBECCS system, we rerun two sets of cases under the CCS-only scenario (i.e., 0%-biomass) and the CBECCS scenario with a higher co-firing level (i.e., 30%-biomass), with other assumptions unchanged. In 2025, the 15%-biomass case achieves an additional 166 Mt/a (17.2%) of the supply potential relative to the 0%-biomass case, while the 30%-biomass case achieves an additional 113 Mt/a (12.1%) of the supply potential relative to the 15%-biomass case (Supplementary Fig. 5a). The net CO_2 emissions without extra life-cycle emissions of CBECCS plants range from 0.08~1.33 Mt/a, -0.84~0.49 Mt/a, and -3.03~0.59 Mt/a for the 0%, 15%, and 30% biomass cases, respectively (Supplementary Fig. 5b). A detailed consideration of life-cycle emissions would prevent most plants from achieving net negative emissions (Supplementary Fig. 7). For the dynamic assessment in 2040, the mitigation contribution of the 15%-biomass case can exceed that of the 0%-biomass case by 16.1 Mt/a (1%), while the mitigation contribution of the 30%-biomass case can exceed that of the 15%-biomass case by 29.9 Mt/a (2%) (and afterward, Supplementary Fig. 5c). Without biomass substitution mitigation, all CBECCS plants under the 15%-biomass case and 219 of 260 under the 30%-biomass case fail to achieve net negative emissions (Supplementary Fig. 5d). With 30%-biomass co-firing, biomass consumption by CBECCS deployment could amount to a maximum of 0.12 billion tce/a (occurred in the dynamic assessment), accounting for only 5.0% of the total available biomass (including the projected energy crops) in China that year. This situation indicates that large-scale CBECCS deployment in China is unlikely to cause additional severe ecological problems or unsustainable earth boundary threats, such as water and soil nutrient losses, land degradation, food, or energy shortages [55, 138-144].

Single biomass type as co-firing fuel. We also rerun a single type biomass case instead of mixed biomass sources, such as the coal-to-biomass Drax plant in operation in the UK [145]. The results have subtle changes. For example, the total CO_2 emissions reduction potential (supply potential) and the negative emissions potential would decrease by only 2% and 9%, respectively, with the average co-firing ratio slightly changing from 14% to 13% (Supplementary Fig. 23).

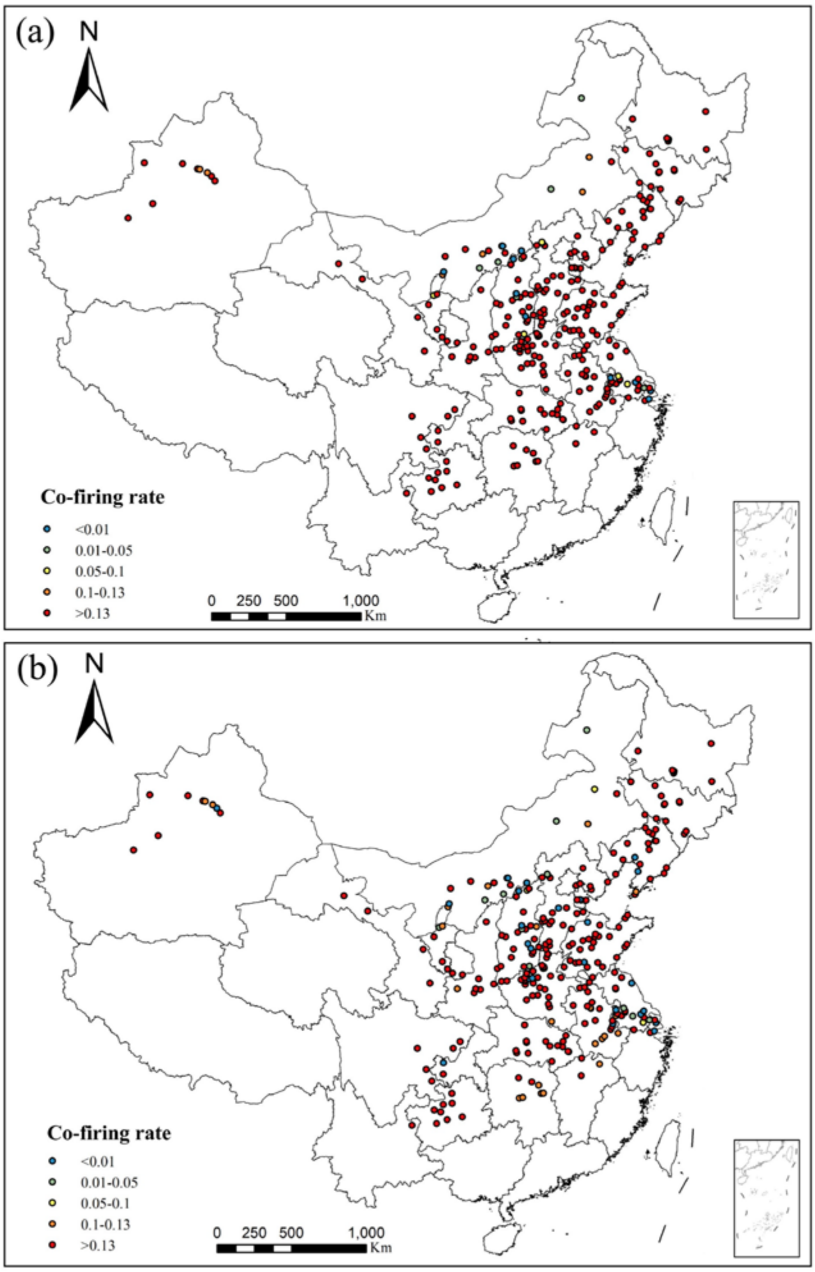

Figure 23. Distribution of the actual co-firing rate for power plants with mixed and single types of biomass sources. (a. represents the case of mixed biomass sources; b. represents the case of a single biomass source. Note: The single biomass source refers to a specific biomass type with the largest volume surrounding each coal-fired power plant within 50 km. Both mapping results are based on the biomass and power plant matching model. Data Credits: All the provincial administrative boundaries are from Ministry of Civil Affairs of the People's Republic of China (http://xzqh.mca.gov.cn/map, Map Content Approval Number: GS(2022)1873))

Limitations and further perspectives

This study still suffers certain limitations in terms of the research boundaries and modelling assumptions. In this study, we did not provide an elaborate assessment of the potential environmental impacts of severe ecological problems or unsustainable Earth boundary threats (e.g., water and soil nutrient losses, land degradation, food, or energy shortages) caused by CBECCS technology deployment but rather an approximate assessment. In the power system, we carefully considered the differences in the hourly fluctuations in variable renewable energy in 31 provinces (via the AF value and electricity demand) and clustered the yearly hourly data into more categories (i.e., 25 clusters) than those considered in other studies (e.g., Zhuo, Du [61,] Green, Staffell [71]), thus contributing to a high temporal resolution with spatial heterogeneity. However, we did not further decompose the national model into a cross-province model, although we did improve the model operation efficiency.

In addition to the internal soft-links of the CBECCS source–sink matching system, the combination model in this study includes three soft-linking mechanisms: (1) the CGE model outputted the national dynamic electricity demand and power sector CO_2 emission trajectory from 2020-2060 to the PSOM model under the carbon neutrality constraint; (2) the maximum CBECCS retrofittable installed capacity in the PSOM model was obtained from the CBECCS source–sink matching model. The technical parameters of CBECCS (e.g., the capital cost, learning rate of the learning curve for the dynamic capital cost and CO_2 emission factor of the biomass resources) were set to ensure consistency with the PSOM model and CBECCS source–sink matching model; and (3) The input variables, e.g., the CBECCS retrofit installed capacity, electricity generation, and mitigation demand every five years, were generated by the PSOM as constraints of the dynamic source–sink matching model. These mechanisms render our model more advanced than traditional macroeconomic models (e.g., Weng, Cai [146]) and dedicated CCS source–sink models (e.g., Fan, Xu [147]).

Nevertheless, certain feedback mechanisms, e.g., those from the PSOM to the CGE model and from the dynamic source–sink matching model to the PSOM, were not characterized, as this would entail a highly complex and time-consuming simulation process [148]. Although the CBECCS static assessment results are unlikely to correspond to China's carbon neutrality pathway, we reported them as a reference for other studies requiring geologically constrained full-chain CBECCS information. In addition, some parameter details may still be uncertain, e.g., the hidden CO_2 emissions that may result from the increased oil consumption were not evaluated in LCA of the EOR opportunity, considering that the average emission factor of oil use is difficult to estimate given the uncertainties in the future use structure (e.g., as a raw material or fuel) and technological development (e.g., petrochemical mitigation technology). The above limitations should be addressed in future studies.

References

1. Fan Y, Liu L-C, Wu G, Tsai H-T, Wei Y-M. Changes in carbon intensity in China: empirical findings from 1980–2003. *Ecological Economics* 2007, **62**(3)**:** 683-691.
2. Zhang W, Zhang L, Zhang C, Yu D. Assessment of the Potential of Forest Biomass Energy in China. *Journal of Beijing Forestry University* 2015, **14**(2)**:** 52-55.
3. Huang J, Wang X, Xu T. Related Questions Research on Biomass Generation Using Agriculture and Forest Residue in China. *Journal of Shengyang Institute of Engineering (Natural Science) (in Chinese)* 2018, **4**(1)**:** 7-18.
4. Sohu. Estimation of biomass energy crop resources reserves in China. 2019

[cited]Available from: https://www.sohu.com/a/308501318_100252878 (in Chinese)

5. Nie Y, Chang S, Cai W, Wang C, Fu J, Hui J*, et al.* Spatial distribution of usable biomass feedstock and technical bioenergy potential in China. *GCB Bioenergy* 2020, **12**(1)**:** 54-70.
6. Kou J, Bi Y, Zhao L, Gao C, Tian Y, Wei S*, et al.* Investigation and evaluation on wasteland for energy crops in China. *Renewable Energy Resources* 2008, **26**(6)**:** 3-9.
7. Zhuang D, Jiang D, Liu L, Huang Y. Assessment of bioenergy potential on marginal land in China. *Renewable and Sustainable Energy Reviews* 2011, **15**(2)**:** 1050-1056.
8. IPCC. *2006 IPCC Guidelines for National Greenhouse Gas Inventories*. Intergovernmental Panel on Climate Change: Bracknell, U.K., 2006.
9. IEA. *Ready for CCS retrofit: The potential for equipping China's existing coal fleet with carbon capture and storage*. International Energy Agency: Paris, 2016.
10. Li K, Shen S, Fan J-L, Xu M, Zhang X. The role of carbon capture, utilization and storage in realizing China's carbon neutrality: A source-sink matching analysis for existing coal-fired power plants. *Resources, Conservation and Recycling* 2022, **178:** 106070.
11. Agbor E, Zhang X, Kumar A. A review of biomass co-firing in North America. *Renewable and Sustainable Energy Reviews* 2014, **40:** 930-943.
12. Fan J-L, Shen S, Wei S-J, Xu M, Zhang X. Near-term CO2 storage potential for coal-fired power plants in China: A county-level source-sink matching assessment. *Applied Energy* 2020, **279:** 115878.
13. Fan J-L, Wei S, Shen S, Xu M, Zhang X. Geological storage potential of CO2 emissions for China's coal-fired power plants: A city-level analysis. *International Journal of Greenhouse Gas Control* 2021, **106:** 103278.
14. Wei Y-M, Kang J-N, Liu L-C, Li Q, Wang P-T, Hou J-J*, et al.* A proposed global layout of carbon capture and storage in line with a 2 °C climate target. *Nature Climate Change* 2021.
15. Bachu, Stefan. Review of CO2 storage efficiency in deep saline aquifers. *International Journal of Greenhouse Gas Control* 2015, **40:** 188-202.
16. Dahowski RT, Dooley J, Davidson C, Bachu S, Gupta N. *Building the Cost Curves for CO2 Storage: North America*. IEA Greenhouse Gas R&D Programme, 2005.
17. Diao Y, Zhu G, Jin X, Zhang C, Li X. Theoretical potential assessment of CO2 geological utilization and storage in the Sichuan Basin. *Geological Bulletin of China* 2017, **36**(6)**:** 1088-1095.
18. Li X, Wei N, Liu Y, Fang Z, Dahowski RT, Davidson CL. CO2 point emission and geological storage capacity in China. *Energy Procedia* 2009, **1**(1)**:** 2793-2800.
19. Baik E, Sanchez DL, Turner PA, Mach KJ, Field CB, Benson SM. Geospatial analysis of near-term potential for carbon-negative bioenergy in the United States. *Proceedings of the National Academy of Sciences* 2018, **115**(13)**:** 3290-3295.
20. Tian Q, Zhao D, Li Z, Zhu Q. Robust and stepwise optimization design for CO2 pipeline transportation. *International Journal of Greenhouse Gas Control* 2017, **58:** 10-18.
21. IEA. Net Zero by 2050. Paris: IEA; 2021.
22. Zhang D, Wang Z, Sun J, Zhang L, Li Z. Economic evaluation of CO2 pipeline transport in China. *Energy Conversion and Management* 2012, **55:** 127-135.
23. ZGW. China steel price. 2022 [cited]Available from: https://hq.zgw.com/chart.html
24. Lu H, Ma X, Huang K, Fu L, Azimi M. Carbon dioxide transport via pipelines: A systematic review. *Journal of Cleaner Production* 2020, **266:** 121994.

25. Lu H, Ma X, Huang K, Fu L, Azimi M. Carbon dioxide transport via pipelines: A systematic review. *Journal of Cleaner Production* 2020, **266**.
26. SAC. Equipment and pipe insulation standards. 1989 [cited]Available from: https://wenku.baidu.com/view/b75553a8443610661ed9ad51f01dc281e53a56ac?aggId=b75553a8443610661ed9ad51f01dc281e53a56ac&fr=catalogMain
27. Fan J-L, Li Z, Li K, Zhang X. Modelling plant-level abatement costs and effects of incentive policies for coal-fired power generation retrofitted with CCUS. *Energy Policy* 2022, **165:** 112959.
28. Fajardy M, Mac Dowell N. Can BECCS deliver sustainable and resource efficient negative emissions? *Energy Environ Sci* 2017, **10**.
29. Parajuli R, Løkke S, Østergaard PA, Knudsen MT, Schmidt JH, Dalgaard T. Life Cycle Assessment of district heat production in a straw fired CHP plant. *Biomass and Bioenergy* 2014, **68:** 115-134.
30. Lu X, Cao L, Wang H, Peng W, Xing J, Wang S*, et al.* Gasification of coal and biomass as a net carbon-negative power source for environment-friendly electricity generation in China. *Proceedings of the National Academy of Sciences* 2019, **116**(17)**:** 8206-8213.
31. IPCC. Climate Change 2014 Synthesis Report; 2014.
32. Dias AC. Life cycle assessment of fuel chip production from eucalypt forest residues. *The International Journal of Life Cycle Assessment* 2014, **19**(3)**:** 705-717.
33. Fajardy M, Mac Dowell N. Can BECCS deliver sustainable and resource efficient negative emissions? *Energy & Environmental Science* 2017, **10**(6)**:** 1389-1426.
34. Qin X, Mohan T, El-Halwagi M, Cornforth G, McCarl BA. Switchgrass as an alternate feedstock for power generation: an integrated environmental, energy and economic life-cycle assessment. *Clean Technologies and Environmental Policy* 2006, **8**(4)**:** 233-249.
35. Lu W, Zhang T. Life-cycle implications of using crop residues for various energy demands in China. *Environmental science & technology* 2010, **44**(10)**:** 4026-4032.
36. NBS. *China City Statistical Yearbook 2020*. China Statistics Press, 2021.
37. Zhang X, Xu M, Xu D, Zhong P, Peng X, Fan J. Carbon footprint assessment of coal‑to‑hydrogen technology combined with CCUS in China. *China population, resources and environment* 2021, **31**(12)**:** 1-11 (in Chinese).
38. Oberschelp C, Pfister S, Raptis CE, Hellweg S. Global emission hotspots of coal power generation. *Nature Sustainability* 2019, **2**(2)**:** 113-121.
39. Li N, Chen W. Modeling China’s interprovincial coal transportation under low carbon transition. *Applied Energy* 2018, **222:** 267-279.
40. Xian Y, Wang Q, Fan W, Da Y, Fan J-L. The impact of different incentive policies on new energy vehicle demand in China's gigantic cities. *Energy Policy* 2022, **168:** 113137.
41. Gao J, Xu X, Zheng F, Huo R. Coal carbon emission inventory calculation and uncertainties analysis based on life cycle analysis. *China Coal* 2017, **43**(6)**:** 22-26.
42. Yang B, Wei Y-M, Hou Y, Li H, Wang P. Life cycle environmental impact assessment of fuel mix-based biomass co-firing plants with CO2 capture and storage. *Applied Energy* 2019, **252:** 113483.
43. Xian Z, Mao X, Dong X, Ping Z, Xueting P, Fan JL. Carbon footprint assessment of coal‑to‑hydrogen technology combined with CCUS in China. *China population，resources and environment* 2021, **31**(12)**:** 1-11.

44. Yang B, Wei Y-M, Liu L-C, Hou Y-B, Zhang K, Yang L*, et al.* Life cycle cost assessment of biomass co-firing power plants with CO2 capture and storage considering multiple incentives. *Energy Economics* 2021, **96:** 105173.
45. Li J, Wang R, Li H, Nie Y, Song X, Li M*, et al.* Unit-level cost-benefit analysis for coal power plants retrofitted with biomass co-firing at a national level by combined GIS and life cycle assessment. *Applied Energy* 2021, **285:** 116494.
46. IEA. Zero-emission carbon capture and storage in power plants using higher capture rates; 2019.
47. Agbor E, Oyedun AO, Zhang X, Kumar A. Integrated techno-economic and environmental assessments of sixty scenarios for co-firing biomass with coal and natural gas. *Applied Energy* 2016, **169:** 433-449.
48. Xing B. Research on the potential reduction of coal transportation cost in China. *Coal Economic Research* 2022, **42**(03)**:** 22-27.
49. MOT. Transportation Statistics Yearbook of China 2019. 2019 [cited]Available from: https://www.mot.gov.cn/tongjishuju/
50. NEA. National Electricity Price Supervision Notice in 2018; 2019.
51. Zhang Q, Zhou D, Zhou P, Ding H. Cost Analysis of straw-based power generation in Jiangsu Province, China. *Applied Energy* 2013, **102:** 785-793.
52. Lu X, Liang C, Wang H, Peng W, Xing J, Wang S*, et al.* Gasification of coal and biomass as a net carbon-negative power source for environment-friendly electricity generation in China. *Proceedings of the National Academy of Sciences* 2019, **116**(17).
53. Joint Research C, Institute for E, Transport, Elbersen B, Dalla Longa F, Ruiz P*, et al. The JRC-EU-TIMES model : bioenergy potentials for EU and neighbouring countries*. Publications Office, 2015.
54. Xing X, Wang R, Bauer N, Ciais P, Cao J, Chen J*, et al.* Spatially explicit analysis identifies significant potential for bioenergy with carbon capture and storage in China. *Nature Communications* 2021, **12**(1)**:** 3159.
55. Fajardy M, Mac Dowell N. Can BECCS deliver sustainable and resource efficient negative emissions? *Energy & Environmental Science* 2017, **10**(6)**:** 1389-1426.
56. MOST. Development Roadmap of Carbon Capture, Utilization and Storage Technology in China. 2019.
57. McFarland JR, Reilly JM, Herzog HJ. Representing energy technologies in top-down economic models using bottom-up information. *Energy Economics* 2004, **26**(4)**:** 685-707.
58. Commission NDaR. Typical power load curves in each provincial power system. 2019 [cited]Available from: https://www.ndrc.gov.cn/xxgk/zcfb/tz/201912/P020191230336066090861.pdf
59. Ortega-Vazquez MA, Kirschen DS. Optimizing the Spinning Reserve Requirements Using a Cost/Benefit Analysis. *IEEE Transactions on Power Systems* 2007, **22**(1)**:** 24-33.
60. CEC. *China Electric Power Statistical Yearbook 2021*. China Statistics Press: Beijing, 2021.
61. Zhuo Z, Du E, Zhang N, Nielsen CP, Lu X, Xiao J*, et al.* Cost increase in the electricity supply to achieve carbon neutrality in China. *Nature Communications* 2022, **13**(1)**:** 3172.
62. Wright TP. Factors affecting the cost of airplanes. *Journal of the Aeronautical Sciences* 1936, **3:** 122-128.
63. Heuberger CF, Rubin ES, Staffell I, Shah N, Mac Dowell N. Power capacity expansion planning

considering endogenous technology cost learning. *Applied Energy* 2017, **204:** 831-845.
64. NASA. Modern-Era Retrospective analysis for Research and Applications, Version 2(MERRA-2). 2022 [cited]Available from: https://gmao.gsfc.nasa.gov/reanalysis/MERRA-2/
65. Gelaro R, McCarty W, Suárez MJ, Todling R, Molod A, Takacs L*, et al.* The Modern-Era Retrospective Analysis for Research and Applications, Version 2 (MERRA-2). *Journal of Climate* 2017, **30**(14)**:** 5419-5454.
66. AG M. Meteonorm Version 8. 2022 [cited]Available from: https://meteonorm.com/
67. CNREC. Renewable Energy Data Sheet 2019: China National Renewable Energy Center; 2019.
68. Li M, Virguez E, Shan R, Tian J, Gao S, Patiño-Echeverri D. High-resolution data shows China's wind and solar energy resources are enough to support a 2050 decarbonized electricity system. *Applied Energy* 2022, **306:** 117996.
69. Dobos AP. PVWatts Version 5 Manual. United States; 2014.
70. Commission NDaR. Typical power load curves in each provincial power system; 2019.
71. Green R, Staffell I, Vasilakos N. Divide and Conquer? k-Means Clustering of Demand Data Allows Rapid and Accurate Simulations of the British Electricity System. *IEEE Transactions on Engineering Management* 2014, **61**(2)**:** 251-260.
72. Ojeda JJ, Volenec JJ, Brouder SM, Caviglia OP, Agnusdei MG. Evaluation of Agricultural Production Systems Simulator as yield predictor of Panicum virgatum and Miscanthus x giganteus in several US environments. *GCB Bioenergy* 2017, **9**(4)**:** 796-816.
73. Wang C. Comparison and preliminary study on biological characteristics of different switchgrass varieties in western Jilin Province. *Northeast Normal University* 2016.
74. Sun J. Study on Developmental physiology and suitable harvest time of switchgrass seeds. *Northeast Normal University* 2015.
75. Zhan W-j, Ren J-x, Jin S-h, Huang Y-j, Pan Y-h, Zheng B-s. Research progress on agronomic characteristics of Miscanthus. *Journal of Zhejiang A&F University* 2012, **29**(1)**:** 119-124.
76. Leng G, Huang M, Tang Q, Leung LR. A modeling study of irrigation effects on global surface water and groundwater resources under a changing climate. *Journal of Advances in Modeling Earth Systems* 2015, **7**(3)**:** 1285-1304.
77. Warszawski L, Frieler K, Huber V, Piontek F, Serdeczny O, Schewe J. The Inter-Sectoral Impact Model Intercomparison Project (ISI–MIP): Project framework. *Proceedings of the National Academy of Sciences* 2014, **111**(9)**:** 3228-3232.
78. Hempel S, Frieler K, Warszawski L, Schewe J, Piontek F. A trend-preserving bias correction – the ISI-MIP approach. *Earth Syst Dynam* 2013, **4**(2)**:** 219-236.
79. Dai Y, Shangguan W, Duan Q, Liu B, Fu S, Niu G. Development of a China Dataset of Soil Hydraulic Parameters Using Pedotransfer Functions for Land Surface Modeling. *Journal of Hydrometeorology* 2013, **14**(3)**:** 869-887.
80. Liao W, Liu X, Xu X, Chen G, Liang X, Zhang H*, et al.* Projections of land use changes under the plant functional type classification in different SSP-RCP scenarios in China. *Science Bulletin* 2020, **65**(22)**:** 1935-1947.
81. Danaci D, Bui M, Petit C, Mac Dowell N. En Route to Zero Emissions for Power and Industry with Amine-Based Post-combustion Capture. *Environmental Science & Technology* 2021, **55**(15)**:** 10619-10632.
82. Jiang K, Feron P, Cousins A, Zhai R, Li K. Achieving Zero/Negative-Emissions Coal-Fired Power Plants Using Amine-Based Postcombustion CO2 Capture Technology and Biomass

Cocombustion. *Environmental Science & Technology* 2020, **54**(4)**:** 2429-2438.

83. Panja P, McPherson B, Deo M. Techno-Economic Analysis of Amine-based CO2 Capture Technology: Hunter Plant Case Study. *Carbon Capture Science & Technology* 2022, **3:** 100041.
84. Brandl P, Bui M, Hallett JP, Mac Dowell N. Beyond 90% capture: Possible, but at what cost? *International Journal of Greenhouse Gas Control* 2021, **105:** 103239.
85. IEAGHG. Towards Zero Emissions CCS from Power Stations using Higher Capture Rates or Biomass: IEA Greenhouse Gas R&D Programme; 2019.
86. He R. Geographical distribution of biomass energy and access on its development and utilization in China. Master thesis, Lanzhou university, Lanzhou, 2012.
87. Xie G, Zhuang H, Wei W, Zhuo Y, Guang X. *Non-food energy plants: principles of production and marginal cultivation*. China Agricultural University Press: Beijing, 2011.
88. Xu Z, Yang L. The resources of miscanthus in sichuan and its development and utilization prospect. *Prataculture and animal husbandry* 2009, **0**(9)**:** 22-27.
89. Xiao L, Yi Z. Distribution and Climate Model of Four Type Species of Miscanthus in China. *Acta Agrestia Sinica* 2017, **25**(4)**:** 685-690.
90. Fu J. Assessment of the development potential of non-food fuel ethanol in China. University of Chinese Academy of Sciences, Beijing, 2015.
91. Hu S, Gong Z, Jiang D. Brief introduction of a bio-energy crop-Panicum virgatum. *Pra Tacultu Ra L Science* 2008, **25**(6)**:** 29-33.
92. Wu C, Chen X, Sun Y, Jiang M, Yan K, Zhang L. Marginal Land-Based Biomass Energy Production in Yellow River Delta. *Adv Mater Res-Switz* 2014, **2912:** 544-549.
93. Sun F, Wang D, Yuan J, Chen Z. Research progress and research value of miscanthus. *Henan agricultural* 2017(4)**:** 48-49.
94. Liu W, Sang T. Potential productivity of the Miscanthus energy crop in the Loess Plateau of China under climate change. *Environmental Research Letters* 2013, **8**(4)**:** 04003.
95. Xie X, Zhou F, Zhao Y, Lu X. A summary of ecological and energy-producing effects of perennial energy grasses. *Acta Ecologica Sinica* 2008, **28**(5)**:** 2329-2342.
96. Xie G, Guo X, Wang X, Ding R, Lin HU, Cheng X. An Overview and Perspectives of Energy Crop Resources. *Resources Science* 2007, **29**(5)**:** 74-80.
97. NBS. *China Energy Statistics Yearbook 2017*. China Statistical Press: Beijing, 2017.
98. Wang M. The greenhouse gases, regulated emissions, and energy use in transportation (GREET) model (version GREET 2019). Illinois, 2019.
99. Li G, Lv M. *Atlas of China's petroliferous basins (2nd Edition)*: Beijing, 2002.
100. Markit IHS. Energy & Natural Resources. 2019 [cited]Available from: https://ihsmarkit.com/industry/energy.html
101. Center for Hydrogeology, Environmental Geology Survey. *Suitability evaluation map of CO2 Geological storage in main sedimentary basis in China and its adjacent sea area*. Geological Publishing House: Hebei, 2017.
102. NBS. *China Energy Statistics Yearbook 2019*. China Statistical Press: Beijing (in Chinese), 2019.
103. Zhang X, Huang X, Zhang D, Geng Y, Tian L, Fan Y*, et al.* Research on the Pathway and Policies for China's Energy and Economy Transformation toward Carbon Neutrality. *Journal of Management World* 2022, **38**(01)**:** 35-66.
104. China Electricity Council. *China Electric Power Yearbook 2021*, 2021.
105. World Resources Institute. Global Power Plant Database. [cited]Available from:

https://datasets.wri.org/dataset/globalpowerplantdatabase
106. China National Renewable Energy Information Management Centre. Construction of biomass power generation in various provinces in 2020. 2020 [cited]Available from: https://news.bjx.com.cn/html/20210204/1134651.shtml
107. Chinese Wind Energy Association. Installed capacity of offshore wind for provinces at the end of 13th Five-year Plan. 2020 [cited]Available from: https://www.smelz.cn/article/zixun/detail-45127.html
108. China Energy Storage Alliance. White Papers of Research on Chinese Energy Storage Industry. 2020 [cited]Available from: https://www.xdyanbao.com/doc/auonxjt0if?bd_vid=10001695266172045651
109. State Grid Energy Research Institute. *China Energy & Electricity Outlook*, 2020.
110. Liang Y, Yu B, Wang L. Costs and benefits of renewable energy development in China's power industry. *Renewable Energy* 2019, **131:** 700-712.
111. National Renewable Energy Laboratory (NREL). Cost Projections for Utility-Scale Battery Storage: 2021 Update; 2020.
112. China Electricity Council. Research on Flexible Operation and Life Extension Operation of Coal-fired Unit; 2019.
113. China Nuclear Energy Associate. Statistics of Chinese mainland Nuclear Power Plant Operating Reactor Years. 2018 [cited]Available from: https://www.china-nea.cn/site/content/35677.html
114. China Nuclear Energy Associate. National Nuclear Power Operation from January to December 2020. 2020.
115. National Energy Administration. Reserve rate of power system. 2017 [cited]Available from: https://view.officeapps.live.com/op/view.aspx?src=http%3A%2F%2Fzfxxgk.nea.gov.cn%2Fauto84%2F201705%2FP020170510400277383807.docx&wdOrigin=BROWSELINK
116. China Electric Power Planning & Engineering Institute. *Report On China's Electric Power Development 2020*, 2020.
117. National Renewable Energy Laboratory. 2021 annual technology baseline electricity data. 2021 [cited]Available from: https://atb.nrel.gov/electricity/2021/data (2021)
118. Xie G-h. Progress and Direction of Non-Food Biomass Feedstock Supply Research and Development in China. *Journal of China Agricultural University* 2012, **17**(6)**:** 1-19.
119. Venturi P, Venturi G. Analysis of Energy Comparison For Crops in European Agricultural Systems. *Biomass and Bioenergy* 2003, **25**(3)**:** 235-255.
120. Hu Sm, Gong Zx, Jiang Ds. Brief Introduction of a Biorenergy Crop-Panicum Virgatum. *Pratacultural Science* 2008, **25**(6)**:** 29-33.
121. Ma Y-q, Hao Z-q, Xiong S-j, Liu J-l. Present Status and Future of Switchgrass Going to Scale Plantation in China. *Journal of China Agricultural University* 2012, **17**(6)**:** 133-137.
122. Zuo Ht, Yang Xs, Chen Q. Research Progress of Cellulosic Herbaceous Energy Plants. *Biomass Energy* 2008**:** 261-266.
123. Zong Jq, Guo Aj, Chen Jb, Liu Jx. A Study on Biomass Potentials of Perennial Gramineous Energy Plants. *Pratacultural Science* 2012, **29**(5)**:** 809-813.
124. Vogel KP. Switchgrass. *Warm‐Season (C4) Grasses*, 2004, pp 561-588.
125. Fan X-f, Hou X-c, Zuo Ht, Wu J-y, Duan L-s. Biomass Yield and Quality of Three Kinds of BioenergyGrasses in Beijing of China. *Scientia Agricultura Sinica* 2010, **43**(16)**:** 3316-3322.

126. Bouton JH. Bioenergy Crop Breeding and Production Research in the Southeast, Final Report for 1996 to 2001. United States; 2003.
127. Liu J, Williams JR, Zehnder AJB, Yang H. GEPIC – Modelling Wheat Yield and Crop Water Productivity with High Resolution on a Global Scale. *Agricultural Systems* 2007, **94**(2)**:** 478-493.
128. Sun F, Wang D, Yuan J, Chen Zj. Research Progress and Research Value of Miscanthus Sinensis. *Shen Tai Nong Ye* 2017, **11:** 48-49.
129. Xie G-h, Guo Xq, Wang X, Ding Re, Hu L, Cheng X. An Overview and Perspectives of Energy Crop Resources. *Resources Science* 2007, **29**(5)**:** 74-80.
130. Liu W, Sang T. Potential productivity of the Miscanthus Energy Crop in the Loess Plateau of China under Cimate Change. *Environmental Research Letters* 2013, **8**(4)**:** 044003.
131. Xie G, Peng L. Genetic Engineering of Energy Crops: A Strategy for Biofuel Production in ChinaFree Access. *Journal of integrative plant biology* 2011, **53**(2)**:** 143-150.
132. Yi Z-l. Exploitation and Utilization of Miscanthus as Energy Plant. *Joumal of Hunan Agricultural University (Natural Sciences)* 2012, **38**(5)**:** 455-463.
133. Yu Y-C, Yi Z-L, Zhou G-k. Research Progress and Comprehensive Utilization of Miscanthus. *Chinese Bulleting Sciences* 2014, **26**(5)**:** 474-480.
134. Alpine WJM, Shield IF, Walsh LRE, Mccracken AR, Wilson H, Gilleland J*, et al.* Rothamsted Research Willow (Salve spp.) Breeding Programme; Multi-Site Yield Trial Results 2011. *Aspects of Applied Biology* 2011(112).
135. Xue S, Lewandowski I, Wang X, Yi Z. Assessment of the Production Potentials of Miscanthus on Marginal Land in China. *Renewable and Sustainable Energy Reviews* 2016, **54:** 932-943.
136. Jiang D, Hao M, Fu J, Liu K, Yan X. Potential bioethanol production from sweet sorghum on marginal land in China. *Journal of Cleaner Production* 2019, **220:** 225-234.
137. Duan H, Zhou S, Jiang K, Bertram C, Harmsen M, Kriegler E*, et al.* Assessing China's efforts to pursue the 1.5°C warming limit. *Science* 2021, **372**(6540)**:** 378.
138. CSLF. Technical Summary of Bioenergy Carbon Capture and Storage (BECCS): Carbon Sequestration Leadership Forum; 2018.
139. Smith P, Davis SJ, Creutzig F, Fuss S, Minx J, Gabrielle B*, et al.* Biophysical and economic limits to negative CO2 emissions. *Nature Climate Change* 2016, **6**(1)**:** 42-50.
140. Jones MB, Albanito F. Can biomass supply meet the demands of bioenergy with carbon capture and storage (BECCS)? *Glob Change Biol* 2020, **26**(10)**:** 5358-5364.
141. Heck V, Gerten D, Lucht W, Popp A. Biomass-based negative emissions difficult to reconcile with planetary boundaries. *Nature Climate Change* 2018, **8**(2)**:** 151-155.
142. Wilhelm WW, Johnson JMF, Karlen DL, Lightle DT. Corn Stover to Sustain Soil Organic Carbon Further Constrains Biomass Supply. *Agronomy Journal* 2007, **99**(6)**:** 1665-1667.
143. Yang Y, Zhang P, Zhang W, Tian Y, Zheng Y, Wang L. Quantitative appraisal and potential analysis for primary biomass resources for energy utilization in China. *Renewable and Sustainable Energy Reviews* 2010, **14**(9)**:** 3050-3058.
144. Amundson R, Biardeau L. Soil carbon sequestration is an elusive climate mitigation tool. *Proceedings of the National Academy of Sciences* 2018, **115**(46)**:** 11652-11656.
145. Katie F. Drax's 2014 results show decarbonization project on time, budget 2015 [cited]Available from: https://www.woodpelletservices.com/documents/Drax%20FEB2015.pdf

146. Weng Y, Cai W, Wang C. Evaluating the use of BECCS and afforestation under China's carbon-neutral target for 2060. *Applied Energy* 2021, **299:** 117263.
147. Fan J-L, Xu M, Yang L, Zhang X. Benefit evaluation of investment in CCS retrofitting of coal-fired power plants and PV power plants in China based on real options. *Renewable and Sustainable Energy Reviews* 2019, **115:** 109350.
148. Tang H, Zhang S, Chen W. Assessing Representative CCUS Layouts for China's Power Sector toward Carbon Neutrality. *Environmental Science & Technology* 2021, **55**(16)**:** 11225-11235.